TECHNISCHE UNIVERSITÄT MÜNCHEN
Lehrstuhl für Chemie der Biopolymere

Helix Backbone Dynamics of the Alzheimer Amyloid Precursor Protein Transmembrane Domain - a γ-Secretase Substrate

Oxana Pester

Vollständiger Abdruck der von der Fakultät Wissenschaftszentrum Weihenstephan für Ernährung, Landnutzung und Umwelt der Technischen Universität München zur Erlangung des akademischen Grades eines

Doktors der Naturwissenschaften

genehmigten Dissertation.

Vorsitzende:	Univ.-Prof. Dr. I. Antes
Prüfer der Dissertation:	
	1. Univ.-Prof. Dr. D. Langosch
	2. Univ.-Prof. Dr. B. Küster

Die Dissertation wurde am 18.04.2013 bei der Technischen Universität München eingereicht und durch die Fakultät Wissenschaftszentrum Weihenstephan für Ernährung, Landnutzung und Umwelt am 26.06.2013 angenommen.

‘Nothing in life is to be feared, it is only to be understood.
Now is the time to understand more, so that we may fear less.’
Marie Curie

Acknowledgements

It is my pleasure and an opportunity I shall not miss to thank all the people who have supported, influenced and motivated me during my PhD thesis.

Foremost, I would like to express my sincere gratitude to my advisor Prof. Langosch. He gave me scientific freedom as well as inspiration to my research work. I thank him for being an attentive and encouraging discussion partner and sharing my passion for science.

My sincere thanks go to Prof. Küster (Chair of Proteomics and Bioanalytics) for being my second examiner and offering me to apply my ideas on his mass spectrometry equipment and for the opportunity of peptide synthesis. I also thank him for the discussions we had.

I thank Prof. Antes (Theoretical Chemical Biology and Protein Modelling Group) for showing interest in my projects and being the chair of the examination committee.

I am also grateful to:

Dr. Christina Scharnagl for sharing her knowledge in molecular dynamics simulations and in biophysics in general, for proofreading my thesis and being a stimulant companion during my thesis.

The whole molecular dynamics simulation group (Daniel and Philipp Hornburg, Rasmus Pröbstle, Simon Widmaier, Matthias Mörch and Christina Scharnagl) for their contributions, intense exchange of experiences, and discussions which sometimes became very philosophic.

Walter Stelzer and Dr. Bernhard Poschner for sharing their expertise in DHX and Dr. Markus Gütlich for his technical and laboratorial expertise.

Hannes Hahne and Andrea Hubauer from the Chair of Proteomics and Bioanalytics for their help introducing me to the Amazon ETD ion trap and the peptide synthesizer.

Christian Ried for his friendship and for writing a mass spectrometry data evaluation programme easing my work and for his valuable discussions in my research projects.

My colleague Jan Kirrbach and from the Bioinformatics Group Sindy Neumann, Nadia Latif and Angelika Fuchs for their profound friendship and group mentoring.

My lab colleagues (Jana Herrmann, Steffi Unterreitmeier, Steven Verhelst, Ellen Schneider, Eliane Küttler, Christoph Kutzner, Martin Seybold, Ute Haedke, Oliver Vosyka, Sevnur Serim, Rashmi Srivastava, Marcella Langer and more) for the fantastic atmosphere and funny moments in the lab. Special thanks go to Aline Schindler for correcting the typos in my thesis and having a good time together.

All students working with me during my PhD (Julia Leberfinger, Milena Dürrbaum, Daniel Hornburg, Christoph Kutzner and Rasmus Pröbstle) for their contributions to my work and the knowledge I gained from their questions and the many laughs we had.

And finally:

My family and my friends for their continuous encouragement and motivation and for being there when I needed them.

Johannes for giving me comfort and support in times where labwork did not give me reason for laughing and bestowing me with happy moments and strength.

Contents

Abstract

Proteolysis of transmembrane helices within lipid membranes is of great importance for regulatory processes in the cell. Also, it represents one of the major molecular causes of Alzheimer's disease (AD). Herein, the amyloid precursor protein (APP), a bitopic membrane protein, is subject to two major proteolytic events. The latter is the sequential proteolysis of the α-helical transmembrane domain (TMD) by the intramembrane γ-secretase scissoring at two possible initial ε-sites and working in a three to four residue stepwise manner giving Aβ peptides of different lengths. A general feature of γ-secretase TMD substrates are helix-destabilising residues such as Val and Ile residing near the cleavage sites. This proposes that transient local unfolding of the substrate helix is required in order to be sterically available for water and the two Asp residues representing the active site of γ-secretase. To enhance the understanding of the AD's etiology, this thesis deals with the structural characterisation of the APP TMD, particularly with its helix dynamics.

Amide deuterium/hydrogen exchange kinetics were recorded with electrospray ionisation mass spectrometry in order to probe helix dynamics of APP TMD model peptides. The N-terminal GxxxG motif harbouring dimerisation domain exchanges much faster than the C-terminal cleavage region. This means that the dimerisation domain exhibits pronounced backbone flexibility, whereas the cleavage domain has comparatively moderate hydrogen bond stabilities. Since Thr residues occurring at the initial ε- and at a γ-cleavage site stabilise the cleavage region, Thr to Val mutations enhanced backbone dynamics in this domain. The lack of additional hydrogen bonding between the Thr side chain and the fourth next amino acid's carbonyl oxygen as reported by molecular dynamics simulation studies explains this finding. Further, the Thr/Val mutated cleavage region expresses similar backbone dynamics compared to non-APP-TMDs which are hallmarked by their average amino acid composition of TMDs. To map the backbone dynamics of the C-termini of the cleaved APP TMD fragments, peptides consisting of constant oligo-Leu helix and variable octa-residue fragments of the APP TMD were tested. Results show that backbone dynamics of the free C-termini of the fragments are increased from the C-terminus towards the γ-sites.

Major conclusions are the following: The sequence defines helix dynamics, as seen for the APP TMD and non-APP-TMDs with average residue composition. General enhancers for backbone dynamics are Gly, whereas Thr causes the opposite. The Thr residue H-bonding in the APP TMD may be possibly interpreted as molecular switch

between intra- and intermolecular interaction facilitating a correct orientation relative to the enzymatic cleft. The sequential cleavage from the C-terminus towards the γ-site, once initiated, is suggested to be eased due to frayed C-termini of the substrate helix fragments.

With regard to other TMDs, the APP TMD helix backbone characterisation motivates further systematic analysis of relationships between helix dynamics and biological function, as already exemplified by intramembrane proteolysis and lipid vesicle fusion.

Zusammenfassung

Die Proteolyse von membranständigen Helices in Lipidmembranen spielt eine wichtige Rolle in den regulatorischen Prozessen einer Zelle. Zudem stellt sie eine der molekularen Hauptursachen der Alzheimer Krankheit dar. In diesem Zusammenhang erfolgen am Amyloid Vorläufer Protein (APP), ein bitopisches Membranprotein, zwei wichtige proteolytische Ereignisse. Das letztere ist die sequentielle Proteolyse der α-helikalen Transmembrandomäne (TMD) durch die intramembrane γ-Sekretase, die bei zwei möglichen ε-Schnittstellen beginnt und alle drei bis vier Aminosäurereste schneidet. Somit ergeben sich Aβ-Peptide unterschiedlicher Länge. Eine Gemeinsamkeit der γ-Sekretase-Substrate ist die Anwesenheit von Helix-destabilisierenden Seitenketten wie Val und Ile, die sich in unmittelbarer Nähe zu den Spaltstellen befinden. Daher liegt es nahe, dass eine transiente und lokale Auffaltung der Substrathelix eine Voraussetzung für die Proteolyse ist. Denn Wasser und die zwei Asp Seitenketten, die das aktive Zentrum der γ-Sekretase darstellen, müssen die zu schneidende Peptidbindung räumlich erreichen. Um einen weiterführenden Beitrag zum Verständnis der Ätiologie der Alzheimer Krankheit zu geben, beschäftigt sich diese Dissertation mit der strukturellen Charakterisierung der APP-TMD, vor allem mit seiner Helixdynamik.

Die Aufnahme von Deuterium-Wasserstoff-Austausch (DHX) - Kinetiken an Amiden mithilfe der Elektrospray-Ionisation-Massenspektrometrie war die Methode der Wahl, um die Helixdynamik von APP-TMD-Modellpeptiden zu untersuchen. In der N-terminalen GxxxG gekennzeichneten Dimerregion erfolgt der DHX sehr schnell im Vergleich zur C-terminalen Spaltregion. Dies bedeutet, dass die Dimerisierungsregion eine ausgeprägte Rückgratflexibilität aufweist, wohingegen die Spaltregion der TMD moderate Wasserstoffbrücken-Stabilitäten besaß. Thr Seitenketten, die sich einerseits in einer initialen ε- und andererseits in einer γ-Spaltstelle befinden, stabilisieren die Spaltregion. Deswegen erhöhte sich ihre Rückgratdynamik als Thr- durch Val-Seitenketten in dieser Sequenz ersetzt wurden. Das Fehlen einer zusätzlichen Wasserstoff-Brücke zwischen der Thr Seitenkette und dem Carbonylsauerstoff der viertnächsten Aminosäureeinheit laut vorangegangenen Moleküldynamiksimulationsstudien begründet dieses Ergebnis. Außerdem zeigt die Spaltregion, in der Thr/Val-Mutationen auftreten, eine ähnliche bzw. leicht erhöhte Dynamik im Vergleich zu Nichtsubstrat-TMDen, die durch ihre durchschnittliche Aminosäurezusammensetzung in TMDen gekennzeichnet sind. Um die Peptidrückgratdynamik der C-Termini verschiedener APP-TMD Spaltfragmente zu bewerten, wurden Peptide benutzt, die sich aus einem konstanten oligo-Leu-Helixteil

und einem variablen APP-TMD-Teil aus acht Aminosäuren zusammensetzen. Die Ergebnisse zeigen, dass die Rückgratdynamik der freien C-Termini der Fragmente sich mit jeder weiteren Spaltstelle vom C-Terminus zu den γ-Spaltstellen hinweg erhöhte.

Die hauptsächlichen Schlussfolgerungen sind folgende: Die Sequenz bestimmt die Peptidrückgratdynamik, wie es für die APP-TMD sowie andere TMD-Modelle beobachtet wurde. Allgemeine Verstärker der Peptidrückgratdynamik sind Gly-Reste, wohingegen Thr Seitenketten das Gegenteil verursachen. Die zusätzliche H-Brücke der Thr Seitenkette in der APP-TMD könnte so interpretiert werden, dass sie als molekularer Schalter zwischen intra- und intermolekularer Interaktion dient und somit eine korrekte Orientierung in der enzymatischen Tasche ermöglicht. Für die Spaltserie, beginnend vom C-Terminus der APP-TMD in Richtung zu den γ-Spaltstellen, wird vorgeschlagen, dass, wenn sie einmal initiiert wurde, sie durch das Ausfransen der C-Termini der gebildeten Substrathelixfragmente erleichtert wird.

In Hinsicht auf andere TMDen motiviert die Charakterisierung des Helixpeptidrückgrats der APP-TMD weitere Arbeiten, die die systematische Analyse von Beziehungen zwischen der Helixdynamik und der biologischen Funktion betreffen, wie es bereits beispielhaft für die Intramembranproteolyse und Lipidvesikelfusion gezeigt wurde.

1 Introduction

Life is based on unique architecture and its ability to change, regarding each layer - from the organism to the molecule. The smallest brick of an organism is the cell separated by a selectively permeable biological membrane from the environment. It is composed of a phospholipid bilayer with embedded proteins and separates two reaction spaces, either the cell content from the environment or two compartments within the cell. This concept helps to maintain the balance between the uptake of new building blocks and the disposal of unusable material and enables multiple reactions to occur simultaneously.

Important key players of a biological membrane are the membrane proteins. They account for at least 50% by weight relative to the lipid content [McCloskey and Poo, 1986]. One of their functions is to mediate the transport of molecules, i.e. external signals in order to respond to environmentally stimuli. Also they enable cell-cell communication. Further, they maintain the energy balance due to formation of chemical and electrical gradients across the membrane. And, they participate in intramembrane proteolysis. As a consequence, membrane proteins hold diverse and essential functions to sustain life in a cell.

This is why it does not surprise that many diseases are associated with the malfunction or altered behaviour of membrane proteins. 70% of all drug targets are membrane protein associated [Yildirim *et al.*, 2007]. Major reasons are misassembly and misfolding of membrane proteins, dysregulated membrane protein function and amyloidogenic degradation products of membrane proteins [Sanders and Myers, 2004]. The neurodegenerative Alzheimers's Disease is prevailing for the latter reason. In year 2010, about 0.8 million German people were counted to be affected according to the Deutsche Alzheimer Gesellschaft [Bickel, 2010].

Remembering that unique architecture designs each layer of life, the architecture of a membrane protein respectively its ability to be flexible determines its role. This thought is also attributable to the Alzheimer's Disease because the Amyloid Precursor Protein (APP), an integral membrane protein, is starring a major role in it. It is subject to proteolysis occurring within the membrane. Certain structural aspects such as orientation of the substrate to the enzyme, secondary structure, electron density distribution of the molecule groups, accessible cleavage sites and conformational dynamics of the substrate have an impact.

Since this work deals with the structural properties of the APP transmembrane domain

(TMD), the following introduction will face the structural features of transmembrane domains in general. This is followed by introducing the principle of methods probing the structural properties of TMDs. Finally, current knowledge on the intramembrane proteolysis in Alzheimer's Disease and its requirements will be gathered and summarized.

1.1 Structural Properties of Transmembrane Domains

1.1.1 Characteristics of Transmembrane Domains

Transmembrane domains are substantial regions of integral membrane proteins. Together with peripheral membrane proteins they belong to the class of membrane-associated proteins. They comprise between 20% and 30% of all proteins encoded in already sequenced genomes [Wallin and von Heijne, 1998].

Integral membrane proteins are classified into bitopic or polytopic membrane proteins. Bitopic membrane proteins have a single α-helical transmembrane domain, whereas polytopic proteins consists of several transmembrane segments which form either an α-helix bundle or a β-barrel within a membrane.

How many transmembrane segments (TMS) a membrane protein contains and how they are oriented across the membrane define the topology of a membrane protein. For most membrane proteins the positive inside rule helps to determine the orientation of TMSs, that means whether membrane proteins are classified into C_{in}-N_{out}, C_{in}-N_{in}, C_{out}-N_{in} or C_{out}-N_{out}. If a hydrophobic TMS region is followed by a protein subsequence enriched with positively charged amino acid residues, the probability is high that this subsequence is located in the cytoplasm [Heijne, 1986]. With this, it can be distinguished whether the C-terminus of the protein resides in the cytoplasm (in) or in the extracellular region (out) [von Heijne, 2006]. In addition, there exist membrane proteins with undefined orientation. To name a few reasons, TMSs do not insert completely into the membrane or introduction of the nascent polypeptide into the membrane by the translocon machinery occurs in both orientations. A full description of exceptions is enlisted in the review of von Heijne [2006].

In the following the focus will be on α-helical transmembrane segments as they are present both in bitopic and α-helix bundle membrane proteins and subject to this thesis.

The hydrophobic amino acid residues Ala, Ile, Leu and Val constitute 45% of TMS residues, together with Gly and Phe it is 63% [Ulmschneider *et al.*, 2005]. As the peptide backbone is polar and water is absent in a membrane, intramolecular hydrogen bonds between backbone atoms are stable. Consequently, a helical conformation of the polypeptide is ideal. Since the hydrophobic residues of the TMS point towards the lipid-tails of the lipid bilayer, the polar backbone is hidden from the apolar environment. Due to a hydrophobicity gradient across the membrane, there is a certain residue distribution dependent on the position in the membrane. Aliphatic residues and Phe

reside in the TMS centre, whereas Trp and Tyr prefer to be in the flanking regions residing between the lipid tail and the lipid head group region. This is supported by calculating the statistical free energies of membrane insertion using a set of 46 high-resolution X-ray structures [Ulmschneider *et al.*, 2005]. Charged or polar residues occur up to 5% [Ulmschneider *et al.*, 2005]. Arkin and Brunger [1998] distinguish between bitopic and polytopic membrane proteins. They found that polar residues have a higher frequency in polytopic membrane proteins which can be explained with the shielding of polar residues inside the helix-bundle.

The length of a TMS is about 20 to 30 amino acids (aa) with an average of 26.3 ± 5.6 aa and 33.7 Å ± 18.2 Å, respectively [Ulmschneider *et al.*, 2005]. Such a helix fits into the hydrophobic core of the lipid bilayer with an average thickness of 30 Å. To avoid the hydrophilic lipid head group region (each 15 Å thick) TMSs tilt away from the membrane normal, in average 24 ± 14° [Ulmschneider *et al.*, 2005]. This may result from hydrophobic mismatch, if the TMS is longer or the hydrophobic thickness is shorter (called positive mismatch) [de Planque and Killian, 2003]. A negative hydrophobic mismatch results from the reversed scenario.

Transmembrane helices are also known to interact with each other. They can pack via the knobs-into-hole principle, which means residues of one helix fit into the space between residues of the opposite helix [von Heijne, 2006]. Also, small residues such as Ser, Ala or Gly allow helices to be in close contact. The GxxxG motif is a prominent pattern to mediate helix-helix-interaction [Senes *et al.*, 2004, 2000]. Electrostatic interactions are also found between polar and/or ionizable side chains of two transmembrane helix monomers [Herrmann *et al.*, 2010].

Eilers and colleagues characterised TMSs of 11 membrane proteins in terms of packing. Comparing helices in soluble proteins and those of the investigated membrane proteins, they discovered that TMS helices are packed tighter on average. Reasons for that are the small residues of Gly and Ala and the hydroxyl-containing side chains of Ser and Thr. The latter residues are argued to form hydrogen bonds with the helix backbone at residues at $i - 3{,}4$ positions [Baker and Hubbard, 1984, Ballesteros *et al.*, 2000, Eilers *et al.*, 2000, Gray and Matthews, 1984]. The packing theory of Eilers was complemented by the work of Hildebrand *et al.* [2005]. They discovered that transporter and channel membrane proteins are more loosely packed than soluble proteins. Therefore, it is proposed that some membrane protein regions should have deficiencies in packing in order to fulfil their function.

1.1.2 The Peptide Bond and the Hydrogen Bond

To understand what determines a polypeptide and which basics contribute to helix folding and dynamics, an introduction into the nature of a peptide bond and a hydrogen bond is given.

The peptide bond is formed when two amino acids condense with the expulsion of a water molecule. Its atom group consists of the carbon and oxygen atom from the former carboxyl group delivered by the first amino acid and the nitrogen and hydrogen atom of the former amino group provided by the second amino acid. Together with the α-carbon atoms of both amino acids, the six atoms form a plane (demarcated in Figure 1.1).

The stabilisation by resonance structures due to hydroxylimine-amide tautomerism explains the planarity. The bond between the carbonyl carbon and the nitrogen cannot rotate any more freely because the double bond character accounts to 40% resonance [Sigel and Martin, 1982]. Consequently, the tautomerism of the amide bond results in a dipole moment of around 3.5 Debye [Creighton, 1993]. The partial charges δ^+ and δ^- are depicted in Figure 1.1. The peptide bond favours the *trans*-position over the *cis*-form because the rotation of the lone electron pair of the nitrogen is restricted due to the amide planarity and the chain tails favour opposite directions due to steric hindrance.

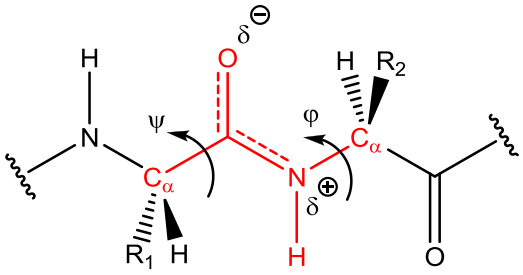

Figure 1.1: Geometry of the peptide backbone with a *trans*-peptide bond.

The planes, which can be described as quadrilaterals with the carbon, oxygen and hydrogen atoms as vertices, are connected by the vertices represented by the α-carbon atoms. Thus, a chain of connected amide bond planes builds the peptide backbone.

The bonds between the α-carbon and the carbonyl carbon (C_α-C) and between the nitrogen and α-carbon (C_α-N) are able to rotate freely, thus the planes face each other at certain angles. These are the torsion angles Ψ (N-C_α-C-N) and Φ (C-N-C_α-C) (see Figure 1.1). The free rotation of the C_α-C and the C_α-N is limited by the interactions of the atoms among each other and steric influences by the amino acid residues. Hence, the polypeptide accommodates certain Φ and Ψ angle ranges.

Because the amide bond is both a hydrogen bond donor and acceptor, a polypeptide is able to adapt to regular structure patterns, such as α-helices or β-sheets. A hydrogen bond is a short-ranged interaction between $X - H \cdots A$, in other words it is a local bond and $X - H$ acts as a hydrogen donor towards the electronegative partner A. The hydrogen is bound itself to an electronegative partner, called here X. In case of regular secondary structures in peptides and proteins, backbone H-bonds exist between the electronegative carbonyl oxygen (H-bond acceptor) and the amide hydrogen bound to

the electronegative nitrogen (H-bond donor). Beside this H-bond type, X and A do not have to be extremely electronegative, the C_α-atom and the π-system of an aromatic side chain are also possible [Steiner, 2002, Weiss *et al.*, 2001]. Indeed, $C_\alpha - H \cdots O$- and $C_\alpha - H \cdots \pi$-interactions have been identified in polypeptides [Bella and Berman, 1996, Brandl *et al.*, 2001].

The strength of a hydrogen bond ranks between the strength of a covalent/ionic bond and that of a non-covalent van-der Waals interaction. Ben-Tal and colleagues determined the energy of an amide hydrogen bond between N-methylacetamide dimers to be in vacuum 28 kJ/mole [Ben-Tal *et al.*, 1997]. As a general rule in solvent, the dissociation energy accounts for approximately 8-42 kJ/mole [Creighton, 1993]. The interaction length ranges between 1.65-2.63 Å for $N - H \cdots O$ hydrogen bonds according to electron density studies from neutron or X-ray diffraction data [Espinosa *et al.*, 1998]. The donor and the acceptor engage in a certain angle to each other ($\angle\ X - H \cdots A$). Ideal angles in intramolecular hydrogen bonds in helices are approximately 180° [Baker and Hubbard, 1984, Kim and Cross, 2002]. Also, a hydrogen donor is able to share its hydrogen to several acceptors which are the so called bifurcated or trifurcated hydrogen bonds [Steiner, 2002].

The total energy of a hydrogen bond can be dissected into contributions from electrostatics, polarisation, charge transfer, dispersion and exchange repulsion. Often the last two mentioned contributions are combined to the "van der Waals"-term which is described as a Lenard-Jones Potential. For each hydrogen bond type, contributions have different extents [Morokuma, 1977]. The $N - H \cdots O$ H-bond is dominated by electrostatic and charge-transfer energy, which applies for a hard acid-hard base pair using the Pearson's hard/soft-acid/base (HSAB)-concept. Contrariwise, a $C_\alpha - H \cdots \pi$-interactions is driven by dispersion and polarization energies, equivalent to a soft acid-soft base pair [Hobza and Havlas, 2000, Pearson, 1963, Weiss *et al.*, 2001].

Further properties of hydrogen bonds are the ability to alter the geometry of covalent bonds, for instance it is able to stretch or compress the $X - H$ bond [Steiner *et al.*, 2002]. Additionally, in α-helices intramolecular hydrogen bonds are enforced due to π-binding cooperativeness. The N-H groups are polarised via the charge flow of π-bonds which is represented by the carbonyl of the amide bond. This is of course again reasoned by its zwitterionic resonance form [Steiner, 2002].

Hydrogen bonds can be also reduced in their free energy. It can be influenced by the surrounding geometry and/or can be decreased due to the entropic cost when the donor and the acceptor adopt a fixed position. Solvent polarizability reduces also hydrogen bond strength when it is dominated by electrostatic contributions [Bowie, 2011]. Solvent will act also as a competitor if it is able to form hydrogen bonds, i.e. water interacts with the amide bond thus destabilising secondary structure [Fersht *et al.*, 1985].

In transmembrane domains, backbone hydrogen bonds are more stable than in water soluble isolated helices. As the lipid bilayer lacks water and has a low dielectric

constant ($\varepsilon(H_2O)$=80; ε(membrane core)=2), it is devoid of potential hydrogen bond donors/acceptors [Dilger *et al.*, 1982, Hildebrand *et al.*, 2004]. The length of backbone hydrogen bonds is shorter in TMS and they occur on more regular basis than backbone hydrogen bonds in globular proteins. Also, backbone hydrogen bonds in TMS can bifurcate, i.e. having two hydrogen bond acceptors. These are interactions in the $i, i-3$ and $i, i-4$ manner resulting in a 3_{10}- and α-helix respectively [Hildebrand *et al.*, 2004]. Side chain hydrogen bonds between TM helices tend to have similar strengths in membranes compared to side chain hydrogen bonds in water soluble proteins [Bowie, 2011].

1.1.3 Secondary Structure of Transmembrane Domains

In addition to β-barrel shaped membrane proteins, transmembrane domains can adopt α-helical conformations. These are part of either bitopic membrane proteins or polytopic ones which form α-helical bundles. In globular and membrane proteins it is the most frequent conformation beside β-sheets, β-turns and random coiled structures [Bigelow *et al.*, 2004, Bowie, 2005, Creighton, 1993]. Advantages are the decrease in energy cost of burying the polar backbone from the surrounding lipids, the parallel aligning of the helix to the membrane normal to avoid disruption of the lipid packing and favourable van der Waals interactions between the apolar side chains and the hydrocarbons of the lipid [Deber and Li, 1995, Jennings, 1989, Unwin and Henderson, 1984].

Helices are right-handed screws stabilised by hydrogen bonds within the polypeptide chain. Hydrogen bonds between the amide hydrogen of amino acid i and the carbonyl oxygen of the forth next amino acid $(i-4)$ in sequence characterise the α-helix. One turn comprises 3.6 amino acid residues, in which one residue is translated by 1.5 Å along the helical axis and turned by 100° towards its neighbour residue. The resulting pitch of a turn is 5.4 Å [Richardson, 1981]. The torsion angles for a classical α-helix formation found in proteins are for Φ -62° and for Ψ -41° [Barlow and Thornton, 1988]. The peptide backbone is in the centre and the residues protrude outward from the helical backbone and point into the opposite direction to the helix direction (helix direction: from N- to C-terminus). As a result of the geometrical properties, the helix represents a tightly packed formation. Because the residues of a TMD face the hydrophobic lipid tail region of the membrane, they are mostly of a hydrophobic nature.

Attributed to the residue alignment, steric consequences for the conformation evolve. Two residues which have one neighbour in between point into opposite directions, whereas residues i, $i-3$, $i-4$ and $i-7$ are aligned horizontally being thus in close proximity and affecting helix stability [Doig *et al.*, 2005]. Therefore, only a selection of residues will account for helix formation and stabilisation. These are for example Ala, Leu, Met and Glu for globular proteins. Helix destabilising residues are Gly, Pro, Tyr and Ser [Levitt and Greer, 1977]. These propensities were concluded from statistical

analysis of residues occurring in a certain secondary structure type based on known three-dimensional protein structures [Chou and Fasman, 1974]. In a study for α-helical propensities of amino acids in n-butanol mimicking the membrane environment Leu, Phe and the β-branched amino acids Val and Ile were identified to be helix-stabilising [Liu and Deber, 1998]. The physicochemical properties for stabilising/destabilising a helix will be discussed further in section 1.1.4 (p. 11).

Another important property of an α-helix is its dipole character. Due to the dipole moment of the amide bond and its extension along the backbone by its hydrogen bonds, the helix has a total dipole moment with a positive N-terminus and a negative C-terminus [Hol *et al.*, 1978]. The three amide hydrogens at the N-terminus and the three carbonyl oxygens at the C-terminus cannot participate in intramolecular hydrogen bonding because there are no available bonding partners due to the end of the chain. Therefore the positive and negative partial charges on the N- and the C-terminus are localised and enforce the dipole character of the helix. The 50% H-bond saturation at the termini leads to local destabilisations of a helix which is called fraying. In globular proteins, side chains of opposite partial charges are often found at the termini and can therefore stabilise them [Bryson *et al.*, 1995]. In membrane proteins, polarizable and charged residues are often found in the TMD region facing the lipid/ water phase and differ in amount between TMDs of bitopic and polytopic membrane proteins [Arkin and Brunger, 1998, Ulmschneider *et al.*, 2005]. These residues can interact with the polar lipid head groups. Though a stabilisation effect on the helix termini by this would be case dependent. The helix termini are rather stabilised by the lipid bilayer packing surrounding the helix and thus reducing its fraying compared to helices in globular proteins.

Beside the α-helix, there exist also π- and 3_{10}-helices. Hydrogen bonds are formed between the amino acids i and $(i-5)$ for π- or $(i-3)$ for 3_{10}-helices [Richardson, 1981].

1.1.4 Conformational Stability and Dynamics of Transmembrane Helices

The conformational stability of peptides and proteins is expressed as the change in free energy ΔG° for folding under physiological conditions [Pace, 1990]. This principle applies for helix-random coiled transition of TMS, as well (see equations 1.1 and 1.2).

$$\alpha - Helix \underset{k_{fold}}{\overset{k_{unfold}}{\rightleftharpoons}} Random\ Coil \tag{1.1}$$

$$\Delta G^\circ = -RT\ lnK_{fold} \quad with \quad K_{fold} = \frac{k_{fold}}{k_{unfold}} \tag{1.2}$$

k_{fold} ...rate constant of folding
k_{unfold} ...rate constant of unfolding
K_{fold} ...equilibrium constant of folding

The thermodynamic equilibrium of the folding/unfolding process is described as the ratio of the unfolded to folded species concentrations or of its rate constants k_{unfold} to k_{fold} and gives information about the stability of the structure. The free energy of helix stability is described by its enthalpic and entropic contributions.

$$\Delta G^\circ = \Delta H^\circ - T\Delta S^\circ \tag{1.3}$$

TM helix stabilisation is driven by hydrogen bond formation, by van der Waals interactions between side chain atoms and with the backbone, packing of side chains and entropy loss caused by side chain rotation restriction, respectively [Langosch and Arkin, 2009, Scholtz *et al.*, 1991, Yang and Honig, 1995]. For soluble helices and TM helices at the polar region of lipid bilayers, stabilisation is driven in addition by the hydrophobic effect (burying the hydrophobic surface upon folding) [Deber and Li, 1995].

The hydrogen bond formation in the $i, i-4$ manner results in a favourable enthalpy for helix formation [Scholtz *et al.*, 1991]. In section 1.1.2 (p. 9) it has been already mentioned that the extension of a helix contributes positively to the helix stability since the hydrogen bond strength is increased by the elongation of the π-binding cooperativeness. Though the entropic loss caused by limited combinations of torsion angles Φ and Ψ destabilises a helix, the enthalpy contribution is large enough to compensate it. The rotational freedom of side chains contributes to the conformational entropy [Creamer and Rose, 1994]. In fact, it results in the differences of free energy for helix stability. The side chain rotamer distributions vary in different backbone conformations and thus contribute to the intrinsic helical propensity of a residue [Creamer and Rose, 1995].

The examples Gly and Ala shall demonstrate the contrast in favourising a conformation as their residues differ in one methyl group. A Gly rich peptide engages in random coil structure [Hermans *et al.*, 1992]. This results from the entropic gain of rotational freedom of the dihedral angles Φ and Ψ. It outweighs the enthalpy contribution of hydrogen bonding. Furthermore, the absence of a C_β-carbon atom in Gly reduces the enthalpic contribution for helix formation. The non-polar interaction between C_β and the helix backbone is known to stabilise the helix [Blaber *et al.*, 1993, Go *et al.*, 1968, Luque *et al.*, 1996, Yang and Honig, 1995]. In contrast, a polyAla peptide favours the α-helix because the enthalpy contribution outvotes the entropic one [Hermans *et al.*, 1992]. Because of the presence of the methyl group in Ala, the dihedral angles Φ and Ψ are similarly constrained in the helix state compared to the coil state. Therefore the entropic loss upon helix folding is reduced [Hermans *et al.*, 1992, Luque *et al.*, 1996].

The enthalpy gain is realised by the interaction of the C_β-carbon atom of Ala with the backbone which is helix stabilising [Hermans *et al.*, 1992, Yang and Honig, 1995].

Extending the side chain beyond the C_β-carbon atom will result in side chain entropy loss upon folding. Creamer and Rose have established a ranking based on the entropy loss determined by the side chain rotamer distributions: Ala < Leu < Trp < Met < < Phe < Ile < Tyr < Val [1992]. This supports the statistical propensities that Leu acts as a strong helix-builder, both in globular and membrane proteins. The β-branched amino acid residues Val, Ile and Thr are known to be helix-breaking in globular proteins. By contrast, in TMS Val and Ile are discussed to be helix-promoting due to their hydrophobicity. The saturation of the polar backbone by H bonds is thus strong that the side chains having contact with the hydrophobic lipids should be themselves of hydrophobic nature [Liu and Deber, 1998]. Still, Val and Ile will increase its dynamics [Langosch and Arkin, 2009]. The reason for the destabilising properties is their constrained rotational movements in a helical conformation. In detail, for Val,

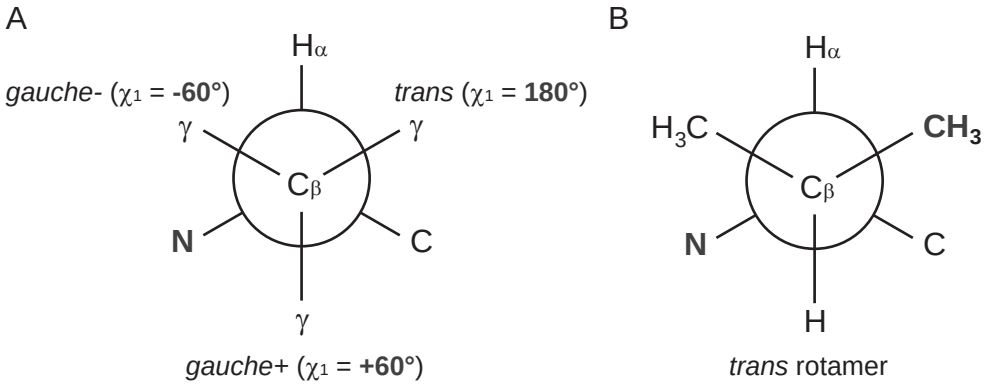

Figure 1.2: Newman Projection of peptide backbone with side chain γ positions in the staggered form. A: Nomenclature of rotamer conformation positions. The dihedral angle χ_1 describes the alignment between the amide nitrogen and the C_γ-carbon atom; B: *trans*-Rotamer of Val. χ_1-assignment is based on the right-hand branch of C_β. Scheme is based on references from [Dunbrack and Karplus, 1994, Hansen and Kay, 2011, Lovell *et al.*, 2000].

Ile and Thr there are three possible rotations in the staggered form of the Newman projection having the C_α-C_β-carbon bond as the rotational centre: *gauche+*, *gauche-* and *trans* rotamers. In helices only the *trans* rotamer for Val and Ile is possible (see Figure 1.2). Two out of three motions are hindered due to sterical reasons. Thus, the conformational entropic cost of helix formation increases. Branching at the C_γ-carbon atom such as in Leu does not constrain the rotation to such an extent. For Leu the *trans* and *gauche-* C_β-rotamers are favourable in helices [Dunbrack and Karplus, 1994, Quint *et al.*, 2010, Renfrew *et al.*, 2008]. Being able to engage in one additional rotameric state explains Leu to be a good helix former.

Thr as the third β-branched residue will occupy mostly *gauche-* rotamers in helices both in soluble and membrane proteins (hydroxyl group in *gauche-* and methyl group in *trans* position as C_β is a R stereo centre in the L-amino acid) [Chamberlain and Bowie,

2004]. In this side chain rotamer position hydrogen bonding of the hydroxyl-group of Thr to the next helix turn is possible supporting helicity and putting Thr in an exceptional position in face of limited rotamer possibilities.

Pro is not able to participate in hydrogen bonding because its amide function is tertiary in peptides. Also the ring confines the torsion of the peptide bond so that a Pro containing helix is destabilised and kinks. Yet, Pro is sometimes beneficial in terms of TMS orientation. It induces high flexibility and can change the orientation of a helix to other interacting TMS partners which is important for the fulfillment of biological functions [Cordes *et al.*, 2002].

Beside intrinsic side chain properties, the solvent environment has a great impact on helix formation and stability [Deber and Li, 1995]. As mentioned in section 1.1.2 earlier, water destabilises intramolecular polypeptide hydrogen bonds when they are mainly contributed by electrostatic interaction. In other words, the dipoles of clustered water weaken the dipole of the amide bond and soften polarisation. Hence, this decreases hydrogen bond strength. But foremost, water acts as a hydrogen bond competitor [Bowie, 2011]. Therefore, transmembrane helices in lipid bilayers have an advantage as the acyl chains of the phospholipids lack hydrogen bond partners.

An ideal solvent for solubilising hydrophobic helices should have a low polarity and concomitant a low dielectric constant [Deber and Li, 1995]. Such a solvent excludes competing H-bond partners and thereby enforces local intramolecular electrostatic interactions such as H-bonds [Buck, 1998, Thomas and Dill, 1993].

In order to study TMD structures, alcohols and halogenated alcohols are used as alternative for model membranes. Deber and Li discovered that increasing the chain length of the alkanol from methanol to propanol, helicity of Ala based host guest TMDs was increased [1995]. This effect even masked the intrinsic helix propensity of the guest residue in the synthetic TMD as no differences in their circular dichroism were observed. Major reason for this helix formation is the strengthening of intramolecular H-bonds [Arvinte and Drake, 1993, Deber and Li, 1995, Muga *et al.*, 1994].

Halogenated alcohols such as trifluoroethanol (TFE) were found to be best in mimicking the membrane. TFE for instance has a dielectric constant of ε=26.14 [Eckstrom *et al.*, 1960, Tanaka *et al.*, 2000]. Therefore TFE is often used as a cosolvent with water to study transmembrane helices. A systematic analysis by Hirota *et al.* of each molecule group in the halogenated alcohol was performed revealing that the hydrocarbon chain length respectively branching, the halogen substitution and the alcohol function contribute in an additive manner to the α-helix formation: The length and bulkiness of the hydrocarbons contributed positively to helix formation. So did the halogens in the following order: F<Cl<Br. The number of halogens was proportional to the effectiveness of helicity. The alcohol function though had a negative effect due to its polarity [Hirota *et al.*, 1998]. Further, halogenols form micelle-like structures as it is common for alcohol/water mixtures which enclose the polypeptide as clathrate structures and hinder water to form H-bonds [Gast *et al.*, 1999, Hirota *et al.*, 1997, Hong *et al.*, 1999, Kuprin *et al.*, 1995]. TFE and hexafluoroisopropanol (HFIP) clusters were seen from 0 to 80% (v/v) with an average size of 5 to 10 Å and at 30% (v/v) with 14 Å as the greatest diameter measured with X-ray and/ or dynamic light scattering [Hong

et al., 1999, Reiersen and Rees, 2000]. Further TFE titration experiments of H-bond capable *o*-hydroxybenzoic acid (salicylic acid) and non-H-bond capable *p*-hydroxybenzoic acid showed that with increasing TFE concentration the strength of hydrogen bonds increased [Luo and Baldwin, 1997]. Mechanistically, the TFE micelles surrounding the peptide produce a hydrophobic micro environment. As a result the local and bulk concentration of TFE deviate from each other. Analysis of a MD simulation on the helical melittin at a bulk concentration of 30% (v/v) revealed a local TFE concentration of 80% (v/v). Thus, giving a 2.5 fold increase and resulting in a local low polarity despite the bulk environment [Roccatano *et al.*, 2002]. The dielectric constant of an 80% (v/v) TFE-water mixture is between 33.56 and 39.98 [Gente and La Mesa, 2000]. Since the dielectric constant of the environment is low and TFE with its hydroxyl group represents a good H-bond donor but a "poorer H-bond acceptor compared to water" [Buck, 1998], the peptide backbone prefers to form intramolecular hydrogen bonds to satisfy both carbonyl oxygens and amide hydrogens [Llinas and Klein, 1975, Roccatano *et al.*, 2002, Shiraki *et al.*, 1995]. Hence, a random coil structure is destabilised by TFE micelles [Storrs *et al.*, 1992]. As hydrophobic TFE-peptide interactions are weak, hydrohobic interactions within the peptide are not affected [Roccatano *et al.*, 2002]. So far the mentioned arguments apply also to non-halogenated alcohols. What gives the difference is the negative inductive effect of the fluorine atoms of TFE respectively HFIP. They pull the electron density of the hydroxyl oxygen towards the hydrocarbon chain making the hydroxyl group more acidic (pK_a[TFE]=12.4, pK_a[EtOH]=15.9, pK_a[H_2O]=15.7) [Brown *et al.*, 2010]. In turn, a better self-association between TFE molecules occurs, whereas ethanol molecules have a weaker H-bond network among the hydroxyl groups and prefer to interact with the competing water molecules. This is the reason why micelle-like structures among TFE molecules are better stabilised. An additional specific interaction between trifluoromethyl groups and hydrophobic side chains of the peptide is not given as they were not detected via NMR studies and in general only weak affinities to the polypeptide chain are discussed [Buck, 1998, Storrs *et al.*, 1992]. Another reason why TFE is a suitable cosolvent for studying intrinsic dynamics properties of TMDs. TFE and its colleagues are also known for stabilising β-sheets, β-turns and β-hairpins. A good review is written by Buck [1998].

Other additives to enhance TMD solubility and helix stabilisation are detergents forming micelles such as SDS [Zhong and Johnson, 1992].

When speaking about helix stability described by the equilibrium between unfolded and folded, respectively random coil and α-helix, and its causes of destabilisation, helix dynamics need to be considered, as well. The transmembrane domain as a secondary structure element is able to move within its constraints by the lipid bilayer, other surrounding TM helices and its polypeptide extensions both at the N- and C-termini, called also rigid body motions [Langosch and Arkin, 2009]. This is important for light activation of rhodopsin and angiotensin II type-1 receptor activation for example [Farrens *et al.*, 1996, Miura *et al.*, 2003]. Timescales of such motions lie in nanoseconds [Henzler-Wildman and Kern, 2007]. Going further into detail, fluctuations along the TM helix such as bending at hinge regions, caused by Pro, or side-chain rotations lie within picoseconds to nanoseconds [Cordes *et al.*, 2002, Henzler-Wildman and Kern, 2007, Mukherjee *et al.*, 2006]. Vibrational motions like stretching and twisting of

bonds have frequencies in femtoseconds [Henzler-Wildman and Kern, 2007]. As a result of all mentioned motions, transient hydrogen bond opening and closing events occur which enhance helix dynamics [Langosch and Arkin, 2009, Poschner *et al.*, 2009, Quint *et al.*, 2010]. SNARE mediated vesicle fusion is one of the examples where TM helix dynamics is related to function [Langosch *et al.*, 2001]. Also in membrane proteolysis, dynamics is a requirement for Rhomboid substrates [Urban and Freeman, 2003].

To study the dynamics of TM helices the combination of circular dichroism and hydrogen deuterium exchange experiments as these are applied in this thesis are appropiate and meaningful methods. Their principles are further introduced in sections 1.2.1 (p. 16) and 1.2.2 (p. 18). Also molecular dynamic simulations increase the understanding of helix dynamics [Quint *et al.*, 2010].

1.2 Measuring the Structural Properties of TM Helices

In this section the principles of the measurement methods for secondary structure analysis (section 1.2.1, page 16) and helix dynamics (section 1.2.2, p. 18) are explained. It shall give an understanding how the principles of the applied techniques are connected to the structural properties of the peptides.

1.2.1 Circular Dichroism

Circular dichroism (CD) spectroscopy is used to determine the secondary structure of peptides and proteins in a rapid manner. Because polypeptides possess stereo centres, they can absorb differently strongly left and right circularly polarised light (equation 1.4) [Woody, 1995]. This leads to dual chromaticity justifying the name dichroism.

$$\Delta\varepsilon = \varepsilon_L - \varepsilon_R \text{ ; with } \varepsilon_L \neq \varepsilon_R \tag{1.4}$$

ε_L ...extinction coefficient of left circularly polarised light
ε_R ...extinction coefficient of right circularly polarised light

The chromophores of polypetides are the peptide bonds and aromatic side chains. The amide bond has a stronger absorbance than aromatic side chains in the far ultraviolet (UV) spectral region (180-250 nm). The characteristic electronic transitions for the peptide bond are the π-π^* at 190 nm and n-π^* transitions at 210-220 nm with molar extinction coefficients 7000 M^{-1} cm^{-1} and 100 M^{-1} cm^{-1} respectively. The involved electrons belong to the molecular orbital π of the carbonyl oxygen and carbonyl carbon atom and to the non-binding molecular orbital n contributed by the carbonyl oxygen atom [Johnson, 1985]. The energy of incident light has to exceed a certain value ΔE to elevate the electrons from the ground to the excited state because these are discrete energy states (see equation 1.5 with h as Planck's constant and ν as frequency) [Snatzke, 1981].

$$\Delta E = h \cdot \nu \tag{1.5}$$

When the freely moving π and n electrons interact with the incident electromagnetic wave, they are shifted in two ways. Electrons are excited and occupy another molecular orbital, thus a temporary deficit in negative charge of the abandoned molecular orbital and a temporary excess in negative charge of the newly occupied molecular orbital occur. The balance points of "positive" and negative charge do not coincide anymore. An electric transition dipole moment $\vec{\mu}$ arises which is prerequisite for light absorption. Yet, this will happen only, when the electric field strength $\vec{E}$ of incident light has the same polarisation direction. If the electromagnetic wave has another polarisation direction, the interaction will be weaker and the extent of absorption will become smaller. In mathematical terms, the strength of light absorption is proportional to the square of $\vec{\mu}$. Once electrons have stabilised in their new orbital, $\vec{\mu}$ vanishes [Snatzke, 1981].

The other way to interact with incident light is a shift in which the movement of electrons becomes circular. With the electron movement from one to the other molecular orbital, the charge rotates and like in a circular current, it induces temporarily a magnetic dipole moment, the magnetic transition dipole moment $\vec{m}$. The scalar product of both transition dipole moments $\vec{\mu}$ and $\vec{m}$ define the rotation strength R. This describes the extent of rotating the polarisation plane, the so called ellipticity [Snatzke, 1981].

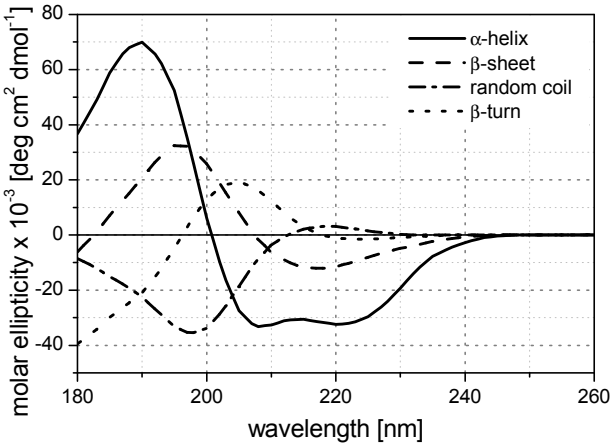

Figure 1.3: Circular dichroism spectra of single secondary structure elements.

So how is CD light used to determine the secondary structure of proteins and peptides? The C_α-atom and the carbonyl carbon atom of the peptide bond constitute chiral centers. Though the C_α-atoms are not directly responsible for CD light absorption because all their electrons are involved in sp^3-bonds, the C_α-atoms and their connected side chains are part of the conformation of the molecule. In other words, the secondary structure describing dihedral angles Φ and Ψ define the direct electronic environment of the π and n orbitals of the peptide bond and change the energy of incident light taken up by the electrons to get to their excited states [Johnson, 1985, Snatzke, 1981].

The resulting CD spectrum of a polypeptide is a linear combination of single CD spectra for each secondary structure type, namely the α-helix, β-sheet, β-turn and random coil [Sreerama and Woody, 1994]. Their corresponding CD-spectra are depicted in Figure 1.3. Different approaches treat CD spectra of polypeptides with mixed secondary structures. The most prominent one is the singular value decomposition applied on a set of CD spectra taken

from known three-dimensional structures. With this, a reconstruction of secondary structure contents is made from a CD spectrum of a polypeptide with unknown structure [Compton and Johnson, 1986, Greenfield, 2007, Park *et al.*, 1992, Whitmore and Wallace, 2008].

1.2.2 Probing Helix Dynamics with Hydrogen Deuterium Exchange

Since amide hydrogens of the peptide backbone participate in hydrogen bond formation, they are sensitive probes for the structural stability of α-helical peptides. Hence, the kinetics of deuterium hydrogen exchange is suitable to measure its structural stability.

Peptide hydrogens which take part in polar covalent bonds with oxygen, nitrogen or sulphur are competent in exchange with protons from the bulk solvent. This accounts for positions at the terminal amino and carboxyl groups, at polar side chains and amide hydrogens of the peptide backbone. Hydrogens bound to carbon atoms will not exchange [Englander and Kallenbach, 1984].

The underlying principle of the hydrogen exchange is a proton transfer [Eigen, 1964]. The following example shall illustrate this. The proton is transferred from the proton donor PepH to a proton acceptor via an hydrogen bridged complex resulting in a new donor-acceptor pair (equation 1.6). To complete exchange, the resulting proton acceptor Pep^- receives a proton from another proton donor (equation 1.7). In case of the peptide the initial proton donor is the peptide PepH and the initial proton acceptor a solvent molecule, e.g. a hydroxide ion. The formation of a hydrogen bridged complex between a proton donor and acceptor is controlled by diffusional collisions. Once it is formed, it dissociates immediately via equilibration.

$$PepH + OH^- \rightleftharpoons (PepH...OH^- \rightleftharpoons Pep^-...H_2O) \rightleftharpoons Pep^- + H_2O \tag{1.6}$$

$$Pep^- + H_2O \rightleftharpoons (Pep^-...H_2O \rightleftharpoons PepH...OH^-) \rightleftharpoons PepH + OH^- \tag{1.7}$$

The hydrogen exchange reaction is either base- or acid-catalysed. The mechanism for amide hydrogens is based on the ampholytic character of the peptide bond (see Figure 1.4). In base-catalysis the hydroxide ion abstracts a proton from the amide. Thus, the peptide bond is converted to an imidate anion which is subsequently reprotonated while abstracting a deuteron from deuterium oxide. Acid catalysis begins either with N- or O-protonation. Going for N-protonation, the deuterated amide function is again deprotonated and the peptide bond is re-established. In contrast, O-protonation begins with the protonation of the carbonyl oxygen and acidifies the amide hydrogen. This allows the abstraction by a water molecule. An imidic acid intermediate is formed and is reversed to an amide taking up a deuteron from a deuterated hydronium-ion. The O-protonation is favoured over the N-protonation because the carbonyl-oxygen is more basic than the nitrogen (pK_a= 0 respectively = -7) [Brier and Engen, 2008, Fersht, 1971].

Hydrogens bound to side chains and the peptide termini exchange faster than the amide hydrogens due to their lower pK_a values. The pK_a for side chains is below 13 and for OH^- protonation at 15.7 which means proton transfer is facilitated from a stronger to a weaker acid

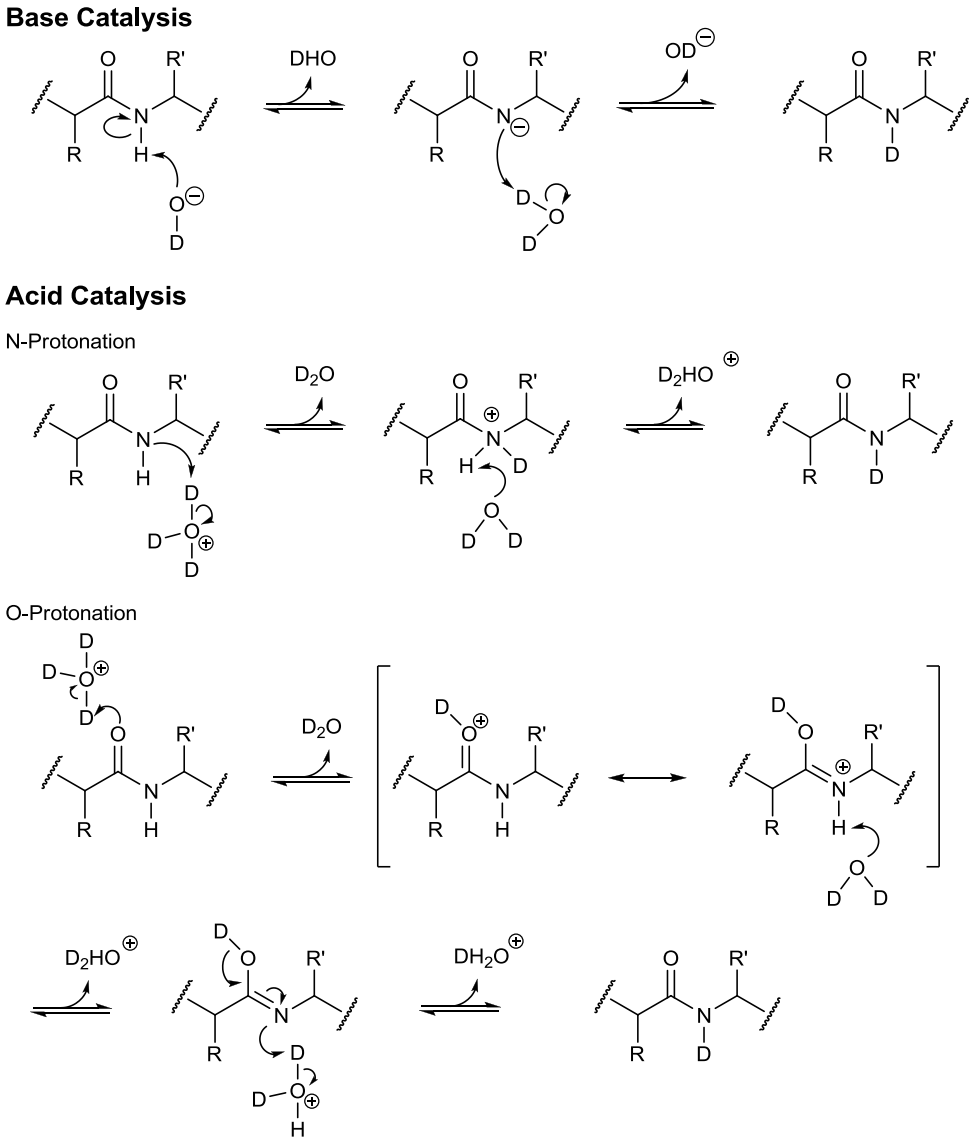

Figure 1.4: Mechanism of backbone amide hydrogen deuterium exchange. Scheme is adapted from [Brier and Engen, 2008] and based on [Perrin, 1989].

[Englander, 2006, Englander *et al.*, 1972]. Hence, the exchange rates are dominated mainly by diffusion-limited collision [Brier and Engen, 2008]. Amide hydrogens have a pK_a value at 18.5 therefore exchange occurs more slowly [Eriksson *et al.*, 1995, Molday and Kallen, 1972]. Consequently, the measured exchange encompasses the exchange of amide hydrogens.

As introduced in section 1.1.4 (page 11) the conformational stability of a peptide or a protein is described as the change in free energy between the folded and the unfolded conformation under physiological conditions [Pace, 1990]. In the case of an α-helical peptide, the stability of hydrogen bonds reflects the stability of the helical backbone. Since amide hydrogens participate in these H-bonds, hydrogen deuterium exchange probes the conformational stability respectively dynamics of an α-helix.

$$NH_{cl} \underset{k_{cl}}{\overset{k_{op}}{\rightleftharpoons}} NH_{op} \xrightarrow{k_{ch}} ND_{op} \underset{k_{op}}{\overset{k_{cl}}{\rightleftharpoons}} ND_{cl} \tag{1.8}$$

The intramolecular hydrogen bond in which an amide hydrogen NH_{cl} is involved opens and frees the amide hydrogen NH_{op} to be then competent for exchange for a deuteron from the solvent. The hydrogen bond closes and the amide deuteron is the new H-bond-donor ND_{cl}. All reactions are reversible. Because deuterated solvent is in excess, the exchange reaction itself is forwarded to one direction. The rate constants k_{op} for the opening process, k_{cl} for the closing process and the chemical exchange rate k_{ch} describe the reaction sequence known also as Linderstrøm-Lang model (equation 1.8) [Dempsey, 2001].

Since the exchange rate of an unprotected amide hydrogen is defined by the proton transfer reaction along a hydrogen bridge to the proton-acceptor and can be only catalysed by a strong acid (H_3O^+) or a strong base (OH^-), the chemical exchange rate depends on the pH value. The overall exchange rate is then the chemical exchange rate k_{ch} which is defined by equation 1.9 [Woodward and Hilton, 1980]. Contributions from acid-, base- and water-catalysis account for it.

$$k_{ch} = k_{H_3O^+}[H_3O^+] + k_{OH^-}[OH^-] + k_{H_2O} \tag{1.9}$$

Considering the peptide in the folded state, the overall exchange rate for an amide hydrogen is defined as the fraction of the product of the forward reactions and the sum of all rate constants described in equation 1.8. The definition is depicted in equation 1.10.

$$k_{ex} = \frac{k_{op} \cdot k_{ch}}{k_{cl} + k_{op} + k_{ch}} \tag{1.10}$$

Since hydrogen bonds reside mainly in the closed state ($k_{cl} >> k_{op}$), equation 1.10 is reduced to equation 1.11.

$$k_{ex} = \frac{k_{op} \cdot k_{ch}}{k_{cl} + k_{ch}} \tag{1.11}$$

From this two cases can be differentiated. Case one is when the forming rate of a hydrogen bond is higher than the transient exchange ($k_{cl} > k_{ch}$). The probability of exchange of a single amide hydrogen in one single opened hydrogen bond event is less than one. Therefore the overall exchange rate k_{ex} is defined by the occurrence of opening events and the probability of exchange during a single opening event [Kaltashov and Eyles, 2005] (see equation 1.12). This case describes the so called EX2 mechanism.

$$k_{ex} = k_{op} \cdot \frac{k_{ch}}{k_{cl}} = K_{op} \cdot k_{ch} \tag{1.12}$$

In case two, the transient exchange occurs faster than the closing of a hydrogen bond ($k_{cl} < k_{ch}$). A single opening event suffices for an amide hydrogen to exchange. Hence, the closing process is the rate-limiting step and the overall exchange rate is correlated to the rate constant k_{op}. This is termed as EX1 mechanism (equation 1.13)

$$k_{ex} = k_{op} \tag{1.13}$$

Amide hydrogen exchange is pH dependent as mentioned earlier. Using an unstructured peptide such as poly-DL-alanine (PDLA), the amide reference exchange rate constants $k_{H_3O^+}$, k_{OH^-} and k_{H_2O} were determined at 20°C and low salt conditions from NH to ND exchange resulting in 41.7 $M^{-1}min^{-1}$, $1.12 \cdot 10^{10}$ $M^{-1}min^{-1}$ and $3.16 \cdot 10^{-2}$ $M^{-1}min^{-1}$ respectively [Bai *et al.*, 1993]. This enables to plot the logarithm of the exchange rate of an amide in an unstructured peptide as a function of pH with the help of equation 1.9 (see Figure 1.5). The exchange rate constant has its minimum at pH 3 approximately.

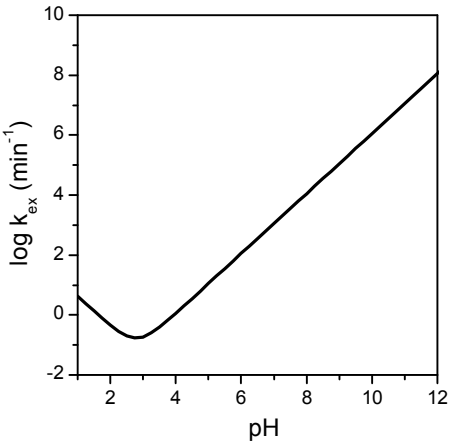

Figure 1.5: pH dependence of amide hydrogen exchange. The curve is redrawn with the reference exchange rate constants of PDLA measured at 20°C and low salt concentration and equation 1.9 [Bai *et al.*, 1993, Dempsey, 2001].

The pH at which the rate constant is at its minimum can be calculated also by equation 1.14 [Leichtling and Klotz, 1966] (note that pK_W for D_2O is 15.05).

$$pH_{min} = \frac{1}{2}\left[pK_W + log\frac{k_{H_3O^+}}{k_{OH^-}}\right] \tag{1.14}$$

From figure 1.5, it can be concluded that exchange at pH 3 is contributed by acid- and base-catalysis equally. The slope of the curve below pH 3 is -1 and above +1 and gives rise to a first-order pH dependence of k_{ex}. This means that below pH 3 exchange is dominated by acid-catalysis and above pH 3 by base-catalysis [Brier and Engen, 2008]. Water-catalysis contributes to the overall exchange around pH 3, below and above it has little effect [Gregory *et al.*, 1983]. The exchange rate increases 10fold for each pH unit distant from the pH minimum. Also the influence of base-catalysis is 8 orders of magnitude higher than the acid-catalysis comparing the reference exchange rate constants of PDLA [Dempsey, 2001].

The different pH dependence of acid- and base-catalysed exchange can be explained by considering the pK_a values of each involved partner. Based on the proton transfer events in both types of catalysis the rate-limiting step for base-catalysis is the proton abstraction of the amide hydrogen and for acid-catalysis the protonation step. The

reason for that is the proton transfer from a weaker acid to a stronger acid. The pK_a for the deprotonation of an amide function is 18.5 and for protonation of a hydroxide ion 15.7 [Englander and Kallenbach, 1984]. The difference in pK_a is -3 ($\Delta pK_a = pK_a(acceptor) - pK_a(donor)$) resulting in a proton transfer rate of 10^{-3}. This means, in one in thousand collisions a proton is successfully transferred. The pK_a value for protonation of the amide function is -13 and for hydronium-ion -1.74. The resulting proton transfer rate is 10^{-11} [Englander *et al.*, 1972, Englander and Poulsen, 1969]. In an unprotected amide function the resulting exchange rate k_{ex} is the chemical exchange rate k_{ch} (see equation 1.9) with either base-catalysis or acid-catalysis contribution. The rate constants k_{OH^-} and $k_{H_3O^+}$ are defined as $10^{\Delta pK_a} \cdot k_D$ with the diffusion rate constant $k_D = 10^{10} M^{-1} s^{-1}$ [Englander and Kallenbach, 1984]. These rate constants are in the same order of magnitude as the determined reference exchange rate constants for PDLA. With equations 1.15 and 1.16 the overall exchange rate can be determined dependent on the pH. Here again, the rate constants k_{ex} for base- and acid-catalysis are equal in contribution at pH 3.

$$k_{ex} = 10^{-3} \cdot k_D \cdot [OH^-] = 10^{(pH-7)} s^{-1} \tag{1.15}$$

$$k_{ex} = 10^{-11} \cdot k_D \cdot [H_3O^+] = 10^{(-1-pH)} s^{-1} \tag{1.16}$$

Further, k_{ch} depends on the contribution of the side chains due to their steric and inductive effects on the amide hydrogen. Therefore equation 1.9 can be also described by correcting the second-order rate constants for acid, base and water catalysed hydrogen exchange with the factors A_L, A_R, B_L and B_R for effects of the neighbouring side chains (equation 1.17) The designation L and R signifies whether the side chain is on the left or the right position of the amide function. The correction factors are listed in reference [Bai *et al.*, 1993].

$$k_{ch} = k_{H_3O^+} \cdot A_L \cdot A_R \cdot [H_3O^+] + k_{OH^-} \cdot B_L \cdot B_R \cdot [OH^-] + k_{H_2O} \cdot B_L \cdot B_R \tag{1.17}$$

Temperature is another parameter influencing hydrogen exchange. With equation 1.18 the chemical exchange rate constant k_{ch} can be corrected based on the Arrhenius theory with T as temperature, E_a as activation energy and R as gas constant. According to the different catalysts the activation energies E_a account for 14, 17 and 19 kcal mol^{-1} for $k_{H_3O^+}$, k_{OH^-} and k_{H_2O} respectively [Bai *et al.*, 1993]. The amide exchange rate constant increases threefold with each 10 K increment [Bai *et al.*, 1993, Brier and Engen, 2008]. A temperature increase will lead also to an altered pH thus influencing additionally the exchange rate [Englander *et al.*, 1972, Englander and Kallenbach, 1984, Englander and Poulsen, 1969].

$$k_{ch} = k_{ch}(293K) \cdot exp\left(-\frac{E_a}{R}\left[\frac{1}{T} - \frac{1}{293}\right]\right) \tag{1.18}$$

In summary, the chemical hydrogen exchange is influenced by pH, temperature, side chains, solvent and isotope effects. Taking into account that an amide hydrogen is involved in hydrogen bonds, this leads to protection against exchange and slows the exchange rate. In the works of Rohl and Baldwin [1994] an amide hydrogen in helical and non-helical alanine based peptide structure was examined giving a 10fold decrease in exchange when the amide hydrogen was involved in hydrogen-bonding. The 10fold exchange rate decrease is also confirmed on the peptide apamin in the works of Dempsey [1986].

1.3 Intramembrane Proteolysis in Alzheimer's Disease

To understand why helix dynamics is important to the etiology of Alzheimer's Disease, the following chapter introduces intramembrane proteolysis in general (sec. 1.3.1, p. 23) and in more detail in the example of Alzheimer's Disease (sec. 1.3.2, p. 24). For this example, both protease (sec. 1.3.3, p. 26) and substrate (sec. 1.3.4, p. 29) are further described in their influences and properties. Finally, the link between helix dynamics and intramembrane proteolysis is derived (sec. 1.3.5, p. 31 and sec. 1.3.6, p. 33).

1.3.1 Principles of Intramembrane Proteolysis

Hydrolysis of a peptide bond within a peptide or a protein catalysed by an enzyme is defined as proteolysis [Barrett and McDonald, 1986, Bergmann and Niemann, 1937]. When proteolysis occurs within a membrane and the transmembrane domain of a bitopic membrane protein is subject to proteolysis, it is called intramembrane proteolysis [Brown *et al.*, 2000]. Because water is needed as another educt for hydrolysis, intramembrane proteolysis is something exceptional because water is not included in lipid bilayers due to their hydrophobic nature. Thus, proteases involved in intramembrane proteolysis are first themselves membrane proteins and second they are able to capture water inside the lumen of the protease to facilitate the proteolysis of a transmembrane domain [Wolfe and Kopan, 2004].

Comparable to soluble proteases there exist also classifications for membrane proteases signified by their amino acids constituting the active site. Intramembrane cleaving proteases (I-CLiPs) can be grouped into serine, aspartyl and metalloprotease classes. Cysteine I-CLiPs were yet not discovered [Erez *et al.*, 2009]. I-CLiPs belong to the polytypic membrane proteins, thus having several TMSs. The catalytic site is mostly represented on two TMSs. A prominent representative for metalloproteases is the site-2-protease (S2P) with a catalytic site comprising **HE**xx**H** at one TMS and L**D**G at the other TMS. Serine proteases are represented by the rhomboids with Gx**S**G and **H** as the active site. Signal peptide peptidase (SPP) and presenilin (PS) in the γ-secretase-complex belong to the aspartyl protease family with Y**D** and LGxG**D** as

active site. Excellent reviews for intramembrane proteolysis are from Beel and Sanders [2008], Erez *et al.* [2009] and Wolfe [2009].

The consequence of intramembrane proteolysis is the release of the cytosolic and the extracellular/lumenal domain of the membrane protein. A major function of this process represents signalling [Brown *et al.*, 2000]. The released cytosolic part acts as a transcription factor inside the nucleus or the deliberated extracellular part activates receptors of neighbouring cells or even both domains play a significant role [Erez *et al.*, 2009]. Other functions were discussed, such as the remove of remnant membrane protein stubs as a "proteasome of the membrane" [Kopan and Ilagan, 2004]. Some intramembrane proteolysis events require the proteolysis of the lumenal/extracellular domain of the membrane protein substrate. This two-step cleavage mechanism is then called as regulated intramembrane proteolysis (RIP) [Brown *et al.*, 2000, Lemberg, 2011, Selkoe and Kopan, 2003]. The first cleavage event is often called as ectodomain shedding [Arribas and Borroto, 2002, Lichtenthaler *et al.*, 2011].

When the membrane protein fragments are released from the membrane, they contain parts of the transmembrane domain. Hence, when the solute environment changes, the TMD regions of the released domains may interact differently and also structural alterations can occur due to the hydrophobic effect. An extreme case would be the refolding from an α-helical to a β-ladder shaped state associating with others to β-sheets. Oligomerisation and/or aggregation are the structural consequences [Johannsen, 2003, Lichtenthaler *et al.*, 2011].

1.3.2 The Etiology of Alzheimer's Disease

Alzheimer's Disease (AD) is one of the most prevalent forms of dementia occuring in mid-to-late life [Morris, 1999]. 98% of incidences are attributed to a sporadic form, whereas 2% stem from inherited forms, which is the familial Alzheimer's Disease (FAD). Major hallmarks of AD are the neurofibrillary tangles and amyloid plaques which were already described by the disease's discoverer Alois Alzheimer [1907]. Affected brain regions are the cortex, hippocampus, amygdala and basal forebrain [Sisodia, 1999]. Neurofibrillary tangles consist of the hyperphosphorylated microtubuli-associated protein tau which is prone to aggregation. These intracellular deposits are also characteristic for other dementia forms such as frontotemporal dementia (FTD) [Goedert and Spillantini, 2006]. But typical for AD are the extracellular amyloid deposits [Goedert and Spillantini, 2006]. They are composed mainly of the amyloid β peptides with varying lengths [Glenner and Wong, 1984, Masters *et al.*, 1985]. They derive from regulated intramembrane proteolysis of the amyloid precursor protein [Annaert and De Strooper, 2002, Goldgaber *et al.*, 1987, Kang *et al.*, 1987, Selkoe and Kopan, 2003]. Yet, the central molecular cause for neuronal degeneration in AD are the soluble oligomers of Aβ peptides and not the amyloid plaques [Darocha-Souto *et al.*, 2011, Klein *et al.*, 2001, Lue *et al.*,

1999, McLean *et al.*, 1999, Walsh *et al.*, 2002]. They impair synaptic structure and plasticity leading to synaptic dysfunction and neuronal death [Haass and Selkoe, 2007]. Which stoichiometric conformer of soluble Aβ oligomers causes toxicity remains unclear [de Strooper, 2010]. Predominant forms of Aβ peptides are Aβ40 and Aβ42 which differ in two residues at the C-terminus. The highest toxicity results from Aβ42 because of its higher propensity to oligomerise and to aggregate [Lambert *et al.*, 1998]. It is argued whether the dodecamer of Aβ42 is the neurotoxic species [Bernstein *et al.*, 2009, Lesne *et al.*, 2006] and its oligomerisation pathway distinguishes Aβ42 from Aβ40 [Bitan *et al.*, 2003]. In the scientific community, discussion on the mechanism how Aβ peptides oligomerise and aggregate in human bodies, *in vivo* and *in vitro* is still going on [de Strooper, 2010]. Ideas include a nucleation and elongation mechanism with low-order and high-order oligmers and protofibrils as intermediates [Chiti and Dobson, 2006, Straub and Thirumalai, 2011] and fibrils as endproducts. An accompanying feature for the Aβ release is the unfolding into random coil and refolding to β-pleated sheets of Aβ peptides [Bartolini *et al.*, 2007, Xu *et al.*, 2005]. Whether refolding occurs right after cleavage within the membrane, immediatedly after contact with the lumen/ extracellular site or upon oligomer formation is yet not clearly revealed [Bernstein *et al.*, 2009, Lesne *et al.*, 2006].

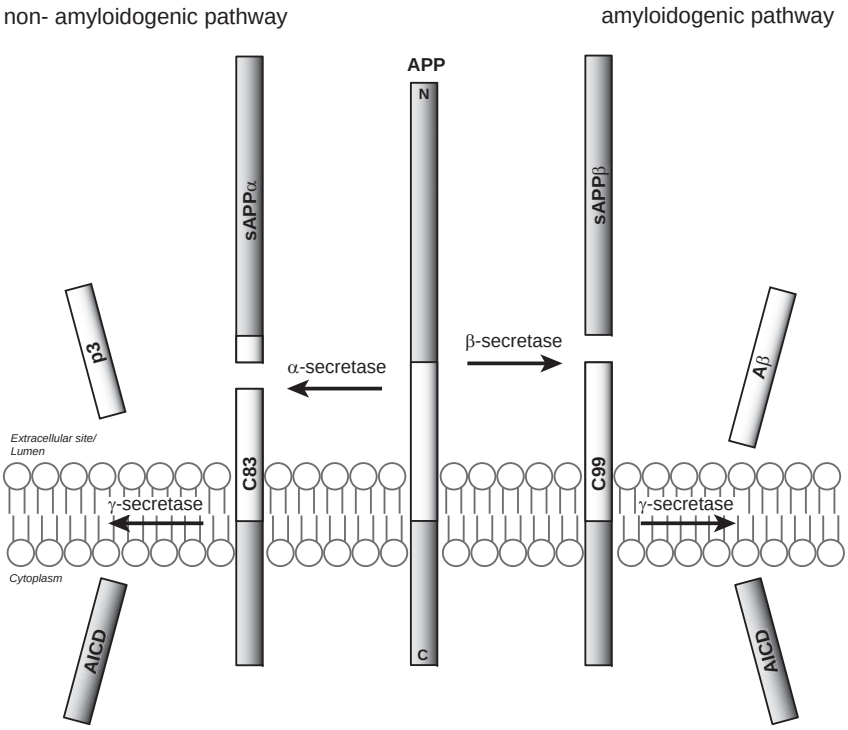

Figure 1.6: Processing Pathway adapted from reference [Lazo *et al.*, 2008]

The amyloid precursor protein can be cleaved via two alternative processing pathways (see Figure 1.6). Only the amyloidogenic pathway leads to Aβ peptides. Both begin with the shedding at the extracellular site of APP. In the non-amyloidogenic pathway the α-secretase ADAM10 (a disintegrin and metalloprotease) cleaves after position

Lys687 of APP770 [Asai *et al.*, 2003, Huovila *et al.*, 2005]. A large extracellular soluble fragment sAPPα is released and a C-terminal stub C83 remains in the membrane. In contrast, the β-secretase, also called β-site APP cleaving enzyme (BACE), sheds after position Met671 of APP770 and secretes a soluble sAPPβ fragment [Cole and Vassar, 2008, Vassar, 2004]. A membrane remnant C99 is produced and hence defines the N-terminus of the so called Aβ peptides. In a second step the C-terminal membrane stub (C83 or C99) is proteolysed by the γ-secretase at multiple positions in the TMD sequence of the C-terminal stub, thus releasing the APP intracellular domain (AICD) into the cytoplasm and varying lengths of the p3 respectively the Aβ peptides into the lumen or extracellular site. Aβ metabolism occurs on the plasma membrane, in the secretory and endosomal pathway including also the trans-Golgi compartment [Lazo *et al.*, 2008].

Throughout life these processes are ubiquitous in the human body with a low level of Aβ peptides produced [Moghekar *et al.*, 2011, Seubert *et al.*, 1992, Shoji *et al.*, 1992]. In sporadic AD, the equilibrium between both processing pathways shifts towards increasing Aβ-production [de Strooper, 2010]. The analysis of cell culture media experiments reveal a composition of 90% Aβ40 and 5-10% Aβ42, which is likely to be similar for the production in diseased humans [Suzuki *et al.*, 1994, Younkin, 1998]. In many FAD cases, mutations in either the APP or in γ-secretase lead to an increased ratio of Aβ42 to Aβ40, thus enhancing severeness of AD or shifting the disease onset to mid life [Kaether *et al.*, 2006]. The triggers for the sporadic diseases' onset remain unsolved, yet risk factors such as age were found. A genetic risk factor was identified for carrying the ε4-allele of the apolipoprotein E [Poirier *et al.*, 1993, Saunders *et al.*, 1993]. Statistically more AD incidences were found with this genotype. Influences from the environment, diet or level of education are considered as well [Luchsinger and Mayeux, 2004].

1.3.3 Assembly, Structure and Function of the γ-Secretase

γ-Secretase is the responsible enzyme for the sequential proteolytic cleavage of the C99 fragment. Beside this, other roles are found in the transport and degradation of membrane proteins, cell adhesion, endoplasmic reticulum Ca^{2+} regulation and cell signalling [Coen and Annaert, 2010].

It is itself a multi subunit membrane protein complex which is only functional with at least four subunits: presenilin-1 or -2 (PS-1 or PS-2), anterior pharynx-defective-1 (APH-1), presenilin enhancer-2 (PEN-2) and nicastrin (NCT) (Figure 1.7) [Edbauer *et al.*, 2003]. The formation of the complex begins with the assembly of nicastrin and APH-1 in the endoplasmic reticulum [LaVoie *et al.*, 2003]. PS joins the pre-complex. After this, PEN-2 completes the assembly and initiates maturation of the whole complex. The active complex is then transported to the plasma membrane or endosomal compartments

[Dries and Yu, 2008, LaVoie *et al.*, 2003, Niimura *et al.*, 2005].

Presenilin is the subunit with proteolytic activity. It consists of 9 transmembrane segments with the N-terminus in the cytoplasm and the C-terminus in the lumen or extracellular site [Laudon *et al.*, 2005]. The catalytic site is represented by two aspartates D257 at TMS 6 and D385 in a conserved GxGD motif at TMS7 (numbering belongs to human PS; UniProtKB accession number: P49768) [Wolfe *et al.*, 1999]. The γ-secretase is mature when presenilin undergoes sequential autocatalytic endoproteolysis in the intracellular loop between TMS 6 and 7 beginning at residue 292 and ending at residues 299 [Fukumori *et al.*, 2010]. This results into the N- and C-terminal fragments, PS-NTF and PS-CTF, existing now as a heterodimer and representing the catalytically active form [Capell *et al.*, 1998, Dries and Yu, 2008, Thinakaran *et al.*, 1996, 1998].

Nicastrin is a highly N-glycosylated bitopic membrane protein with type I topology. Its extracellular domain binds to the substrate. In detail, the carboxyl group of Glu333 in the DYIGS and peptidase domain (DAP) binds to the α-amino group of C99 and thus positions the substrate for cleavage (pointed out in Figure 1.7). [Shah *et al.*, 2005]

APH-1 acts as a scaffold to stabilise the complex. With its 7 TMS, it associates with NCT and PS [Lee *et al.*, 2002]. One of its important motifs is the GxxxG motif in TMS 4 [Lee *et al.*, 2004].

With PEN-2 the maturation of the γ-secretase-complex is enabled [Prokop *et al.*, 2004]. It facilitates the autoproteolysis of presenilin and the maturation of the subunit nicastrin [Kim and Sisodia, 2005b, Steiner *et al.*, 2002]. Also it was found that PEN-2 enhances enzyme activity [Shiraishi *et al.*, 2004]. The interaction between PEN-2 and PS is localised at TMS 1 of PEN-2 and TMS 4 of PS [Kim and Sisodia, 2005a, Watanabe *et al.*, 2005].

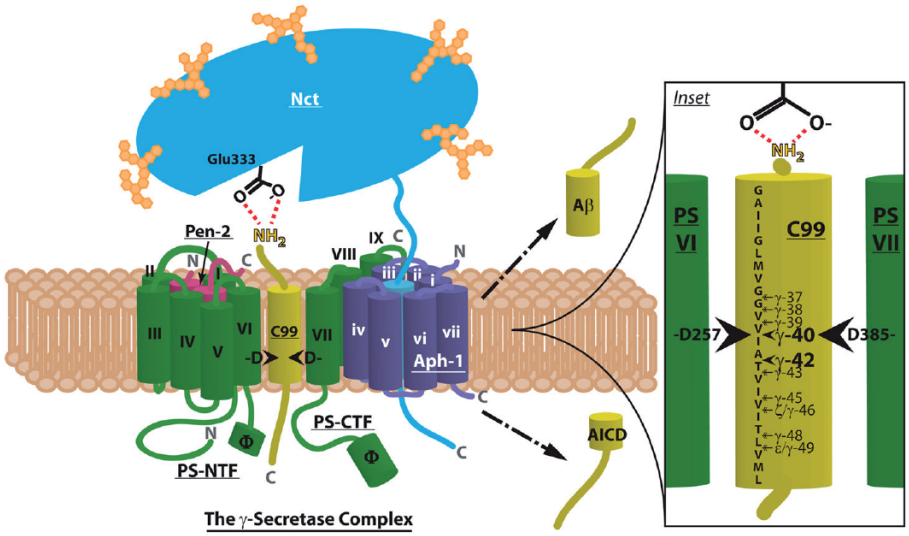

Figure 1.7: The Structure of the γ-secretase. PS-NTF comprises TMS 1 to 6 and PS-CTF comprises TMS 7 to 9. Illustration was taken from reference [Dries and Yu, 2008].

Until now few structural elucidations of the γ-secretase were published due to the

extreme difficulty to enrich and reconstitute the membrane based complex [Steiner *et al.*, 2008]. Osenkowski *et al.* have resolved a cryoelectron microscopy structure of γ-secretase at 12 Å resolution [2009]. It shows potential regions such as solvent-accessible cavities at the cytoplasmic site, a possible substrate binding surface groove in the transmembrane region of the complex and several domains on the extracellular face of the complex. This is concomitant with the work of Lazarov *et al.* [2006] which revealed an aqueous intramembrane space and two pores.

Special focus was put on each TMS in presenilin. With cysteine scanning mutagenesis (SCAM) and hydrophilic sulfhydryl-directed reagents, TMS 6, 7 and 9 were identified to be exposed to a water-containing cavity, which means that the catalytic site is within an aqueous pore [Sato *et al.*, 2006, Tolia *et al.*, 2006, 2008]. Additionally, it is verified that the two catalytic aspartates are opposed to each other [Tolia *et al.*, 2006]. The substrate binding sites are distinct from the active site [Kornilova *et al.*, 2005, Watanabe *et al.*, 2005]. One binding site represented by nicastrin is mentioned a few paragraphs earlier. Other candidates for substrate binding are TMS 2 and the lumenal region of TMS 6, eventually also TMS 9 [Watanabe *et al.*, 2010, Wolfe, 2010]. Further, TMS 1 was discovered to face the catalytic pore as proved by SCAM experiments [Takagi *et al.*, 2010]. It was found to be close to the GxGD and the PAL motif of the PS-CTF. Residues Val82, Leu85 of TMS 1 are regarded as potential subsite involved in substrate recognition. In addition, Takagi and colleagues discuss a cooperative function as catalytic plug represented by TMS 1, 7 and 9. Val94 of TMS 1 could possibly interact with other TMDs based on hydrophobic nature [Takagi *et al.*, 2010]. For the APP as substrate, there is another interaction site between Lys625 of isoform APP695 and an unknown site of γ-secretase [Kukar *et al.*, 2011].

Another attempt for structural elucidation is the solution-state NMR structure of PS-CTF reconstituted in SDS micelles (PDB key:2KR6). It shows TMS 7 as half a helix and TMS 9 as a kinked helix [Sobhanifar *et al.*, 2010].

Knowledge gathered from soluble Asp proteases and a study by Singh *et al.* [2009] suggested that the most probable mechanism of the proteolysis reaction is as follows [Brown *et al.*, 1992, Pearl and Blundell, 1984, Rodriguez *et al.*, 1993, Suguna *et al.*, 1987]. Two steps, the formation of the geminal diol intermediate and the breakage of the scissile peptide bond, lead to the cleavage. In soluble Asp proteases it has been shown that one of the two Asp is protonated and the other one deprotonated [Coates *et al.*, 2006, 2008, Rajamani and Reynolds, 2004, Yu *et al.*, 2006]. The latter one acts as a base and activates a water molecule by H-bonding to it. Thus, the formed hydroxide ion can attack as a nucleophile the carbonyl carbon of the peptide bond of a polypeptide substrate. Simultaneously a proton is transfered from the protonated Asp to the carbonyl oxygen leading to a tetrahedral intermediate. In the second step, the carbonyl reforms by breaking the carbon nitrogen bond. The nitrogen bond abstracts further a proton from the protonated Asp of presenilin which belonged once to the

water molecule. A suggested scheme taken from literature is shown in Figure 1.8. In the computational study of Singh *et al.* [2009] the formation of the geminal diol intermediate was discovered to be the rate-limiting step.

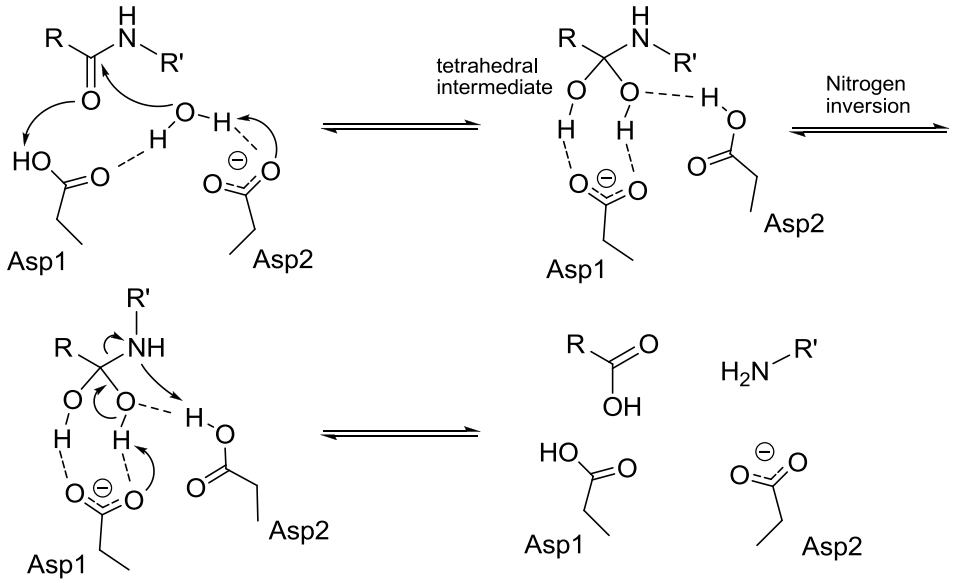

Figure 1.8: Suggested catalytic mechanism for soluble aspartyl protease catalysed proteolysis adapted from [Coates *et al.*, 2006, Singh *et al.*, 2009]. Dashed lines indicate H-bonds. The water molecule H-bonding between both aspartates was found in X-ray structures of soluble Asp proteases.

1.3.4 The Amyloid Precursor Protein

The amyloid precursor protein (APP) is a type I integral membrane protein with one transmembrane domain (Uniprot Protein Knowledgebase-Entry: P05067). It belongs together with amyloid precursor-like proteins to the APP family [Kaden *et al.*, 2011]. It is ubiquitously expressed throughout the body and is enriched in brain, kidneys, heart and spleen [Tanzi *et al.*, 1988]. Dependent on the tissue, differently spliced variants were found [Tang *et al.*, 2003]. The three major isoforms are APP770, APP751 and APP695 mainly produced in the brain (numbers indicate the amino acid length of the proteins). APP770 and APP751 are expressed predominantly in non-neuronal cells and APP695 predominantly in neuronal cells [Haass *et al.*, 1991, Kitaguchi *et al.*, 1988, Menendez-Gonzalez *et al.*, 2005]. The longer isoforms contain a 56 residue long Kunitz type serine protease inhibitor domain in the extracellular site of APP. APP770 additionally carries a 17 residue long OX2 region in its ectodomain [Kitaguchi *et al.*, 1988, Lazo *et al.*, 2008]. Paralogues are the amyloid precursor-like proteins APLP-1 and -2 in human [Kaden *et al.*, 2011].

APP is structured in three major regions. The longest with 600 aa is the ectodomain followed by the transmembrane domain from residue Gly700 to Leu723 according to APP770 nomenclature and for Aβ-numbering from residue 29 to 52. In detail, the

ectodomain contains two larger domains, E1 and E2. The E1 domain comprises the growth factor-like and a copper-binding subdomain [Kaden *et al.*, 2011] and a α-helix rich E2 domain. Figure 1.9 A shows a schematic representation. In the ectodomain two dimerisation sites reside beside another one in the transmembrane domain represented by consecutive GxxxG motifs (from residue 25 to 38, Aβ-numbering) [Gorman *et al.*, 2008, Kaden *et al.*, 2008, Munter *et al.*, 2007, Sato *et al.*, 2009]. Cholesterol titration experiments combined with NMR measurements and Ala scanning mutagenesis reveal that Gly700 and Gly704 bracketing one of the GxxxG dimerisation motifs represent a binding site for cholesterol, as well [Barrett *et al.*, 2012]. Beside this, the extracellular site holds two heparin- and one collagen-binding domains [Beher *et al.*, 1996], copper- and zinc-binding motifs [Multhaup, 2006], acidic and Thr rich domains, multiple disulfide bonds, sites for N- and O-glycosylation, sulfonation and phosphorylation [Bush *et al.*, 1992, Lazo *et al.*, 2008, Walter *et al.*, 1997]. This suggests that APP is interacting with molecules from an organelle lumen or from the extracellular matrix. It is discussed that APP and also the soluble APP ectodomain once it is sequestered by α- or β-secretase may play a role in cell adhesion, cell development and/or function as a cell surface receptor [Kaden *et al.*, 2011]. The intracellular domain is very short and has 47 amino acids. A possible role is the modulation of gene transcription together with other adapter proteins once the intracellular domain is released after regulated intramembrane proteolysis [Cao and Sudhof, 2001].

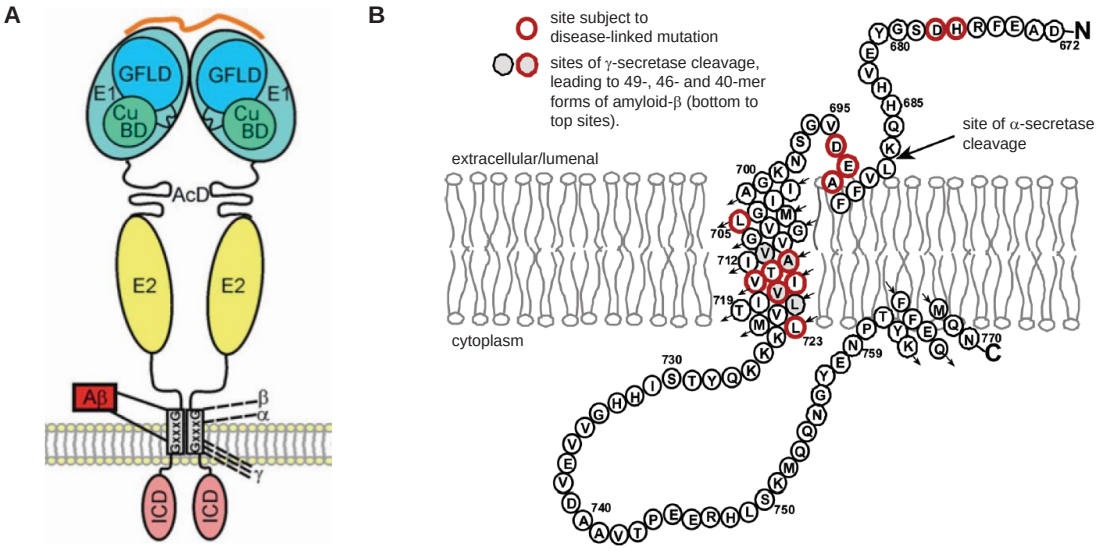

Figure 1.9: APP (A) and C99 (B) Models from references [Kaden *et al.*, 2011] and [Beel *et al.*, 2008]

The three-dimensional structure of APP as a whole is not known. Soluble parts have been crystallised and measured with X-ray diffraction (see UniprotKB entry with accession number P05067). The C99 fragment, which is released from APP proteolysis by β-secretase, was investigated in lysomyristoylphosphatidylglycerol (LMPG) micelles by NMR [Barrett *et al.*, 2012, Beel *et al.*, 2008]. Barrett and coworkers revealed a highly

curved α-helical TMD with Gly708 and Gly709 as apex (Figure 1.9 B) 2012. Both extramembrane regions of C99 have an unordered structure with two exceptions. One helix turn was located between residue Leu688 to Asp694 close to the α-cleavage site and a short helix from residue Tyr762 to Asn770 in the intracellular domain. With solid state-NMR studies, a 42 residue long fragment (Glu693-Val755) including the N- and C-terminal juxtamembrane regions beside the transmembrane domain was investigated in DMPC:DMPG bilayers [Sato *et al.*, 2009]. This work confirmed an α-helical TMD with the exception of a short local unstructured site around Leu720 which is a cleavage site of γ-secretase and Val721 (according to APP770).

Within the cell, APP is localised and trafficked in the endoplasmic reticulum, Trans-Golgi, endosomes, secretory vesicles and plasma membrane [Groemer *et al.*, 2011, Lazo *et al.*, 2008, Suzuki *et al.*, 2006, Thinakaran and Koo, 2008].

1.3.5 Generation of Aβ Peptides by γ-Secretase

The Aβ peptides derive from the sequence of APP. In regulated intramembrane proteolysis, their N-terminus is defined by the shedding at the extracellular site of APP caused by β-secretase producing the C99 fragment (see Figure 1.9 B in section 1.3.4, p. 29). Their C-terminus is determined by the γ-secretase-cleavage. Yet, this cleavage occurs several times along the transmembrane domain of C99 and results in Aβ peptides of varying lengths [Kukar *et al.*, 2011, Munter *et al.*, 2007, Qi-Takahara *et al.*, 2005, Sagi *et al.*, 2011, Takami *et al.*, 2009].

It is proposed that the shorter fragments are parts of the longer fragments [Qi-Takahara *et al.*, 2005, Sato *et al.*, 2003, Zhao *et al.*, 2005]. A model was developed that the actual endoproteolysis occurs at the ε-cut site giving the AICD fragment and Aβ 48 plus Aβ 49 (for cleavage sites see Figure 1.10) [Weidemann *et al.*, 2002]. These membrane bound Aβ fragments are the precursors for Aβ 45 and Aβ 46 peptides and are cut at the ζ-sites [Zhao *et al.*, 2004]. The γ-sites at positions 43/ 42 and 40/ 38 yield then smaller Aβ peptides. The model is supported by the fact that the AICD fragment is from 49-99 and 50-99 and not longer [Kukar *et al.*, 2011, Qi-Takahara *et al.*, 2005, Sato *et al.*, 2003, Takami *et al.*, 2009]. Also the tri- and tetrapeptides were detected with MALDI-mass spectrometry experiments [Takami *et al.*, 2009]. This finding and the certain periodicity of the cleavage sites (every 3rd or 4th next position) suggests as well that the substrate and subsequent intermediates are helical showing a specific face towards the enzyme's active site.

In sum, two product patterns are distinguished depending on the initial cleavage event: Aβ 49 to Aβ 46 to Aβ 43 to Aβ 40 and Aβ 48 to Aβ 45 to Aβ 42 (cleavage sites are depicted in Figure 1.10 above and below the APP-TMD sequence for the respective product pattern) [Qi-Takahara *et al.*, 2005]. All in all, the γ-secretase cleaves in a progressive and sequential manner.

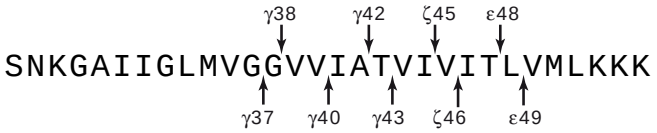

Figure 1.10: Transmembrane domain of APP with its cleavage sites. According to C99 numbering, the depicted sequence shows the range between residue 26 to 55, the actual TMD is from residue 28 to 55. Above the sequence, the Aβ product line for Aβ42 is depicted and beneath the sequence for Aβ 40.

Several factors influencing the product pattern were discovered in the past. One is for example that Lys28 (according to Aβ numbering) is important [Kukar *et al.*, 2011]. Replacing it with an apolar residue leads to shorter Aβ peptides such as Aβ 33 and Aβ 34. An anchoring function for Lys28 is suggested undergoing ionic interactions with the γ-secretase.

The transmembrane domain has N-terminally a consecutive GxxxG motif which was shown via ToxR assays to mediate dimerisation [Munter *et al.*, 2007]. Attenuating the dimer interface by substituting Gly33 to Ile reduces Aβ 42 levels and increases the level of the shorter Aβ 38 peptides. This suggests that dimers of C99 are the substrates although this idea is debated.

FAD mutations at the transmembrane domain of APP are known to increase Aβ 42 levels such as the Austrian T714I mutation (T43I according to Aβ numbering) [Kumar-Singh *et al.*, 2000, van Broeck *et al.*, 2008]. Rescuing wildtype levels, a G33A mutation in the GxxxG motif of the T43I mutant leads to a 60% decrease of Aβ 42 and a 3 fold increase in Aβ 38 levels [Munter *et al.*, 2010].

In order to identify key residues influencing the Aβ product pattern, a phenylalanine scanning mutagenesis along the transmembrane domain of APP combined with ELISA readings of Aβ levels was performed [Lichtenthaler *et al.*, 1999, Tan *et al.*, 2008]. In the research of Lichtenthaler *et al.*, Aβ 42/Aβ 40 ratio decreasing mutations are found to be V44F, I47F and V50F on otherwise wildtype C99. Opposite Aβ 42/Aβ 40 ratio effects were induced by T43F, I45F, L49F and M51F mutations [Lichtenthaler *et al.*, 1999]. Using a Swedish APP mutant (K670N/M671L of APP770; β-cleavage site is M671) phenylalanine mutations within the APP TMD caused in general a decrease in total Aβ load, indeed I45F, T48F and M51F were correlated with the highest reduction in Aβ load, but also with the highest increase of the Aβ 42/Aβ 40 ratio [Tan *et al.*, 2008]. As both works were performed in different cell lines and with different antibodies for Aβ detection a comparison and a mutual confirmation of the results is hard to make.

Another impact on Aβ product pattern is a potentially therapeutic one. γ-Secretase modulators (GSM) and non-steroidal non-inflammatory drugs (NSAID) were discovered to alter the product pattern [Kukar and Golde, 2008, Kukar *et al.*, 2008, Richter *et al.*, 2010, Sagi *et al.*, 2011, Weggen *et al.*, 2001]. The NSAID sulindac sulfide decreases the Aβ 42 production which is compensated by the production of the shorter Aβ 38

peptide [Weggen *et al.*, 2001]. Several experiments suggest that the binding of Sulindac sulfide occurs at the GxxxG motif of the APP-TMD, thus potentially attenuating dimerisation which may explain the reduced Aβ 42 production in favour for shorter Aβ peptides [Richter *et al.*, 2010]. Nonetheless, it is also discussed that NSAIDs and GSMs have another mechanistic way to alter the product pattern. It is suggested that GSMs and NSAID based GSMs modulate γ-secretase's activity by allosteric interaction, thus modifying the enzyme's conformation [Beel *et al.*, 2009, Czirr *et al.*, 2008, Page *et al.*, 2008]. Note beside that the major argument against irreversible inhibition of γ-secretase is the proteolysis of the C-terminal membrane remnant of the NOTCH receptor protein by this protease. This event is crucial for the NOTCH signalling pathway, a key role in tissue development [Selkoe and Kopan, 2003].

1.3.6 Substrate Specificity of γ-Secretase

Having found more than 60 substrates, the question arises which conditions need to be fulfilled for a substrate to be cleaved by the γ-secretase [Beel and Sanders, 2008, Hemming *et al.*, 2008]. One required condition is the orientation in the membrane. The majority of substrates are type I single pass membrane proteins. Note beside, that the aspartyl membrane protease SPP prefers substrates with type II topology probably due to its reversed YD/LGxGD motif [Nyborg *et al.*, 2004]. Another condition is the shedding of the large extracellular site of the substrate, only the short ectodomain will be recognised by nicastrin of the γ-secretase. There exist few exceptions such as the E-cadherin and the VEGF receptor not needing shedding of the extracellular domain [Cai *et al.*, 2006, Marambaud *et al.*, 2002].

Typical of intramembrane proteolysis is the α-helicity of TMD substrates. As explained in section 1.1.3 (p. 10), side chains shield the backbone amide bonds and hinder nucleophilic attack of water due to steric hindrance. Thus, the environment of intramembrane cleaving proteases has to provide both hydrophilic side chains for water capture and appropriate residues for interaction with the substrate. Sequence and structure define the substrate specificity of a membrane protease [Wolfe, 2009]. Yet, no certain key residues in the substrate were discovered. This explains why a lot of mutants are tolerated for TMD processing [Beel and Sanders, 2008]. Further, the analysis by Beel and Sanders reveals little sequence conservation and a low sequence similarity of the 60 substrates [2008].

However, helix dynamics of the substrate plays a significant role in intramembrane proteolysis. In the sterol regulatory element binding protein (SREBP) substrate of S2P protease the neighbouring residues Asp and Pro in the TMD were found to be crucial for TMD cleavability [Wolfe, 2009]. These residues are known to destabilise the helix and support unwinding of the helix, making the scissile amide bond accessible. Also, a Gly-Ala motif in Rhomboid substrates was identified suggesting the requirement

of helix-destabilisation prior cleavage [Urban and Freeman, 2003]. This is valid for SPP substrates, as well [Lemberg and Martoglio, 2002]. Considering substrates of the γ-secretase, β-branched residues such as Val or Ile near the cleavage site could mediate this. A statistical analysis of helical propensities near the initial cleavage site was performed, indicating a potential relevance of helix destabilisation [Beel and Sanders, 2008]. For example, the transmembrane domain of APP, it was found that a destabilised region C-terminal to the ε-cleavage site is necessary for cleavage [Sato *et al.*, 2009]. Despite that, the solution state NMR structure of C99 shows a TMD in a well defined α-helix with no interruptions apart from the general helix fraying at the termini which coincides with the small destabilised region found by Sato et al. [Beel *et al.*, 2008]. Solid-state NMR works by Lu *et al.* give further evidence for non-helical regions in the vicinity of the γ-cleavage sites and on the N- and C-termini of the APP TMD [2011].

Another aspect is the occurrence of a GxxxG motif within the TMD sequence in one quarter of the substrates. This implies the possibility that these TMDs associate to each other and that homodimers may represent the substrate. The works of Munter *et al.* have shown that APP-TMD homodimerisation can regulate the processivity of the γ-secretase, but it does not affect the cleavage efficiency [Munter *et al.*, 2007].

In order to get a detailed picture of substrate specificity, one needs to distinguish the efficiency in substrate binding and cleavage. Further research is needed to unravel its principles.

2 Motivation and Aim of Thesis

As described for helical transmembrane substrates for rhomboid proteases [Urban and Freeman, 2003, Urban and Shi, 2008] and proposed for substrates of the γ-secretase [Beel and Sanders, 2008, Sato *et al.*, 2009], sequence specific helix backbone dynamics was suggested to represent a requirement for intramembrane proteolysis. In other words, the scissile peptide bond of a helical substrate was supposed to be accessible to the catalytic centre of the enzyme and for water. On that account the transmembrane domain of the amyloid precursor protein, which is important for the etiology of Alzheimer's Disease, was characterised with respect to its backbone dynamics.

Thus, the aim of this thesis was to elucidate the secondary structure and the conformational backbone plasticity of the APP TMD. Circular dichroism spectroscopy addressing the first issue and deuterium hydrogen exchange experiments coupled to electron spray ionisation mass spectrometry addressing the latter issue were to be used as suitable methods to study synthetic peptides representing models of the APP TMD.

For example, it is of interest how the dimerisation domain distinguishes itself from the cleavage region. Also the backbone dynamics of TMD sequence fragments was to be studied. Additionally, key residues, influencing backbone dynamics strongly, were to be explored. The influence of small molecules such as non-steroidal anti-inflammatory drugs were to be analysed in their potential to modulate APP TMD backbone dynamics.

Also, differences in helix dynamics between the APP TMD substrate and non-APP-TMDs were to be examined. Non-APP-TMDs included artificial TM sequences based on different contents of Leu and Val and naturally occurring sequences mimicking the average residue composition of transmembrane domains.

Altogether, the work was designed to enrich the information upon structural properties of the APP TMD in regard to understand the mechanism of the consecutive processing of the APP TMD.

3 Materials and Methods

3.1 Materials

3.1.1 Chemicals and Reagents

Standard chemicals were of pro analysi grade and when used for mass spectrometry they were of HPLC or LC-MS grade. Deuterated chemicals had at least 99 atom% of deuterium. The chemicals have been obtained from Sigma-Aldrich (Steinheim), Applichem (Darmstadt), Roth (Karlsruhe) and Merck (Darmstadt). All protic solutions were prepared with deionised water (Millipore filter unit). Nitrogen for mass spectrometry and CD spectrometry was of 5.0 purity and was enriched from air by a nitrogen generator. Argon as collision gas for the mass spectrometer was purchased from Linde, Pullach, Germany and had 5.0 purity.

3.1.2 Instruments and Accessories

The used devices are specified in Table 3.1.

Table 3.1: List of used Instruments and Accesories

Device	Type Designation	Manufacturer
UV/Vis Spectrometer	Ultrospec 3100pro	Amersham Bioscience, USA
Cuvette for UV/Vis	10 mm precision cell, Quartz SUPRASIL	Hellma, Mühlheim, GER
Freeze Dryer	Delta 1-20KD	Christ, Osterode, GER
CD-Spectrometer	J-710 Spectral Polarimeter	Jasco, Easton, MD, USA
Cuvette for CD	106-QS 0.5 mm and 100-QS 1 mm precision cell, Quartz SUPRASIL	Hellma, Müllheim, GER
Water bath	Thermostatic Circulator 2219 Multitemp II	LKB Bromma, USA

(to be continued)

Device	Type Designation	Manufacturer
Cup Sonifier	Branson Sonifier with Cup Resonator	Branson, USA
Fluorescence Spectrophotometer	Cary Eclipse	Varian, Santa Clara, CA, USA
Cuvette for Fluorescence	105.250-QS 10 mm precision cell, Quartz SUPRASIL	Hellma, Müllheim, GER
Mass Spectrometer	Quadrupol-Time of Flight (Q-ToF) Electrospray Ionisation (ESI) mass spectrometer	Waters (Micromass), Manchester, UK
Syringes	1700 Series Gastight Syringes, 50 μl and 500 μl	Hamilton, Bonaduz, CH
Syringe Pump	Harvard Pump 11 Plus Dual Syringe	Harvard, Holliston, MA, USA
Thermocycler	Mastercycler personel	Eppendorf, Hamburg, GER
Thermomixer	Thermomixer comfort	Eppendorf, Hamburg, GER
Centrifuge	Centrifuge Z 233 MK-2	Hermle, Gosheim, GER
Nitrogen Generator	Nitrogen Generator	Linde, Pullach, GER

3.1.3 Software

Programmes and Software which have been applied are listed in Table 3.2.

Table 3.2: List of used Software

software	usage	provider
Masslynx	data recording on mass spectrometer	Waters
Spectra Manager Software	data recording on CD spectrometer	Jasco
Cary Eclipse	data recording on fluorescence spectrometer	Varian
CDNN/PEPFIT	CD data evaluation and secondary structure content determination	[Poschner *et al.*, 2007]

(to be continued)

software	usage	provider
Peak Tracer	MS data evaluation for DHX	programmer is Christian Ried, in house made
Laplace-MEM	HDX kinetic data evaluation	Dr. Marshall, Prof. Zhang [Zhang *et al.*, 1997]
Origin	HDX kinetic data evaluation	OriginLabs Corporation, USA

3.1.4 Peptides

Peptides were synthesised by Fmoc Chemistry and were purchased either from PSL Laboratories (Heidelberg, Germany) with HPLC grade, IZKF Leipzig Core Unit Peptide Technologies (Dr. Sven Rothemund) or the Chair of Proteomics and Bioanalytics, TUM (Prof. Küster) with raw product grade. The sequences of the used peptides are registered in Table 3.3

The purity of peptides was determined by mass spectrometry as a 5 µM solution in 80% (v/v) 2,2,2-trifluoroethanol in 10 mM NH_4Ac. Deuterated peptides were produced by dissolving the peptide lyophilisates in 2,2,2-trifluoroethan(ol-*d*) (d-TFE). The solution was diluted with deuterated 10 mM ammonium acetate buffer pD 7.0 resulting in 80% (v/v) d-TFE and a final peptide concentration up to 400 µM approximately. The samples were sonicated for 10 min, incubated at room temperature (RT) for another 30 min and then lyophilised. The procedure was repeated twice whereas the last incubation step was replaced by an incubation for 15 min at 90°C and by subsequent cooling on ice. The resulting lyophilisates were stored at -20°C.

Table 3.3: Sequences of model peptides

peptide name	sequence	source
A 28-55	KKWKGAIIGLMVGGVVIATVIVITLVMLKKK	A
A 28-44	KKWKGAIIGLMVGGVVIATVKKK	A
A 37-55	KKWKGGVVIATVIVITLVMLKKK	A
A 37-55 T48V	KKWKGGVVIATVIVIVLVMLKKK	B
A 37-55 T43V	KKWKGGVVIAVVIVITLVMLKKK	B
A 37-55 T43V/T48V	KKWKGGVVIAVVIVIVLVMLKKK	B
A 37-55 T43I	KKWKGGVVIAIVIVITLVMLKKK	B
L16	KKKWLLLLLLLLLLLLLLLKKK	A

(to be continued)

peptide name	sequence	source
LV16	KKKWLVLVLVLVLVLVLVKKK	A
LV16 G8P9	KKKWLVLVLVLGPVLVLVLVKKK	A
KTMD01	KKWKLAVSIFLLGGTGFVFVIYIALWMIKKK	A
KTMD02	KKWKIMVLSLFFGLFVFTVAAYIILAFMKKK	A
KTMD03	KKWKLLWIVLLFVFGTGILAYIVCAIVMKKK	A
KTMD04	KKWKSTAVMGAIWMILLFVLKKK	A
KTMD05	KKWKAFIWSAYGIALLVVGLKKK	C
KTMD06	KKWKVWSAFGITFLAMIILLKKK	C
KTMD07	KKWKAGISAGILVFILLLLVKKK	C
KTMD08	KKWKVILTFFVGAAILWLLCKKK	C
KTMD09	KKWKLGLSVGLVGIVVGTVLKKK	C
KTMD10	KKWKCVVLYVASSLFLMVMYKKK	C
KTMD11	KKWKYVWGAFGITFLAMLILKKK	C
KTMD12	KKWKVLGAIVSLILIYAFSTKKK	C
KTMD13	KKWKGTASVALIVILMAIFLKKK	C
mKTMD04	KKWKGGAVMLAIWMILLFVLKKK	C
mKTMD05	KKWKGGIWSAYLIALLVVLLKKK	C
mKTMD06	KKWKGGSAFVITFLAMIILLKKK	C
mKTMD08	KKWKGGLTFFVIAAILWLLCKKK	C
mKTMD12	KKWKGGLAIVSLILIYAFSTKKK	C
mKTMD13	KKWKGGASVALIVILMAIFLKKK	C
AL 35-42	KKKKWLLLLLLLLLLLMVGGVVIA	B
AL 39-46	KKKKWLLLLLLLLLLVVIATVIV	B
AL 42-49	KKKKWLLLLLLLLLLLATVIVITL	B
AL 45-52	KKKKWLLLLLLLLLLLIVITLVML	B
AL 45-52M	KKKKWLLLLLLLLLLLIVITLVMLMMM	B
L19	KKKKWLLLLLLLLLLLLLLLLL	B

A: PSL Laboratories (Heidelberg, Germany); B: IZKF Leipzig Core Unit Peptide Technologies (Dr. Sven Rothemund); C: Chair of Proteomics and Bioanalytics, TUM (Prof. Küster)

3.1.5 Lipids

The synthetic lipids 1-palmitoyl-2-oleoyl-*sn*-glycero-3-phosphocholine (POPC), 1,2-dioleoyl-*sn*-glycero-3-phosphoethanolamin (DOPE), 1,2-dioleoyl-*sn*-glycero-3-phospho-L-serine (DOPS), 1,2-dimyristoyl-*sn*-glycero-3-phosphocholine (DMPC), 1,2-dilauroyl-*sn*-glycero-3-phosphocholine (DLPC), 1,2-dilauroyl-*sn*-glycero-3-phosphoethanolamin (DLPE), 1,2-dilauroyl-*sn*-glycero-3-phospho-L-serine (DLPS) were purchased from

Avanti Polar Lipids (USA) and were delivered as powder or in chlorofom dissolved solution.

3.2 Methods

3.2.1 Peptide Solutions

Lyophilised peptides were stored at -80°C and were accustomed to room temperature for at least 30 min before solution preparation. The desired amount was weighed in a reaction tube (2 ml) and dissolved in trifluoroethanol (TFE) to make 2 mg/ml stock solutions. 15 min cooled sonification enhanced solubility. Insoluble peptide and particles were removed by centrifugation (13000 rpm, 4°C, 10 min). UV/ vis absorbance of the peptide solution containing 50% (v/v) DMSO was measured at 282 nm and a wavelength scan from 220 -320 nm was recorded. The number of occuring tryptophane ($\varepsilon_{282\ nm}$ = 5600 $M^{-1}cm^{-1}$), tyrosine ($\varepsilon_{282\ nm}$ = 1200 $M^{-1}cm^{-1}$) respectively cystine ($\varepsilon_{282\ nm}$ = 100 $M^{-1}cm^{-1}$) determined the molar absorbance coefficient for each peptide. Peptide concentration was then calculated by Lambert-Beer law. Dissolved peptides were stored at -20°C.

3.2.2 Preparation of Small Unilamellar Vesicles (SUVs)

Small unilamellar vesicles (SUV), also named here as liposomes, were used as a model environment for peptides to determine their secondary structure with CD-spectroscopy and to elucidate their backbone dynamics with deuterium/ hydrogen exchange experiments coupled to ESI mass spectrometry.

The lipids POPC, DOPE and DOPS were dissolved in $CHCl_3$ and had each 10 mg/ ml concentration. They were mixed in a ratio 3:1:1 (v/v/v) respectively in a 2 ml reaction tube. 60 µl POPC, 20 µl DOPS and 20 µl DOPE yielded a final 400 µl liposome suspension in buffer with a lipid quantity of 1.25 µmol. Lipid concentration amounts to 3.1 mM using an approximate lipid molecular weight of 800 g/ mol. Alternatively, DLPC, DLPS and DLPE were used (approximate lipid molecular weight is 600 g/mol) (compare Table 3.4.

The final 100 µl $CHCl_3$ were removed by evaporation with the SpeedVac and dried lipids were dissolved in 800 µl cyclohexane. Subsequently, in TFE or HFIP dissolved peptides were added. Different peptide/lipid (P/L) ratios were applied. The working range was between 0.01 and 0.02. To give a nominal P/L-ratio of 0.01 with 0.0125 µmol peptide, 40 µl peptide solution at a 312.5 µM concentration is added to the 800 µl lipid/cyclohexane solution. This results in a TFE or HFIP/ cyclohexane emulsion which is then sonicated 30 seconds to give a well distributed peptide/ lipid texture and is immediately frozen and lyophilised for 21 hours. Noteworthy, a 1:20 (v/v) ratio of TFE

Table 3.4: Exemplified concentrations and volumes for a SUV preparation with a nominal P/L-ratio of 0.02

reagent		concentration	volume [µl]
lipid	DLPC	10 mg/ml	60
	DLPS	10 mg/ml	20
	DLPE	10 mg/ml	20
cyclohexane			800
peptide		625 µM	40
buffer			400

or HFIP/ cyclohexane is maintained. When more peptide/TFE or HFIP solution is added, cyclohexane volume has to be adjusted.

The obtained peptide/ lipid lyophilisates were rehydrated with 400 µl 10 mM NH_4Ac pH 7.5 for mass spectrometry and CD measurements. Using the sample only for CD measurements 400 µl 20 mM NaCl, 10 mM Tris-HCL pH 7.4 were alternatively used. Samples were shaked for 1 h at 37 °C and 1400 rpm in a thermomixer to yield multilamellar vesicles. Then, they were sonicated in a cup resonator with ice cooling for 8 min with 80% amplitude (Output: 35-40%) to produce small unilamellar vesicles. Peptide and lipid aggregates were removed by 20 min centrifugation at 4°C and 13500 rpm. The supernatant containing the SUVs was removed to fresh reaction tubes and was stored at 4-8°C until further usage.

To use peptides integrated into liposomes for DH exchange, fully deuterated peptides (dissolved in dHFIP) were used to make peptide/ lipid emulsions. For rehydration of the peptide/ lipid lyophilisates 400 µl 10 mM ND_4Ac pD 7.5 were utilised.

3.2.3 Determination of Peptide/ Lipid Ratio of SUVs

The determination of the peptide/ lipid (P/L) ratio in SUVs is necessary for quantitation of the secondary structure composition via circular dichroism and for evaluation of the liposome preparation. To determine the concentration of the peptide which is incorporated into liposomes, 135 µl sample is added to 90 µl 10% SDS (w/v), 90 µl absolute ethanol and 225 µl 10 mM NH_4Ac pH 7.5. If SUVs are prepared in another buffer, then 225 µl of this one will be used. The mixture was shaken vigorously for 30 min at room temperature (1400 rpm, Eppendorff thermomixer) to lyse completely the liposomes. Then the mixture was aliquotted into 3 fractions with 160 µl volume each. 10 µl TFE were added to fraction A, 5 µl TFE and 5 µl internal standard (same peptide in TFE with 50 µM concentration as c_{IST}) were added to fraction B and 10 µl internal standard were added to fraction C. 10 µl TFE were added to 160 µl control solution D which contains the lysed liposome without peptide. All aliquots were shaken another 10 min (1400 rpm, room temperature). Emission spectra from 300 to 400 nm were recorded on a fluorescence spectrometer (Varian) with an excitation wavelength at

290 nm for tryptophan which is included in each peptide sequence. Emission values y_{A-D} were read out at the maximum between 325 and 335 nm for aliquots A-C and control solution D was taken as blank. Peptide concentration can thus by determined by the amount of incorporated peptide into the liposomes and the given amount of internal standard which increases in 5 µl steps (V) the fluorescence of the sample. With the help of equation 3.1 the molarity x_{pep} of the peptide can be calculated.

$$x_{pep} = \frac{(y_A - y_D) \cdot c_{IST} \cdot V}{y_C - y_B} \tag{3.1}$$

The dilution factor 0.25 and the initial volume of the liposome suspension have to be considered for concentration determination.

Lipid quantitation in a liposome suspension sample is defined by the determination of phosphate amount. Each used lipid contains a phosphate group and is quantified by the absorbance of the formed molybdophosphate complex. Dublicates were performed or each sample. 7 µl of a 1:4 diluted liposome suspension sample were decomposed with 100 µl 70% perchloric acid at 200°C on a heating block for 1 h. The hydrolytic cleavage of the lipid yields the free phosphate group. Phosphate standard solutions (0, 4.2, 8.3, 12.5, 16.6 and 20.8 nmol with 0.208 mM stock solution) were treated with the same procedure. After the heat treatment samples were cooled. 500 µl 0.44% (w/v) hexa-ammoniumheptamolybdat-4-hydrate solution containing 1.4 (v/v) concentrated sulphuric acid and 500 µl 2.5% (w/v) Fiske Subarrow reducing solution were added to each sample and were well mixed. The Fiske Subbarow Reducer contains 1-amino-2-naphthol-4-sulfonic acid, sodium sulfite and bisulfite [Fiske and Subbarow, 1925]. The samples were then incubated for 10 min at 100°C and afterwards again cooled. The solution was given to cuvettes and its absorbance was measured at 820 nm against a control (0 nmol phosphate). A calibration line is formed by the phosphate standard measurements, which is needed for the phosphate respectively for the lipid quantitation of the liposome suspension samples. The dilution factor 0.25 and the initial volume of the liposome suspension have to be considered for concentration determination.

The P/L ratio was determined by dividing the peptide concentration by the lipid concentration.

3.2.4 Circular Dichroism

Secondary structure of peptides both in isotropic solution, e.g. in TFE/ water mixtures, and integrated in liposomal membranes were determined by circular dichroism spectroscopy.

The measurement of peptide structures in isotropic solutions was carried out at 25 µM, 30 µM or 50 µM peptide concentration and in quartz cuvettes of either 0.5 mm or 1 mm path length at 20°C. The spectrometer recorded CD-spectra from 185 to 260 nm

with a velocity of 100 nm per minute and 1 second signal response. 10 accumulated spectra were averaged to maximize the signal to noise ratio and corrected by a baseline spectrum (derived also from 10 accumulated spectra) which represented the solvent without peptide. For sample preparation the desired peptide amount of stock solutions was taken to a reaction tube. Then solvent was removed by SpeedVac with a pressure of 50 mbar for 20 min. An alternative way for solvent removal was lyophilisation when peptides are known for their high aggregation propensity. Peptides were dissolved in 80% (v/v) TFE in 10 mM NH_4Ac with the respective pH to final concentrations of 25 µM, 30 µM or 50 µM for 10 min in an ultrasound bath. Equilibration time for secondary structure was given at least 3 hours at room temperature.

The measurement of peptides integrated into liposomes was performed at a lipid concentration of 1.5 mM and a peptide/lipid ratio of 2 mol-%. A quartz cuvette of 0.5 mm path length was chosen. Recording took place from 200 to 260 nm at 70°C, 100 nm per minute velocity, 1 second response. 20 accumulated spectra were averaged to maximize the signal to noise ratio and corrected by a baseline spectrum (derived from 20 accumulated spectra) which represented the solvent containing liposomes without peptide.

To determine the secondary structure composition the mean residue ellipticity $[\Theta_{\mathrm{mr}}]$ is calculated from the measured ellipticity Θ.

$$[\Theta_{mr}](\lambda)(MRW) = \frac{\Theta(\lambda) \cdot 100 \cdot M}{n \cdot c \cdot l} \tag{3.2}$$

$[\Theta_{mr}](\lambda)(MRW)$ = mean residue ellipticity in deg cm^2dmol^{-1}
$\Theta(\lambda)$ = ellipticity in mdeg
c = concentration in mg/ ml
l = pathlength in cm
n = number of amino acid residues per peptide

The CDNN/Pepfit Programm computes the relative secondary structures fractions. It is based on an algorithm which compares the measured spectrum with a set of peptide spectra of known secondary structures [Poschner *et al.*, 2007].

3.2.5 Deuterium/Hydrogen Exchange Reactions

To perform deuterium/hydrogen exchange (DHX) reactions on peptides, they were deuterated on their exchangeable positions. The procedure is described in section 3.1.4. The lyophilised deuterated peptides were dissolved in 80% (v/v) dTFE in 10 mM ND_4Ac at the considered pD to final concentrations between 250 and 400 µM. Afterwards concentration was determined, see section 3.2.1. The degree of deuteration

was calculated with equation 3.3.

$$d_r = [(m/z_d - m/z_p) \cdot z - (m_D - m_P) \cdot z] \cdot \frac{100}{D_{max}} \tag{3.3}$$

d_r = degree of deuteration in per cent
m/z_d = mass to charge of deuterated peptide
m/z_p = mass to charge of protonated peptide
z = charge
m_D = mass of a deuteron
m_P = mass of a proton
D_{max} = number of all labile deuterons per peptide

The m/z_d and m/z_p were identified by ESI mass spectrometry with a 10 µM deuterated peptide solution containing 0.5% (v/v) deuterated formic acid (FA) and its fully protonated counterpart (5 µM in 80% (v/v) TFE in 10 mM NH_4Ac, 0.5% (v/v) FA). When deuterated peptides exhibited a minimum of 95% deuteration, they were used further for DHX reactions. 100% deuteration was hard to determine in ESI-MS because very labile deuterons will have exchanged already during the spraying process due to humidity in the ESI chamber.

Performing and recording the deuterium/hydrogen exchange kinetics on peptides two methods were applied, the discontinuous and the continuous one. Kinetics were recorded with the discontinuous method when solutions of deuterated peptide (100 µM in 80% (v/v) dTFE in 10 mM ND_4Ac, final pD 5.0) were diluted 1:20 with protonated solvent (80% (v/v) TFE in 10 mM NH_4Ac, final pH 5.0) to 5 µM final peptide concentration at 20°C. Aliquots were taken out of the exchange reaction tube at different time points and were quenched with ice cooling and formic acid addition (end concentration 0.5% (v/v)), so pH was shifted to pH 3.

Deuterated peptides which are integrated into liposomal membranes underwent exchange reactions as follows. Deuterated liposome suspensions were diluted with protonated solvent (50 mM NH_4Ac in H_2O pH 7.5) at a 1:10 ratio and incubated at a defined temperature (70°C). Isotopic exchange reactions were quenched at different time points with ice cooling and addition of formic acid (end concentration 1% (v/v)), so pH was shifted to pH 3. In both cases, mass to charge ratio of the peptide was measured by ESI-MS.

Recording kinetics with the continuous method, solutions of deuterated peptide (100 µM in 80% (v/v) dTFE in 10 mM ND_4Ac, final pD 5.0) were diluted 1:20 with protonated solvent (80% (v/v) TFE in 10 mM NH_4Ac, final pH 5.0) to 5 µM final peptide concentration at 20°C. Immediately after reaction start the continuously changing mass to charge ratio of the peptide was recorded online by ESI-MS.

When exchange reactions were performed at another pH then deuterated peptide was

dissolved in deuterated solvent mixture with the desired pD and exchange reaction was initiated by dilution with protonated solvent of the same desired pH. In line, DHX was proceeded with peptides incorporated into liposomes.

In the experimental series with NSAID treatment, deuterated peptide was diluted to 200 µM with NSAID containing deuterated solution (80% (v/v) dTFE in 10 mM ND_4Ac, final pD 5.0) with a final NSAID concentration of 2 mM. The peptide-NSAID solution was incubated for 1 h at room temperature including initial vortex and 5 min ultrsonification in a waterbath. Afterwards isotope exchange was carried out with a 1:20 (v/v) dilution factor at 20°C. Used NSAIDs were sulindac sulfide ($\varepsilon_{343\,nm}$=15900 M^{-1} cm^{-1}), sulindac ($\varepsilon_{328\,nm}$=13370 M^{-1} cm^{-1}), fenofibrate (no available extinction coefficient, concentration defined by initial weight) and indometacin ($\varepsilon_{316\,nm}$=6150 M^{-1} cm^{-1}).

The number of protected deuterons $D(t)$ as function of time is the measure for backbone dynamics. In an experiment in isotropic solutions, it is calculated by equation 3.4 which accounts for back exchange due to dilution of deuterated solution with protonated solution.

$$D(t) = (m/z_{d,t} - m/z_p) \cdot z - V_f \cdot D_{max} \tag{3.4}$$

$D(t)$ = number of remaining deuterons as a function of time
$m/z_{d,t}$ = mass to charge of D/H exchanging peptide at time point t
m/z_p = mass to charge of protonated peptide
z = charge
V_f = dilution factor (ratio of deuterated to protonated solvent)
D_{max}=number of all labile deuterons per peptide

The number of remaining deuterons in a DHX experiment in liposomes is calculated by equation 3.5 which encounters the shielding of some amide deuterons by the lipid membrane.

$$D(t) = (m/z_{d,t} - m/z_p) \cdot z \cdot (1 - V_f) \tag{3.5}$$

$D(t)$ = number of remaining deuterons as a function of time
$m/z_{d,t}$ = mass to charge of D/H exchanging peptide at time point t
m/z_p = mass to charge of protonated peptide
z = charge
V_f = dilution factor (ratio of deuterated to protonated solvent)

The exchange kinetics were analysed by the software LAPLACE developed and provided by Zhang *et al.* [1997]. It comprises an algorithm based on the maximun entropy method (MEM). Its theory will be explained in detail in the following chapter.

In short, the program displays a non-dimensional occurence distribution of rate constants out of the kinetic progress of exchange reactions. Because the software was developed for the exchange direction from hydrogen to deuterium, the input data had to be converted from the number of protected deuterons to the number of exchanged deuterons (equation 3.6).

$$H(t) = [n-4] - D(t) \tag{3.6}$$

$H(t)$ = number of exchanged deuterons as a function of time
n = number of amino acid residues of the examined peptide
$D(t)$ = number of remaining deuterons as a function of time

The term $[n-4]$ represents the number of hydrogen-bonded amide deuterons in an ideal α-helix with n amino acid residues length. These n-4 amide deuterons were also considered to be the starting point of an exchange reaction, as the exchange velocity of non-hydrogen-bonded deuterons is higher. This is supported by the number of protected deuterons under stop conditions in the experiment. The programme finally calculates a rate constant distribution for each α-helix. All observed deuterons exhibit a distinct rate constant and contribute to this distribution. Integrating the area beyond the occurence distribution with the help of the software ORIGIN, deuterons within their corresponding rate constant range were summarised into populations.

3.2.6 Kinetic Analysis of Isotope Exchange Reactions

The D/H exchange of a peptide is the sum of all single exchange reactions. Each labile deuteron is exchanging to a hydrogen exhibiting reaction kinetics of first order with a characteristic rate constant. As all single reactions occur parallel the exchange reaction of the peptide can be characterised by a distribution of all rate constants.

One approach to characterise the exchange kinetics is to apply a non-linear curve fit with an exponential function containing three terms (equation 3.7).

$$D(t) = A \cdot exp(-k_A \cdot t) + B \cdot exp(-k_B \cdot t) + C \cdot exp(-k_C \cdot t) + D \tag{3.7}$$

The parameters A, B and C are the counts of exchanging deuterons belonging to a certain population with their corresponding rate constants k_A, k_B and k_C . This means exchanging amide-deuterons are grouped beforehand to certain rate populations which represents an approximation of the exchange kinetics.

Exchange kinetics can be also described by all N exchangeable amide deuterons, i.e. the sum of N exponential functions. Omitting hereby the experimental error would lead to an overinterpretation of the data. Therefore a maximum entropy method is most appropriate to apply in this case which was introduced by Zhang *et al.* [1997]. With its

help exchange kinetics can be expressed as a rate constant distribution taking account of the experimental error. With the highest probability it can extract information out of signals with noise because it chooses that state which leads to the maximised entropy.

Having a peptide with N exchangeable hydrogens its exchange kinetics is expressed by equation 3.8.

$$D = N - \sum_{i=1}^{N} exp(-k_i \cdot t) \tag{3.8}$$

It describes the number of deuterons taken up by the peptide or protein (D) as a sum of exponential functions of the respective deuteron i with its specific rate constant k_i and its reaction time t out of N possible exchangeable sites. Applying a Laplace-Transformation the equation can be transformed into equation 3.9.

$$D = N - \sum_{k=k_1}^{k_2} f_k \cdot exp(-k_i \cdot t) \tag{3.9}$$

Exchange kinetics thus are distinguished by the probability f_k for a reaction system containing rate constants between $log\ k$ and $log\ k + \Delta log\ k$. k_1 and k_2 represent the lowest and highest rate constant one reaction system can exhibit. The range is defined by the number of reaction units and the investigated time period. To include also the experimental error into the rate constant probabilities, entropy of the system has to be considered. When maximising the entropy, it means the uncertainty of the system from which a result will derive and is adjusted by its experimental error. Therefore the definition of entropy S by Skilling and Bryan [1984] is introduced (equation 3.10).

$$S = -\sum_{k=k_1}^{k_2} f_k \cdot \left[ln \frac{f_k}{A} - 1 \right] \tag{3.10}$$

By this, f_k can be determined and is understood as an occurrence probability for rate constant k. A is a user-defined parameter which displays the most probable value for f_k when no other conditions are allocated. When all f_k are equal, then entropy S is at its maximum. This means that the rate constant distribution is parallel to the x-axis. So the maximising entropy process has to be validated under the constraint of the experimental error which leads to equation 3.11.

$$\chi^2 = \sum_{t} \frac{(D_t^{calc} - D_t^{exp})}{\sigma_t^2} \tag{3.11}$$

The constraint of the entropy maximisation is now connected to the standard deviation σ_t^2 at time point t with the number of deuterons D_t^{exp} determined in the experiment and the number of deuterons D_t^{calc} calculated from equation 3.9.

With this an occurrence distribution of rate constants as a function of the logarithm

of rate constants is created.

3.2.7 Mass Spectrometry Acquisition

A Waters Q-ToF Ultima mass spectrometer was used for recording ESI mass spectra of 500 µl reaction volume for continuous measurements and 50 µl discontinuous measurements. The solutions were pumped by a gas tight Hamilton syringe, located in a syringe pump with flows of 2 µl/ min^{-1}. Spectra were acquired in a positive-ion mode with one scan for each second and evaluated with MassLynx 4.0 as described in [Stelzer *et al.*, 2008]. For online measurements, spectra were evaluated with an in house made automated evaluation program (Peak Tracer) giving as output a list of mass/charge ratios for each time point. For signal intensity and data amount reasons, 5 scans were accumulated and every 10 seconds a smoothed and centered mass/charge ratio was read out. The triply charged isotope patterns were smoothed with a Savitzky-Golay algorithm with 25 measuring points and a data pitch of 5 scans. Centering was done by finding the centroid point of 80% peak area. The number of remaining deuterons was calculated from the difference of smoothed and centered triply charged ions of the deuterated and the protonated peptide and corrected for its ionization state, the mass of charge carriers and dilution factors as described in 3.2.5 (page 44).

The following set parameters were applied:

- capillary voltage: 2.0 to 3.0 kV (for liposomes: 2.5 kV)
- cone voltage: 60 V (for liposomes: 35 V)
- RF lens 1: 0V ; RF lens: 2V
- source temperature: 80°C
- desolvation temperature: 150°C (for liposomes: 250°C)
- cone gas flow: 50 l h^{-1}
- desolvation gas flow: 300 l h^{-1}
- LM resolution: 5 V
- HM Resolution: 5 V
- collision energy: 10 eV
- ion energy: 1.6 V
- steering: 0.73 V
- entrance: 0.73V
- pre-filter: 5.0
- transport: 3.0 V
- aperture: 6.0 V
- acceleration: 200 V
- mass range m/z: 400-1600; for liposomes m/z: 650-1200
- scan time: 1 s

- intersection time: 0.1 s
- MS profile with dwell and ramp time was adjusted for each sample in order to increase signal intensity of the triply charged isotope pattern
- tube lens: 70-90 V was adjusted to obtain high resolution
- Offset 1: -2.6-3.6 V was adjusted to obtain high resolution
- Pusher: 945 V
- ToF: 9.1 kV
- Reflectron: 36.0 V
- Pusher Cycle Time: 62 µs
- Multiplier: 550 V
- multi channel plate: 1800-2000 V depending on age

Before beginning the DHX experiment, the resolution was tuned with 1 pmol/ µl insulin dissolved in 50% (v/v) methanol and 1% (v/v) acetic acid solution and calibration was performed with 1 pmol/ µl [Glu^1]-Fibrinopeptid B dissolved in 50% (v/v) methanol and 1% (v/v) acetic acid solution.

3.2.8 Selection of Transmembrane Domains With Similarities to the Average Amino Acid Distribution

The occurrence frequencies of amino acid residues within a transmembrane domain (TMD) were compared with the average occurrence in order to select applicable biological TMDs to compare their backbone dynamics with that of the TMD of the amyloid precursor protein.

Two TMD pools of bitopic membrane proteins were subject of comparison. Pool 1 contains approximately 7600 TMDs derived from bitopic membrane proteins classified in 83 PFAM families [Finn *et al.*, 2010] and retrieved from the SIMAP database [Rattei *et al.*, 2010] (including all database updates until 17.07.2008) and pool 2 comprises representative TMDs of human bitopic membrane proteins filtered from the UniProt Knowledgebase (including all updates until 23.10.2009) and analysed by a cluster analysis. The first one was provided by Sindy Neumann from the Bioinformatics Group of Prof. Dmitri Frishman and the latter from Jan Kirrbach from the research group of Prof. Langosch. In both cases all protein sequences were downloaded from the respective website and were scanned with the transmembrane topology predictor PHOBIUS [Kall *et al.*, 2004]. Then they were filtered by their number of transmembrane domains, and only membrane proteins with a single TMD were displayed and its TMD sequences extracted.

The distribution about the average occurrence frequency of amino acid residues within a transmembrane domain was compiled by Dr. Angelika Fuchs (Bioinformatics Group of Prof. Dmitri Frishman). It results from a non-redundant TMD data set of

20342 bitopic membrane proteins annotated in UniProt Knowledgebase (release 10.0) (analysed databases include updates until 29.07.2008). The data set comprises full length TMDs. Their selection procedure is described in detail by Unterreitmeier *et al.* [2007].

The comparison method is based on the absolute difference value calculation between the occurrence frequency value x of amino acid u ($u = A, C, D, ..., W, Y$) of the investigated TMD and the occurrence frequency value b of amino acid u of the average distribution (equation 3.12). Addition of all differences gives ΔX_{sum}.

$$\Delta X_{sum} = \sum_{u}^{20} |x_{u,TMD} - b_{u,average}| \tag{3.12}$$

The smaller the value for ΔX_{sum} is, the more similar is the investigated TMD to the average occurrence frequency of amino acids. Further selection criteria were:

- $\Delta X_{sum} < 40\%$; this threshold is self-defined to minimize the selection
- $|x_{u,TMD} - b_{u,average}|$ as small as possible for leucine, valine, glycine and isoleucine
- TMD contains no proline
- TMD contains no charged amino acid residues
- if possible, amino acid length = 16 or 24

The design of the selected transmembrane domains had the same flanking regions as the A peptides, i.e. the N-terminal KKWK and the C-Terminal KKK flank with either a 16 or 24 amino acids long core representing the selected TMD. If sequences were longer than the named restriction they were shortened without altering the occurrence frequency distribution too much.

4 Results

In this chapter the results on the structural features and helix dynamics of model peptides mimicking the APP transmembrane domain are presented in six sections. Briefly, in section 4.1 (p. 53) the design of the synthetic peptides is explained. In section 4.2 (p. 55) the experimental outcome of the APP TMD's secondary structure and its dynamics is described. Subsection 4.2.3 (p. 62) contains the results on the influence of NSAIDs on the structural behaviour of APP TMD model peptides. Further, experiments addressing the influence of Thr mutations upon the dynamics of the APP TMD cleavage region are summarised in section 4.3 (p. 64). Section 4.4 (p. 69) encompasses the structural differences between the C-termini of $(Leu)_{11}$-Aβ hybrid model peptides representing different cleavage regions. The last two sections 4.5 (p. 77) and 4.6 (p. 80) deal with the comparison of helix dynamics with non-APP-TMDs, composed of either artificial or natural sequences.

4.1 Design of Model Peptides

To answer the research questions referring to the backbone dynamics of the APP transmembrane domain, several series of model peptides were created (see Table 4.1 on p. 54). Their sequences are composed of a hydrophobic core flanked by short hydrophilic sequences, either KKWK or KKKW for the N-terminus and KKK for the C-terminus. These flanking regions increase the solubility of the peptide in organic solvent/water mixtures. The Trp insertion in the N-terminus enables concentration determination of the peptide in a sample. Trp was placed between the 2nd and 3rd Lys in the KKWK motif because the 3rd Lys belongs to the natural sequence of the APP-TMD. Accordingly, all other sequences were designed like this, save the LV peptides and the hybrid APP-TMD peptides.

For the group of A peptides, three sequences were chosen. Peptide A 28–55 holds the full length APP-TMD and has a core region of 24 aa length. The other two peptides represent two thirds of the N- and C-terminal TMD region, respectively, and possess a 16 aa core sequence length.

The group of A peptide mutants also contains A 37-55 peptides with different Thr replacements to investigate the effect of Thr hydrogen bonding to the backbone. The hydroxyl-group was changed into an apolar methyl-group to prevent side chain H-

bonding, and therefore Val was the optimal amino acid candidate. In addition, the T43I variant was chosen because it is an Austrian FAD mutation [Kumar-Singh *et al.*, 2000, van Broeck *et al.*, 2008].

The hybrid peptides consist of a fixed undeca-Leu sequence and a varying octa-APP-TMD-segment which contain different cleavage sites. To increase their solubility, four Lys were added to the N-terminus, as well as one Trp to determine peptide concentration. As a reference, the 8 aa APP-TMD region was replaced by another 8 Leu (peptide L19). Since at the C-terminus only the carbonyl oxygens are not saturated with H bonds but the possibility for amide hydrogens in an α-helix exists, as is the case for partially proteolysed substrate, the APP-TMD region was placed to the C-terminus in order to get the proper information for helix dynamics.

The LV peptides represent a group which was investigated thoroughly by Poschner *et al.* [2009]. To compare their backbone dynamics with APP-TMD peptides of the same length (23 aa), they were again measured under the same experimental conditions used here.

The group of transmembrane domains from non-APP bitopic membrane proteins (KTMD) was chosen to study backbone dynamics of TMDs with an average composition of residues and to compare this dataset with that of the APP-TMD variants. Modified KTMD peptides whose internal Gly were replaced contain a double Gly motif at the N-terminus similar to A 37-55 in order to be able to compare backbone dynamics.

Table 4.1: Sequences of Model Peptides

Group	Peptide Name	Sequence
A peptides	A 28–55	KKWK GAIIGLMVGGVVIATVIVITLVML KKK
	A 28-44	KKWK GAIIGLMVGGVVIATV KKK
	A 37-55	KKWK GGVVIATVIVITLVML KKK
A peptide mutants	A 37-55 T48V	KKWK GGVVIATVIVIVLVML KKK
	A 37-55 T43V	KKWK GGVVIAVVIVITLVML KKK
	A 37-55 T43V/T48V	KKWK GGVVIAVVIVIVLVML KKK
	A 37-55 T43I	KKWK GGVVIAIVIVITLVML KKK
Hybrid APP-TMD peptides	AL35-42	KKKKW LLLLLLLLLLL MVGGVVIA
	AL 39-46	KKKKW LLLLLLLLLLL VVIATVIV
	AL 42-49	KKKKW LLLLLLLLLLL ATVIVITL
	AL 45-52	KKKKW LLLLLLLLLLL IVITLVML
	AL 45-52M	KKKKW LLLLLLLLLLL IVITLVMLMMM
	L19	KKKKW LLLLLLLLLLL LLLLLLLL

(continued)

Group	Peptide Name	Sequence
LV peptides	L16	KKKW LLLLLLLLLLLLLLL KKK
	LV16	KKKW LVLVLVLVLVLVLV KKK
	LV16 G8P9	KKKW LVLVLVLGPVLVLVLV KKK
Natural TMD peptides	KTMD01	KKWK LAVSIFLLGGTGFVFVIYIALWMI KKK
	KTMD02	KKWK IMVLSLFFGLFVFTVAAYIILAFM KKK
	KTMD03	KKWK LLWIVLLFVFGTGILAYIVCAIVM KKK
	KTMD04	KKWK STAVMGAIWMILLFVL KKK
	KTMD05	KKWK AFIWSAYGIALLVVGL KKK
	KTMD06	KKWK VWSAFGITFLAMIILL KKK
	KTMD07	KKWK AGISAGILVFILLLLV KKK
	KTMD08	KKWK VILTFFVGAAILWLLC KKK
	KTMD09	KKWK LGLSVGLVGIVVGTVL KKK
	KTMD10	KKWK CVVLYVASSLFLMVMY KKK
	KTMD11	KKWK YVWGAFGITFLAMLIL KKK
	KTMD12	KKWK VLGAIVSLILIYAFST KKK
	KTMD13	KKWK GTASVALIVILMAIFL KKK
Modified KTMD peptides	mKTMD04	KKWK GGAVMLAIWMILLFVL KKK
	mKTMD05	KKWK GGIWSAYLIALLVVLL KKK
	mKTMD06	KKWK GGSAFVITFLAMIILL KKK
	mKTMD08	KKWK GGLTFFVIAAILWLLC KKK
	mKTMD12	KKWK GGLAIVSLILIYAFST KKK
	mKTMD13	KKWK GGASVALIVILMAIFL KKK

4.2 Structural Properties of the APP Transmembrane Domain

4.2.1 Primary and Secondary Structure of the APP Transmembrane Domain

In order to map the structure of the APP TMD, sequence analysis (method section 3.2.8, p. 50) and secondary structure determination with circular dichroism (method section 3.2.4, p. 43) were performed.

The APP transmembrane domain has a distinct sequence compared to other TMD sequences. Firstly, it harbours two GxxxG motifs at the N-terminal region known to mediate dimerisation and secondly, it contains a high abundance of helix-destabilising residues such as Gly, Val and Ile. Figure 4.1 shows the relative amino acid composition

for the used model peptides in comparison with the average residue composition in TMDs of bitopic membrane proteins.

Leu represents 19% of residues in average TMDs, whereas only 12.5% occur in A 28–55. The β-branched amino acids Ile, Val and Thr comprise 54% in A 28–55 (62.5% in A 37–55 and 50% in A 28-44) compared to the average which is 29%.

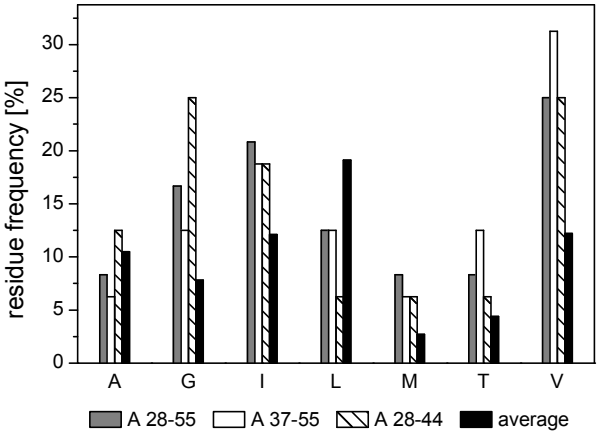

Figure 4.1: Relative amino acid residue composition of A peptide core sequence and the average of TMDs of bitopic membrane proteins. Only residues occurring in the core region of A peptides (16 and 24 aa respectively) are taken for the analysis, excluding the KKWK and KKK flankings.

The circular dichroism analysis for secondary structure determination was performed in 80% (v/v) TFE and 10 mM NH_4Ac. TFE was chosen to support the helical structure of TM peptides, for explanations see section 1.1.4 (p. 14). Water is required to enable isotopic exchange of deuterium to hydrogen to study backbone dynamics. Furthermore, the solvent system mimics the environment of an APP-TMD substrate in the water-containing lumen of the γ-secretase (see section 1.3.3, p. 26).

All three peptides show similar circular dichroism spectra (Figure 4.2 A). The CD spectrum of A 28–55 shows two negative bands at 206.8 nm and 219.5 nm with 32500 and 26600 deg cm^2 dmol^{-1} as mean residue ellipticity ($[\Theta_{mr}]$), an intersection point with the x-axis at 199 nm and a positive band at 190.1 nm with 59400 deg cm^2 dmol^{-1}. These indicators relate closely to those of a regular, in water soluble α-helix: two negative bands at 208 nm and 222 nm with a magnitude of 30000 deg cm^2 dmol^{-1}, an intersection point with the x-axis at 200 nm and a positive band at 190 nm with approximately 70000 deg cm^2 dmol^{-1} [Park *et al.*, 1992].

The CD spectrum of A 28-44 has its negative band intensities slightly increased by 1100 and 3700 units and its positive band intensity slightly decreased by 7600 units compared to those of A 28–55. Its intersection point with the x-axis is shifted to 198 nm. These indicators characterise a slightly decreased α-helix and a slightly increased random coil portion, meaning that the equilibrium between folding and unfolding is shifted towards unfolded structure. For A 37–55, the CD spectrum is similar to that of A 28–55.

The quantitative analysis of the CD spectra with CDNN/ Pepfit confirms the helicity

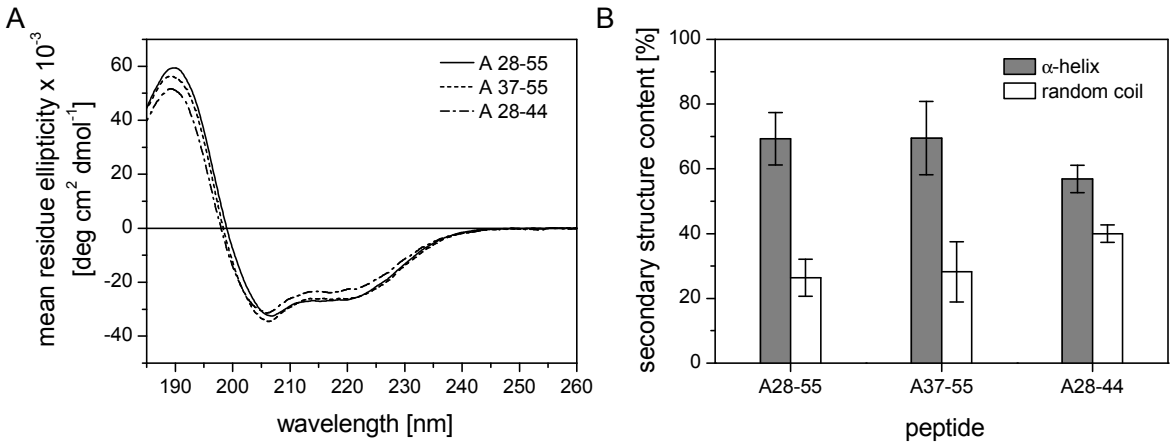

Figure 4.2: Secondary structure analysis of APP TM peptides. A: Average CD spectra of Aβ peptides, 30 µM in 80% (v/v) TFE and 10 mM NH_4Ac, pH 6.3; path length = 0.5 mm; B: α-helix and random coil fractions (evaluation range is 185-260 nm). All values represent means of 3-6 independent measurements.

ranking for the A peptides (Figure 4.2 B): A 28–55 $\approx$ A 37–55 $>$ A 28–44. The α-helix values are 69.3 $\pm$ 8.1% for A 28–55, 69.5 $\pm$ 11.3% for A 37–55 and 56.9 $\pm$ 4.2% for A 28–44. For random coil structure the values are 26.4 $\pm$ 5.7%, 28.2 $\pm$ 9.3% and 40.0 $\pm$ 2.7% respectively. The fractions for β-sheet and β-turn structure are in sum below 4%.

Depending on whether peptides unfold in a dynamic equilibrium locally or globally there are two possible interpretations of secondary structure fractions for a peptide. Part of the peptide molecules unfold completely or all peptide molecules harbour both a helix and a random coil region. Both structure types result in the measured CD spectrum as a linear combination. Table 4.2 expresses the count of residues assigned to secondary structure types which they are part on average.

Table 4.2: Residue Count in Secondary Structure

peptide	α-helix	random coil
A 28–55	21.5 aa	8.5 aa
A 37–55	16.0 aa	6.5 aa
A 28–44	13.7 aa	9.2 aa

All in all, the secondary structure analysis of the A peptides revealed dominantly α-helical shaped structures. This is requisite for investigating their helix dynamics with deuterium hydrogen exchange experiments coupled to mass spectrometry. It is plausible to assume that the ranking of α-helicity results from the excess of Gly and the deficiency of Leu in A 28–44. In face of the helix-destablising Gly-rich motif in A 28–55, its helix is strengthened by the C-terminal peptide extension which has the same sequence as in A 37–55.

4.2.2 D/H Exchange and Backbone Dynamics of the APP Transmembrane Domain

The rationale of this experiment is to elucidate the backbone dynamics of the α-helical APP-TMD with the help of three model peptides consisting of different regions of the APP-TMD. Backbone dynamics in α-helices is hallmarked by the stability of the intramolecular hydrogen bond network. As explained in sections 1.1.4 (p. 11) and 1.2.2 (p. 18), the frequency of local hydrogen bond opening and closing is probed by the isotope exchange between amide hydrogens and deuterons from the bulk solvent because exchange occurs only in an opened conformation due to accessibility of the hydroxide catalyst.

The backbone dynamics of A peptides was measured with deuterium hydrogen exchange experiments coupled to electron spray ionisation mass spectrometry. They were performed by Milena Duerrbaum (method section 3.2.5, page 44) [Dürrbaum, 2010]. The experiment was carried out in a back exchange regime. It was initiated by diluting the fully deuterated peptide (95% D) in protic solvent (80% (v/v) TFE and 10 mM NH_4Ac, at final pH 5) in a 1:20 (v/v) ratio to 5 µM as final concentration at 20°C. The mass spectrometer recorded continuously every second a mass spectrum with m/z values of the deuteron exchanging peptide. Calculating the difference of the m/z values of the deuteron exchanging peptide and the fully protonated peptide corrected by forward exchange gives the number of deuterons protected by hydrogen bonds (see equation 3.4 in section 3.2.5, p. 46). The stability of the helix-forming hydrogen bond pattern is thus reflected by the amide exchange kinetics.

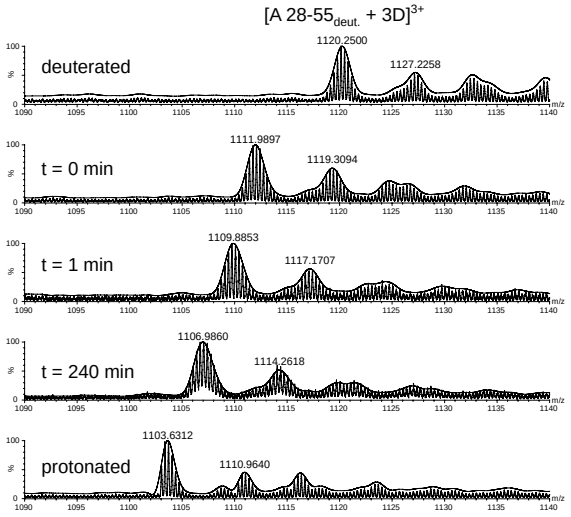

Figure 4.3: Representative mass spectra of A 28–55 from a DHX experiment. Mass spectra were continuously recorded. The isotopic pattern of the threefold charged A 28–55 is depicted in its fully deuterated and protonated state and exchanging states at t=0 (measured under stop conditions), t = 1 min and t = 240 min. Note that the exchange of the heavier deuteron against hydrogen within the peptide leads to lower m/z values in the course of time.

Figure 4.3 (p. 58) shows the isotope pattern of the three-fold positively charged A 28–55 at different exchange states. The gradual shift of the isotope pattern from high to low m/z values indicates an EX2 mechanism (see section 1.2.2, p. 20). Evaluating all isotope patterns over time gives kinetics where different deuterons exchange with different rate constants (Figure 4.4, p. 60). These two observations mean on one hand that the closing rate of hydrogen bonds is higher than the intrinsic isotope exchange rate. And on the other hand it indicates that the opening and closing of H-bonds do not follow a cooperative effect since all deuterons would exchange with nearly the same rate constant demarcating global H-bond folding and unfolding. Therefore, local unfolding of the peptide is the present case. From this, one can conclude that the fractions of secondary structure determined by CD do not rely on differently structured peptide species, but on one peptide species exhibiting both structure types in different regions within the peptide (see section 4.2.1, p. 57). In the kinetic perspective this means also that both structures are interchangeable over time in each single peptide region remembering that the equilibrium constant can be described by its portions of unfolded and folded and by its rate constant of the forward and backward reaction respectively.

The set of A peptides was measured to localise the regions of differently exchanging deuteron populations. Figure 4.4 (p. 60) shows the kinetics of this experiment. For comparability the number of protected deuterons is normalised to the maximum number of hydrogen-bonded amide deuterons in an ideal α-helix. This number is the number of peptide residues subtracted by one representing the N-Terminus and further subtracted by three amide deuterons lacking H-Bond acceptors at the N-Terminus. For A 28–44 and A 37–55 the number is 19 and for A 28–55 it is 27 deuterons.

Since A 28–44 possesses a Gly rich region, this peptide exhibits the highest structural flexibility. A 28–44 begins at t=0 with 77.9 ± 1.4% deuterons (14.8 ± 0.3 D), i.e. 4.2 ± 0.3 of 19 potentially hydrogen-bonded amide-deuterons have exchanged as soon it was diluted in protic solvent under quench condition (pH 2.5 on ice). Hence, these exchanged amide deuterons did not participate in strong H-bonds. In general, deuterons which reside at the termini or the side chains exchange immediately after dilution at stop conditions (see section 1.2.2, p. 19).

Comparing DHX with CD data, the A 28–44 sequence can be divided into an unstructured and a helical region, whereby approx. 9.2 residues belong to the unstructured region and 13.7 residues to the helical region (see Table 4.2 in section 4.2.1, p. 57). The amount of residues within the unstructured region coincides with the number of already exchanged amide deuterons at t=0 min, which accounts for approximately 7-8 residues. These comprise amide deuterons residing in lower time-averaged fractions of H-bonds and thus belonging to residues in the unstructured region and amide deuterons of the last four N-terminal residues. Further, the total number of exchanging amide deuterons (14.5 deuterons within 40 min exchange time) coincides with the residue count attributed to helical structure, that is that these amide deuterons hydrogen-bond

in average more often than deuterons of the above mentioned population. In this case, a full exchange of the α-helical part of A 28–44 was recorded.

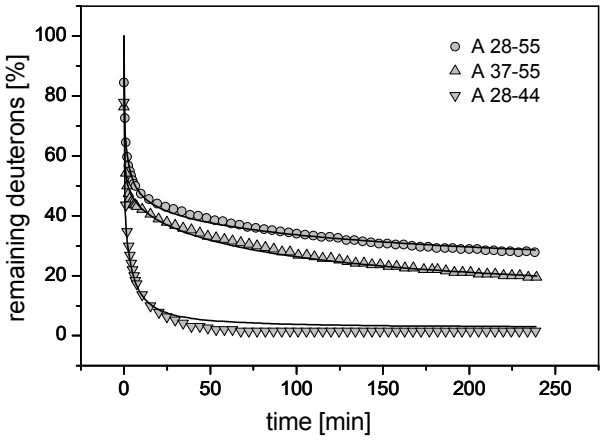

Figure 4.4: D/H exchange kinetics of APP-TMD model peptides. Measurement was performed in 80% (v/v) TFE and 10 mM NH_4Ac, pH 5 at 20°C with a 1:20 dilution and a final peptide concentration of 5 µM. The fraction of remaining deuterons is defined by the ratio of the absolute number of remaining deuterons to the maximum number of hydrogen-bonded amide deuterons in an ideal α-helix (D=19 for A 28–44 and A 37–55 and D=27 for A 28–55). Data points at t=0 min correspond to the numbers of amide deuterium atoms seen after exchange under stop conditions. The data were fit with a maximum entropy method assuming D(t=0 min)=19 (A 28–44 and A 37–55) and D(t=0 min)=27 (A 28–55)(continuous lines). All values represent means of 3 to 4 independent measurements with an average standard deviation of ± 0.8%.

Exchange kinetics of A 37–55 starts with 76.3 ± 3.9% deuterons (14.5 ± 0.7 D) similar to A 28–44. In accordance with Table 4.2 (p. 57), approx. 6.5 residues of A 37–55 are assigned to random coil. Obviously, amide deuterons of these residues belong to the population of the already exchanged amide deuterons at t=0 min (being 4.5 + 3 D). From these, approx. one is assigned to helical structure, since it participates in a H-bond which has a high opening frequency. Within the measuring time, 11 H-bonded amide deuterons have exchanged out of 16 residues assigned to α-helical structure by CD. Hence, a complete exchange of A 37–55 needs more than 4 h.

For A 28-55, a deuteron protection of 84.4 ± 0.7% (22.8 ± 0.2 D) is assessed at t=0 min. 4.2 amide deuterons in very low time-averaged H-bonds and 3 non H-bonded amide deuterons from the N-terminus are lost already at this time point. These 7.5 deuterons can be confirmed by the residue count of 8.5 attributed to random coil (Table 4.2, p. 57). For the helix region it is likewise. A full kinetic coverage of A 28–55 is not given. 15.2 exchanging deuterons determine the kinetics within 4 h. Note please, though the analysis here refers to average values, there is always a distribution of peptides with different exchanged deuteron counts at a time as seen by the broadening of the isotope pattern compared to the $^{12}C/^{13}C$ isotope distribution of exclusively hydrogen or deuteron labelled peptides.

Comparing the kinetics between the model peptides, the order of exchange kinetics

is as follows (from slow to fast): A 28–55 < A 37–55 ≪ A 28–44. This indicates that in A 28–44 H-bonds are in average more open than closed compared to H-bonds of the other A peptides. From this, one can infer that the Gly rich N-terminal region is very dynamic, whereas the cleavage region of the APP transmembrane domain exhibits moderate to fast dynamics.

A software based on Laplace transformation and the maximum entropy algorithm evaluates the DHX data taking the standard deviation into account and extracts a rate constant distribution with distinct deuteron populations, which is shown in Figure 4.5 A (method section 3.2.6, p. 47). The exchange velocity of each amide deuteron is described with its individual rate constants. Taking all together results in one characteristic distribution. This is normalised to the maximum number of hydrogen-bonded amide deuterons in an ideal α-helix. To quantify the populations, integration limits were set as such as to get a reasonable separation of populations.

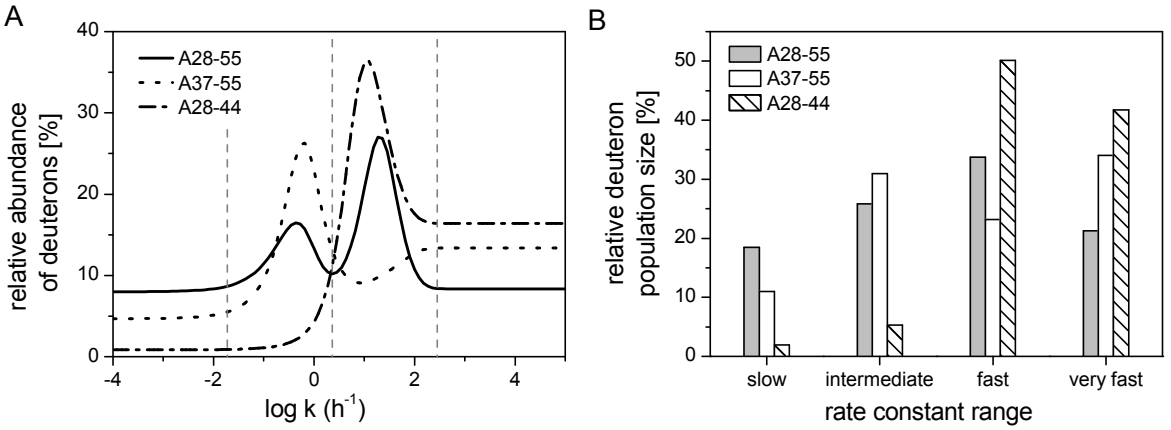

Figure 4.5: Kinetic analysis of D/H exchange with the Maximum Entropy Method. A: Distribution of rate constants. The relative abundance of exchanged deuterons is represented as a function of the decadic logarithm of rate constants for the amide deuterons of the APP-TMD model peptides. For comparability the distribution of rate constants after MEM analysis was normalised to the maximum number of hydrogen bonded amide deuterons in an ideal α-helix. Dashed vertical lines signify the boundaries between four amide deuterium populations "slow, intermediate, fast and very fast". Boundaries are log k (h^{-1}) -1.7273 ($3.122 \cdot 10^{-4}$ min^{-1}), 0.3636 (0.0385 min^{-1}) and 2.4545 (4.746 min^{-1}). B: Relative amount of exchanged deuterons, as determined by the integration of the area beneath the distribution curve within the kinetically distinct populations defined in A.

A 28–55 has two distinct populations with rate constants from $3.122 \cdot 10^{-4}$ to 0.0385 min^{-1} (max at $7.2 \cdot 10^{-3}$ min^{-1}) and from 0.0385 to 4.746 min^{-1} (max at 0.3 min^{-1}). A 28–44 has a single distinct population with high rate constants overlapping with those of the fast exchanging deuteron population of A 28–55 (max at 0.2 min^{-1}), but occurring with a higher relative abundance. The amide deuterons of A 37–55 concentrate in a population coinciding with the intermediate exchanging deuteron population of A 28–55 (max at $11.0 \cdot 10^{-3}$ min^{-1}). Though comparison of backbone dynamics with different helix lengths should be regarded with care (the shorter the

peptide, the higher the impact of helix fraying on the whole peptide), it can be concluded that the full length APP TMD peptide has two regions with distinct dynamics which are reflected by the shorter APP-TMD variants A 28–44 and A 37–55.

Table 4.3: Absolute number of exchanging deuterons from MEM analysis

population	A 28–55	A 37–55	A 28–44
slow	5.0	2.1	0.4
intermediate	7.0	5.9	1.0
fast	9.1	4.4	9.5
very fast	5.7	6.5	7.9

By integrating the area beneath the rate constant curves from MEM analysis within distinct boundaries (demarcated in Figure 4.5 A), a separation into populations is established, illustrated in Figure 4.5 B as a bar plot and compiled in absolute deuteron numbers in Table 4.3. For fast exchanging deuterons, the population size of A 28–44 is twice as high as for A 28–55 and 8% higher than that of A 37–55. The very fast exchanging deuterons include those which exchange immediately after dilution with protic solvent owing to the fact that they belong to random coil region and those which exchange in the first 20 seconds. The half life $t_{1/2}$ of 0.15 min for log k (h^{-1}) 2.4545 (4.746 min^{-1}) assuming a reaction of first order ($t_{1/2} = \frac{ln\,2}{k}$) is supporting this. Those deuterons which exchange beyond 240 min belong to the slow and partly to the intermediate deuteron population. Their half life is higher than 416 min (corresponding to log k (h^{-1}) = -1). Here, the order of population size for each TM peptide is reversed and confirmes the interpretation of the recorded kinetics depicted in Figure 4.4.

The DHX results reveal global information of the helix dynamics in peptides. Due to the design of the chosen model peptides one can distinguish a very dynamic GxxxG region and a moderately dynamic region with almost all cleavage sites in the full length APP TMD.

4.2.3 D/H Exchange and Backbone Dynamics of the APP Transmembrane Domain in Presence of NSAIDS

As mentioned in the introduction, NSAIDs are discussed as γ-secretase modulating agents (see section 1.3.5, page 33). Accordingly, model peptides were treated with NSAIDs to get information about their impact on APP TMD helix dynamics.

The experimental procedures are explained in section 3.2.5 (page 46). In brief, the NSAIDs sulindac sulfide, sulindac, fenofibrate and indometacin dissolved in 80% (v/v) dTFE and 10 mM ND_4Ac (pD5) were added to a deuterated A 28–55 peptide solution. Final concentrations of peptide and NSAID were 200 µM and 2 mM respectively. After one hour equilibration time, the deuterated peptide-NSAID solution was diluted in protic solvent to initiate DHX. As the research of Richter *et al.* suggested a binding of

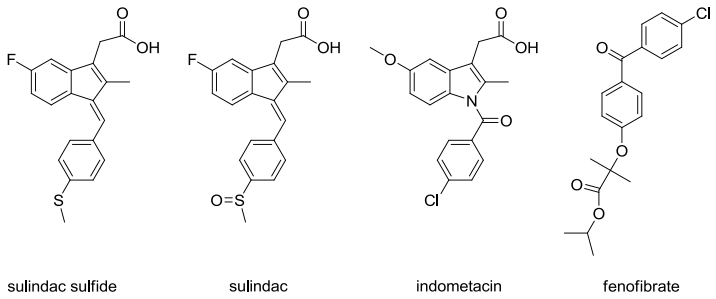

Figure 4.6: Structure of used NSAIDs

sulindac sulfide to the GxxxG motif of the APP TMD with an apparent dissociation constant in the low micromolar range and in the previous section this region was identified to be very dynamic, it is expected that any impact of an NSAID should occur in the short time range [2010]. Therefore, one hour recording time was believed to be sufficient.

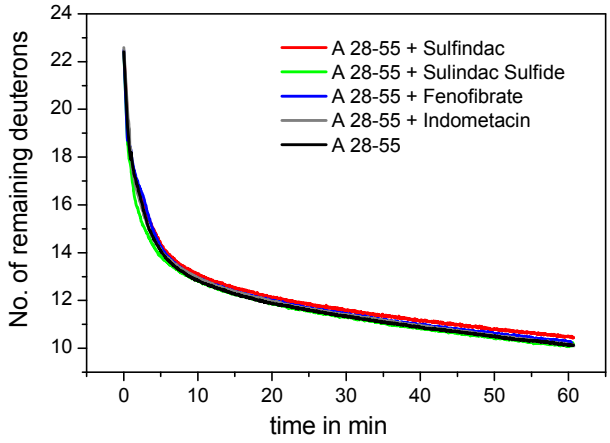

Figure 4.7: D/H exchange kinetics of A 28–55 in presence of NSAIDs. Measurement was performed in 80% (v/v) TFE and 10 mM NH_4Ac, pH 5 at 20°C with a 1:20 dilution and a final peptide concentration of 10 µM and 1:10 peptide/NSAID ratio. Data points at t=0 min correspond to the numbers of amide deuterium atoms seen after exchange under stop conditions. All values represent means of 3 independent measurements with an average standard deviation of ± 0.16 D.

The results of these experimental series indicate no influence by NSAIDs. The DHX kinetics of A 28–55 alone and in presence with any of the NSAIDs are almost identical. During the first 5 min there seems to be some deviation, but is is not significant as the standard deviation of all kinetics overlap with each other. Thus, NSAIDs do not impair the hydrogen bond stability of the APP-TMD under the used conditions.

The kinetics of A 28–55 alone matches with the kinetics of A 28–55 for a dilution from 100 to 5 µM (see Figure 4.4, p. 60). As long as the dilution factor is the same, the kinetics between both concentrations are comparable.

4.3 Impact of Threonine Backbonding on Structural Properties of APP TMD

The sequence of the APP TMD possesses two Thr residues. Thr is known to hydrogen bond to the helix backbone of membrane proteins (commented in section 1.1.1, p. 7) [Gray and Matthews, 1984]. This phenomenon was confirmed in Aβ 26-55 peptide with molecular dynamics simulations performed by Daniel Hornburg [2010]. This motivated further experimental research into APP TMD backbone dynamics. The model peptide A 37–55 was used to see a potential increase in helix dynamics with maximum sensitivity. The residue of choice was Val because the replacement of the polar hydroxyl group by an unpolar methyl group prevents side chain H-bonding. Thr occur on positions 43 and 48 along the APP TMD (Aβ numbering). Single and double mutants were analysed. Additionally, a T43I mutant was created, as it represents the Austrian FAD mutant [Kumar-Singh *et al.*, 2000, van Broeck *et al.*, 2008]. Both circular dichroism and DHX analysises were performed to study the effect of mutants which lack H-bonding by the Thr residue.

4.3.1 Secondary Structure of APP TMD Threonine Mutants

Before DHX analysis can be carried out, the A 37–55 mutant peptides had to be confirmed in their α-helicity in order to conduct helix dynamics comparisons. Further purpose was to study the impact of mutations on the structural flexibility. The experimental procedure for CD is described in section 3.2.4 (p. 43). In short, ellipticities from 185 to 260 nm were recorded for peptides with 30 µM concentration, dissolved in 80% (v/v) TFE and 10 mM NH_4Ac, pH 5.

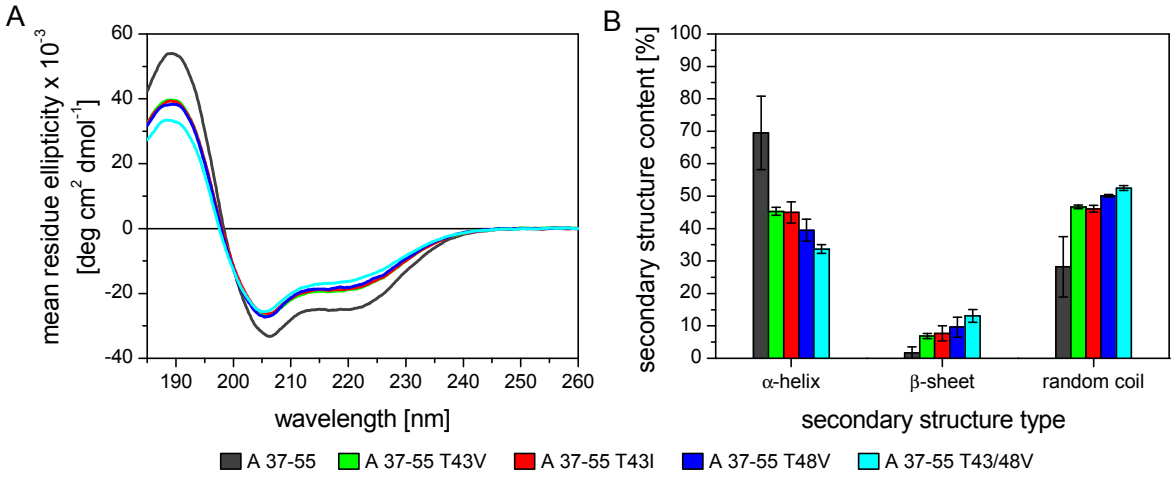

Figure 4.8: Secondary structure analysis of A 37-55 and its Thr mutants. A: Averages of 3 independently measured CD spectra for A 37–55 wild type and each mutant (30 µM in 80% (v/v) TFE and 10 mM NH_4Ac, pH 5, path length = 1 mm); B: α-helix, β-sheet and random coil fractions, CDNN/ Pepfit evaluation from 185 to 260 nm. n=3

Analysing the CD spectra, an increased random coil content of the mutants is observed. A 37–55 forms mainly α-helix with two negative bands at 206.4 nm and 219 nm ($[\Theta_{mr}]_{206.4nm}$= -33200 deg cm^2 dmol^{-1}) , a positive band at 189.3 nm and an intersection with the x-axis at 198.3 nm. The mutant peptides exhibit similar line shapes compared to A 37–55, yet with slight variations. The wavelengths of the maxima of the positive band, the minima of the negative bands and the intersection point shift slightly towards smaller wavelengths within 1 nm difference (blue shift). The order is as follows: A 37-55 > A 37-55 T43I > A 37-55 T43V > A 37-55 T48V > A 37-55 T43V/ T48V. This observation implies the increase of the random coil portion in the mentioned order. The double mutant A 37–55 T43/48V causes the strongest helix-into-random-coil conversion. Due to some β-sheet contents, the shifts towards lower wavelengths are not that pronounced as it would be without it. Taking into account the linear combination of all secondary structure types, a β-sheet structure shifts the helix markers towards higher wavelengths save the second negative band at 222 nm which is shifted towards lower λ.

One may wonder why the absolute ellipticity magnitudes do not reflect the absolute secondary structure content values from CDNN/Pepfit. Instead of 45% helicity for T43 mutants reported by CDNN/Pepfit, a qualitative analysis of the single mutant spectra would give 50-60% α-helicity. This estimate is based on the reconstruction of CD-spectra by linear combination of the pure secondary structure types taken from the peptide spectral information of the CDNN deconvolution data set (see Appendix A Figures A.1 and A.2, p. 145) [Poschner *et al.*, 2007]. Therefore the CDNN/Pepfit evaluation shall be taken with care and comparison between peptides shall be focused more on their CD spectra.

Taken together, the CD analysis of the Thr mutants shows that the prevention of additional side chain H-bonding to the backbone in the APP-TMD induces a gradual equilibrium shift from α-helix to random coil depending on the number of mutations. In other words, the structural flexibility is increased.

4.3.2 D/H Exchange and Backbone Dynamics of APP TMD Threonine Mutants

The differences in α-helix dynamics of the A 37–55 mutant peptides were examined by DHX experiments at pH 5. The slowest kinetic is represented by A 37–55 wild type, followed by A 37–55 T43V, A 37–55 T43I, A 37–55 T48V and A 37–55 T43/48V (see Figure 4.9). The standard deviations of the number of protected deuterons are on average 0.3 deuterons within the first 20 min, with further reaction time the standard deviation is reduced to 0.1 deuteron on average. Hence, the standard deviations are small enough to distinguish the differences between kinetics. At timepoint 10 seconds the peptide order for exchanged deuterons is as follows: A 37–55 wild type, A 37–55 T48V,

A 37–55 T43V, A 37–55 T43I and A 37–55 T43/48V. The exchange of A 37–55 T48V is at the beginning slightly slower than for variant T43I which is reversed after 3 min exchange time. For comparison of absolute values please see Table A.1 in Appendix A (p. 146).

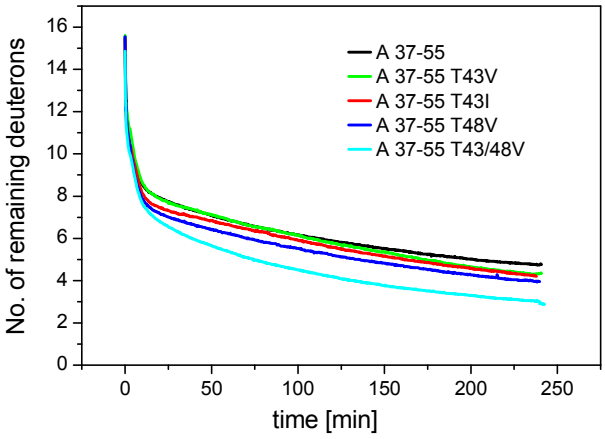

Figure 4.9: D/H exchange kinetics of A 37–55 and its threonine mutants. Online measurement was performed in 80% (v/v) TFE and 10 mM NH_4Ac, pH 5 at 20°C with a 1:20 dilution and a final 5 µM peptide concentration. Data points at t=0 min correspond to the numbers of amide deuterium atoms seen after exchange under stop conditions. All values represent means of 3 independent measurements with an average standard deviation of ± 0.17 D.

Table 4.4: Differences in protected deuterons for Thr mutant DHX at pH 5

$\Delta(D_t)$	A 37–55	T43V	T43I	T48V	T43/48V
19-D_{10s}	5.1	5.7	6.1	5.5	6.3
D_{10s}-D_{240min}	9.1	9.0	8.8	9.6	9.6

Examining Table 4.4 (p. 66), four major amide deuteron groups can be distinguished:

1. Three amide deuterons which do not H-bond at the N-terminus because they lack carbonyl oxygen partners and they do not lie within detection range.

2. Extremely fast exchanging deuterons which are not experimentally accessible due to limited time resolution. These correspond to the difference between 19 (number of H-bonded amide deuterons in an ideal α-helix) and the first real measuring point, in this case 10 sec. Timepoint 0 is measured at quench conditions, at pH 2.5-3, and therefore would not reflect the exchange at the given pH.

3. Amide deuterons which exchange between 10 sec and the endpoint of the measurement (240 min).

4. Slowly exchanging deuterons exchange beyond the end point of measurement (240 min).

Comparing difference values of $\Delta(\mathrm{D}_{10s}\text{-}\mathrm{D}_{240min})$, 9 to 10 deuterons are mapped within the experiment which account for 50% at pH 5. Within the first 10 seconds 5 to 6/7 deuterons have already exchanged ($\Delta(19\text{-}\mathrm{D}_{10s})$. The differences among the model peptides meet the expectations of the experiment. As the single mutants lack one Thr, one amide deuteron less is protected by the hydroxyl mediated H-bond. For the double mutant two amide deuterons less are protected. Which amide deuterons are concerned by these mutations is not revealed by the DHX experiment. But imagining the additional support to the residue $i-4$, the $i-4$ amide deuteron is still able to contact the carbonyl oxygen of residue $i-8$. Abolishing the additional Thr side chain H-bond donor support decreases the chances that residues i and $i-4$ hold together and this decreases the chances of H-bonding between $i-4$ and $i-8$ and/ or the distance between the two turns is extended and thus the amide deuterons of neighbouring amino acids (e. g. at positions $i-1/2/3$) have lower probabilities to occupy in a H-bond.

Another possibility, which needs to be taken into consideration, is that not the amide deuteron is protected by the Thr side chain but the side chain itself is retarded for hydrogen exchange. However, this consideration is not likely because exchange of the Thr side chain is still faster when compared to an unprotected amide deuteron. The exchange at the Thr side chain is catalysed by hydronium-ions below pH 7 and is diffusion controlled. The pKa for O-protonation of the Thr hydroxyl group is approximately 16, therefore the resulting rate constant is still higher than that for the unprotected amide deuteron (see equation 4.1 with diffusion rate constant $k_D = 10^{10} M^{-1} s^{-1}$ and see section 1.2.2, p. 19) [Englander *et al.*, 1972].

$$k_{ex,Thr} = 10^{\Delta pK_a} \cdot k_D \cdot [H_3O^+] = 10^{(16-(-1.74)+10-pH)} s^{-1} \tag{4.1}$$

The maximum entropy analysis reports a rate constant distribution for DHX kinetics at pH 5 (see Figure 4.10, p. 68). It should be noted that the defined deuteron populations are incomparable with groups introduced in Table 4.4.

Since the MEM analysis shows two distinct peaks, groups are indexed as slowly, intermediately fast, fast and very fast exchanging deuterons. The "very fast" group accounts for deuterons which exchange immediately after dilution under quenching conditions and within the first 10 seconds at pH 5 (see Table 4.4). The number of protected deuterons which remain at 240 min exchange time are described by the slow and partly by the intermediate population.

The two peaks for "intermediate" and "fast" deuteron population represent the experimentally accessible DHX kinetics. From this, the T48V variant has two distinct amide deuteron types because its peaks are well separated from each other. Whereas for the T43I and T43V variants only one of both peaks is well distinguished from the baseline and is assigned to intermediately fast exchanging deuterons. As the MEM analysis takes into account the standard deviation, a peak is then well distinguished

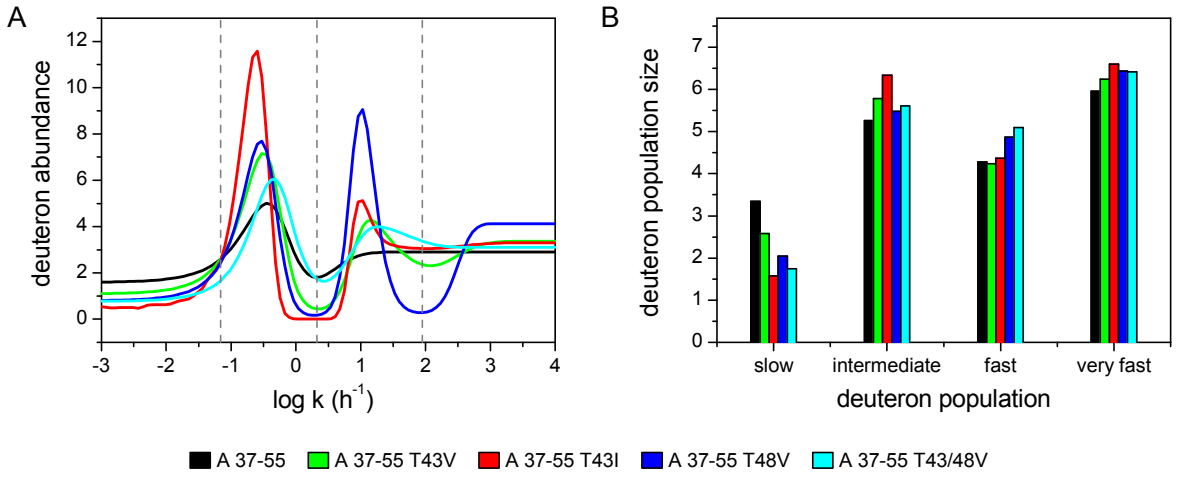

Figure 4.10: MEM Analysis of D/H exchange of A 37–55 wild type and Thr mutants at pH 5. A: Rate constant distribution. The abundance of exchanged deuterons is represented in dependence of the decadic logarithm of rate constants for the amide deuterons of the A 37–55 peptides. Using MEM, D=19 was set, the maximum number of hydrogen bonded amide deuterons in an ideal α-helix. Dashed vertical lines signify the boundaries between four amide deuterium populations. B: Population sizes of different rate constant ranges for A 37–55 threonine mutants. The amount of exchanged deuterons is depicted in bars determined from the integration of the area beneath the distribution curve within the kinetically distinct populations defined in A.

from the baseline when the standard deviation is small enough. Therefore, it seems that for the T48V variant the fast exchanging amide deuterons exhibit a better defined rate constant region than the others for this range. It is likely that increased flexibility in a peptide region can infer pronounced dynamics with increased rate constant variety as seen in the fast population. Since three peptides have mutation T43 in common and show this phenomenon, one may assume that the region around T43 is more dynamic, though the absolute numbers for fast deuterons are higher for the T48 mutant and double mutant than for the T43 mutants and wildtype. The number for intermediate deuterons is slightly higher for the single T43 mutants than for the wildtype at the expense of lower abundance of slowly exchanging deuterons. In addition, A 37–55 has a rate constant distribution with low abundant peaks. One can even say that A 37–55 harbours deuterons with a spectrum of different rate constants.

To summarise the DHX and MEM analysis, the increasing number of Thr mutations goes in hand with increased helix dynamics. The helix destabilisation is likely caused by the lack of an additional H-bond donor by the side chains in position 43 and 48. Also, mutations at position 43 induce a slight increase in kinetics which is seen within the first 3 min of DHX and on the peak broadening of the fast deuteron region in MEM analysis. This suggests that the fast exchanging region is localised around position 43 and mutant T43 increases its dynamics. The double mutant shows all in all more backbone dynamics which is substantiated by the endpoints of DHX and by the population size and maximum shift towards higher rate constants of intermediately

fast and fast exchanging deuterons in MEM analysis. Model peptide T48V exhibits backbone dynamics ranged between the T43 and the double mutant. DHX progression and its higher abundance of fast deuterons at the expense of slow deuterons motivate this finding.

4.4 Structural Properties of Hybrid APP-TMD-Peptides

Since the backbone dynamics of the APP transmembrane domain could affect its sequential processing by γ-secretase, it is of interest to elucidate the helix dynamics of the processed APP TMD parts. Therefore, hybrid peptides were created which have a poly-Leu motif as a helical host sequence and an APP-TMD octapeptide motif as guest sequence. The C-terminal residue reflects a γ-secretase cleavage site, save AL 45-52/ AL 45-52M (see Figure 4.11). The AL peptide sequences overlap in a tri- to tetrapeptide manner.

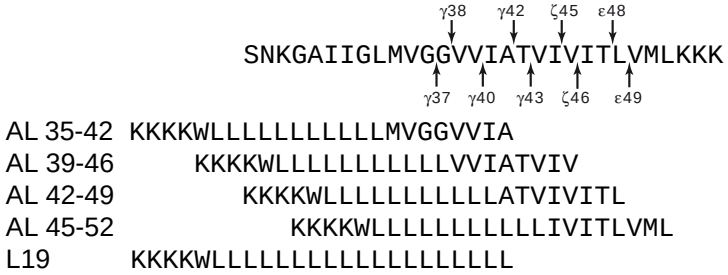

Figure 4.11: Alignment of APP-TMD with hybrid APP-TMD-peptides, including the γ-cleavage sites.

Poor helicity of AL 39-46 and poor solubility of AL 35-42 was observed in 80% (v/v) TFE and 10 mM NH_4Ac, pH 5. Beside loss of comparable helicity, also DHX kinetics was too fast, since approximately three amide deuterons formerly assigned to the hydrogen-bonded population were already lost for detection. Both CD and DHX studies were thus performed with these model peptides embedded into liposomal membranes instead of dissolving them in isotropic solvent. Changing into a more hydrophobic environment with a polarity gradient supports the α-helix' hydrogen bond network in the model peptides and thus facilitates the backbone dynamics evaluation of the guest sequence.

4.4.1 Liposome Integration and Secondary Structure of Hybrid APP-TMD-Peptides

The CD analysis of the hybrid APP-TMD peptides was carried out in DLPC/DLPS/DLPE (3/1/1 (w/w/w) ratio) liposomal membranes with a nominal peptide concentration of 2 mol% at 70°C. Liposome preparation was performed with an HFIP/cyclohexane emulsion because the phase separation is slower between both phases than for the

TFE/cyclohexane emulsion and preserves longer a better peptide/ lipid distribution before it reaches the frozen state (see method section 3.2.2, p. 42). Further, HFIP seems to stabilise better the helix conformation of AL 35-42 and AL 39-46 peptides. In 80% (v/v) TFE and 10 mM NH_4Ac, pH 5, 3% helicity was determined for AL 39-46, and for AL 35-42 CD data do not exist as it dissolved poorly in this solvent. Once a peptide turns into β-sheet conformation, a lipid environment will not reverse this conformational change. Therefore the state of the model peptides needs to be helical in solution in order to be also helical in the liposomal membrane. Table 4.5 enlists the parameters for peptide integration. The nominal final peptide concentration in the liposome suspension was 62.5 µM. Peptide integration into liposomes is reflected by the peptide yield, which is the ratio of measured and initially applied peptide concentration, and the experimentally determined peptide/lipid ratio (see method section 3.2.3, p. 41). Very good peptide yields were obtained for all model peptides apart for L19 which is the reference peptide. L19 has a very long hydrophobic sequence. One explanation could be the increased probability to turn into aggregates and thus not being able to integrate themselves into the lipid bilayer. Another reason would be that the membrane thickness is to small for the L19 integration and causes as such a hydrophobic mismatch which L19 is less able to overcome than the other model peptides leading again to poor integration. The experimentally obtained P/L ratio is almost twice as high as the nominal one apart for L19. This is probably due to pipetting errors since stock solutions were used in which lipids are dissolved in volatile chloroform. Additionally, there is a reasonable probability that a considerable amount of aggregated or insoluble lipids was removed with the centrifugation step after the sonification step for SUV formation.

Table 4.5: Peptide Integration into Liposomes

peptide	peptide concentration [µM]*	peptide yield [%]	lipid concentration [mM]**	P/L ratio [mol %]
L19	27.6 ± 6.8	44.2 ± 10.9	1.53 ± 0.29	1.8 ± 0.2
AL 35-42	73.1 ± 11.1	116.9 ± 17.8	1.42 ± 0.09	5.1 ± 0.5
AL 39-46	60.0 ± 10.0	96.0 ± 15.9	1.51 ± 0.18	4.0 ± 0.3
AL 42-49	49.6 ± 12.5	79.4 ± 20.0	1.34 ± 0.08	3.7 ± 0.9
AL 45-52	50.4 ± 9.2	80.6 ± 14.7	1.37 ± 0.12	3.6 ± 0.8
AL 45-52M	43.5 ± 2.4	69.7 ± 3.9	1.25 ± 0.11	3.5 ± 0.3

* determined with the Trp fluorescence based quantitation method
** determined by the phosphate based quantitation method

The CD analysis is summarised in Figure 4.12. Note that an over- or underestimation of peptide concentration alters the mean residue ellipticity $[\Theta_{mr}]$ and hence also the CDNN evaluation which in turn produces potential evaluation errors. In Figure 4.12 A the CD spectra give a spectrum of varying helix fractions with L19 as the most helical and AL 35-42 as the least helical peptide in the study set. Considering the

concentration values in Table 4.5, the low L19 concentration results in a very pronounced helix spectrum with even 80000 deg cm^2 dmol^{-1} at 195 nm. For an ideal helix, the maximum [Θ_{mr}] is approx. 70000 deg cm^2 dmol^{-1} for the positive band at 190 nm. This is possibly due to an underestimation of L19 concentration. The concentration determination is based on Trp fluorescence and is therefore a sensitive method. Yet, it is possible that for L19 the lower quantitation limit was reached. According to experience, it is recommendable to measure above 8 µM (diluted L19 sample: approx. 7 µM). In addition, L19 possesses a highly hydrophobic sequence possibly having a strong self-association as consequence. Previously, it has been shown that an increase in environment hydrophobicity results in quenching of Trp fluorescence [Alston *et al.*, 2008].

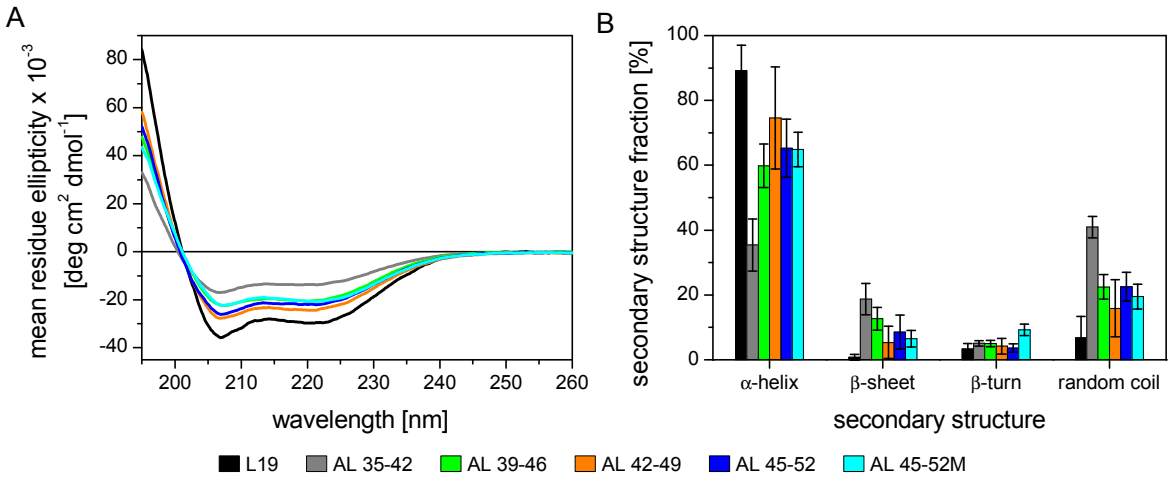

Figure 4.12: Secondary structure analysis of AL hybrid peptides. A: Circular dichroism average spectra of deuterated AL hybrid peptides measured in liposomal DLPC/DLPS/DLPE (3/1/1) membranes at a P/L ratio of approx. 0.03 in 50 mM ND_4Ac pD 7.5 at 70°C; path length = 0.5 mm; B: Secondary structure fractions of peptides determined with CDNN/ Pepfit from A (evaluation range is 205-260 nm). All values represent means of 3-4 independent liposome preparations.

In spite of the mentioned possible errors, the analysis can give the following order with increasing structural flexibility: L19 < AL 42-49 ≤ AL 45-52 ≈ AL 45-52M ≈ AL 39-46 ≪ AL 35-42. The loss in helicity is compensated by small portions of random coil and β-sheet structure. All hybrid peptides have a $KKKKWL_{11}$ sequence in common, therefore the difference in structural flexibility is induced by the guest sequences. With this, a trend in relative flexibility can be observed: APP-TMD 42-49 ≤ APP-TMD 45-52 ≈ APP-TMD 39-46 ≪ APP-TMD 35-42. Remembering the impact of Thr on helix stability described in the previous chapter (p. 64), this order is reasonable as AL 42-49 is the only one with two Thr.

4.4.2 D/H Exchange and Backbone Dynamics of Hybrid APP-TMD-Peptides

Since helix dynamics of the processed APP TMD parts were of interest, helix dynamics of the hybrid APP TMD peptides were studied, as well. Analogue to the experimental conditions for CD experiments, the D/H exchange of the hybrid peptides was initiated via a 1:10 (v/v) dilution of the deuterated peptide liposome suspension (50 mM ND_4Ac pD 7.5) into 50 mM NH_4Ac pH 7.5 at 70°C. A comparison between amide exchange in liposomes and isotropic solution under quench conditions can be viewed in Table A.2 (see Appendix, p. 146). It demonstrates the rapid loss of amide deuterons in isotropic solution preventing the analysis of the C-terminal 8 aa part of the AL peptides which is here of interest.

To deepen penetration of the DHX catalyst (the hydroxide ion) into the lipid bilayer, firstly a thin membrane (hydrophobic thickness of DLPC: ≈ 20 Å) and secondly a high temperature (70°C) were chosen to increase Brownian molecular movement and membrane fluidity. Last, the pH was increased to pH 7.5 for higher basic catalyst concentration [Poschner *et al.*, 2009]. Due to low signal intensities and the need to heat the samples to 70°C, a discontinuous measurement is preferred over a continuous one.

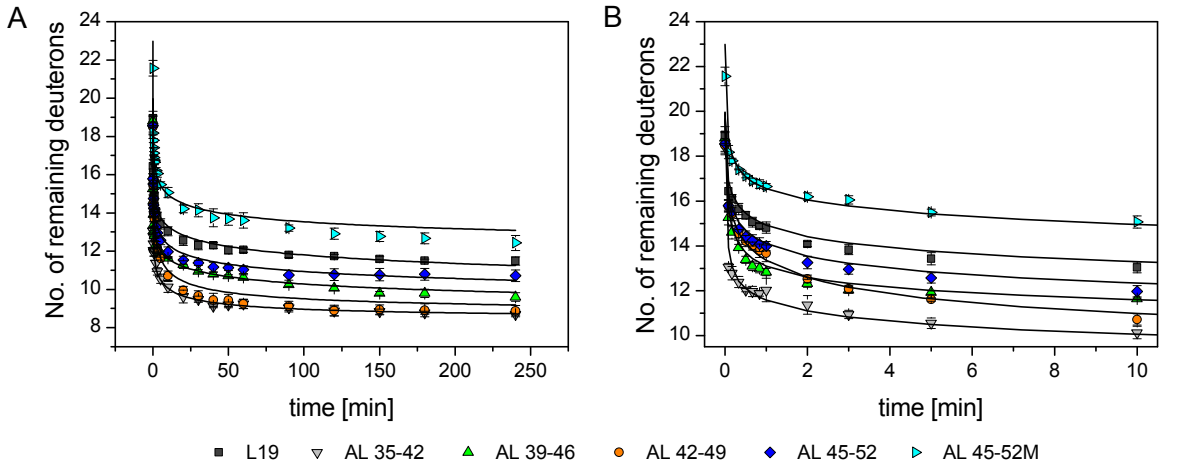

Figure 4.13: A: D/H exchange kinetics of AL peptides in liposomal DLPC/DLPS/DLPE (3/1/1) membranes with 0.03 as P/L-ratio. Kinetics were performed in 50 mM NH_4Ac pH 7.5 at 70°C. Data points at t=0 min correspond to the numbers of amide deuterium atoms seen after exchange under stop conditions. The data were fit with a maximum entropy method using $D_{(t=0\ min)}$ (continuous lines) and an overall exchange of 12 deuterons instead of the number of H-bonded amide-deuterons in an ideal alpha-helix. All values represent means of 3 independent liposome preparations with their standard deviations. B: zoom into the first 10 min of A.

The outcome of the DHX experiment with L19 as reference gives the following kinetics order (Figure 4.13): L19 < AL 45–52 < AL 42–49 < AL 39–46 < AL 35–42. The exchange of model peptide AL 42-49 is within the first 2 min slower than for AL 39–46, after 2 min it accelerates and the order between the two model peptides is reversed (see

Figure 4.13 B). The kinetics of AL 45-52M is the slowest due to a 3 Met extension of AL 45–52.

The first measurement point in liposomal DHX is at t=0 under quench conditions. Approx. 1-1.5 deuterons less than the count of H-bonded amide deuterons in an ideal α-helix are detected. One amide deuteron might be that of Trp and/or that of the last residue of the C-terminus, as helices fray at their endings due to 50% H-bond formation. Within 5 seconds L19 exchanges further 2.5 deuterons and AL 35–42, which is the fastest of the study set, 5.4 deuterons. So the data interpretation is based on the difference of 3 deuterons to each other and on the exchange behaviour over time. The DHX kinetics maps 7-10 exchanged deuterons in this peptide set, i.e. 35% to 50% coverage of the H-bonded amide deuterons assuming an ideal α-helix (for absolute values, please view Table A.2 in Appendix, p. 146).

Studying reference L19, its amide deuterons can be classified into three major groups. One group describes amide deuterons having exchanged immediately after isotope exchange initiation under stop conditions. These include the 3 amide deuterons lacking H-bond acceptors at the N-terminus and perhaps one further amide deuteron being able to H-bond. Note, the first N-terminal residue possesses no amide deuteron. The second group includes those deuterons which exchange during 240 min. For L19 these are approx. 7 deuterons. The third group comprises the non-exchanging deuterons being 12 for L19. Figure 4.14 (p. 74) gives an attempt to assign these three described groups onto L19.

As a consequence of lipid bilayer shielding, the hydroxide catalyst penetrates the lipid bilayer from the surrounding solvent. Based on that consideration, fast exchanging deuterons are assigned to the termini of peptides. Since the positively charged K_4W tag interacts with the negative charges of the lipid head groups, it can be considered as the most accessible one. The non-exchanging deuterons are assigned to the core of the peptide. The poly-Leu sequence forms at this region a very stable helix and DHX is hindered due to the high hydrophobicity in the lipid tail region. With this in mind, we assign the exchanging deuterons detected by the DHX experiment. The K_4W tag maybe followed by another three exchanging amide deuterons. The rest is allocated to the C-terminus.

Applying this approach to the other model peptides and assuming that the L_{11} sequence exchanges with the same behaviour as L19, the additional exchanging amide deuterons are assigned to the C-terminus directed towards the centre of the lipid bilayer. From this, the differences of the C-terminal 8 residue part can be seen. AL 35–42 and AL 42–49 each have three additional accessible amide deuterons from the C-terminus, whereas AL 39–46 has two and AL 45–52 has one additional exchanging amide deuterons with respect to L19. A further refined assignment at residue level in this region is however not feasible.

The kinetic evaluation by the maximum entropy method is depicted in Figure 4.15

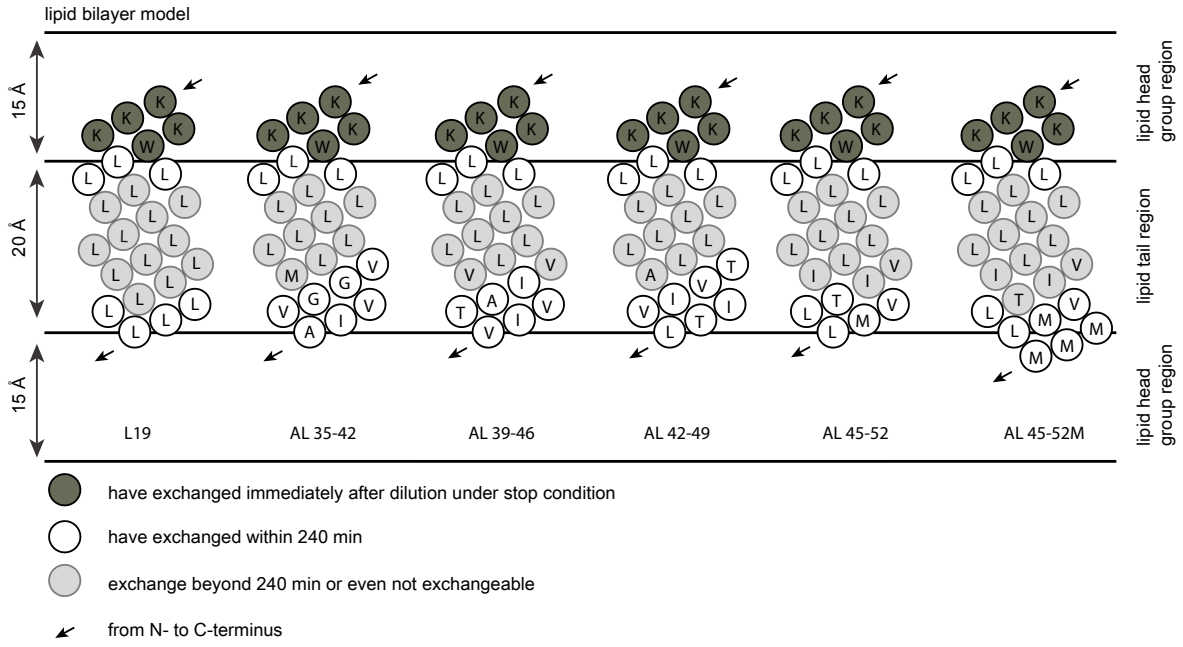

Figure 4.14: Model of deuteron assignment on AL hybrid peptides

(p. 75). In order to refine the population differences among the AL peptides, 12 instead of 20 amide deuterons were used for the computation. The number was reduced because the biggest difference of exchanging deuterons was seen with AL 35–42 (Δ 20-$D_{t=240min}$). Hence, the MEM analysis excluded those deuterons which did not exchange. The same computation conditions were applied for DHX kinetics of AL 45–52M, as well. Two types of populations are distinguished. The region with smaller rate constants (population I) shows rate constant distributions of AL peptides with lower magnitude than that of L19. In population II, deuteron abundances are higher compared to L19. This population exhibits rate constants which can be assigned to a great extent to the amide deuterons observed in the exchange within 240 min including the Trp amide deuteron. Another of these observed amide deuterons falls into the range of population I. Hence, except one deuteron, population II describes most likely both the C-terminal APP-TMD region and the WL_3 part.

Comparing the rate constant distributions with each other, AL 35–42 has a high deuteron abundance with large rate constants. This confirms its fast DHX kinetics. The change in DHX order for AL 39–46 and AL 42–49 is also reflected by the distributions. Whereas AL 42–49 possesses a smaller amount of deuterons with very high rate constants than AL 39–46, the relation reverses below log k (h^{-1}) 2.5. The distribution of AL 45–52 is rather flat with weakly pronounced peaks, and resembles that of L19. Single distinct dynamic or rigid regions within the peptide can not be deduced from that. One might think rather of a linear rate constant gradient for its deuterons. This could be reasoned by the combination of helix stability and accessibility by the hydroxide ion catalyst into the liposomal membrane. The extension of three further amides (3 Met) to the

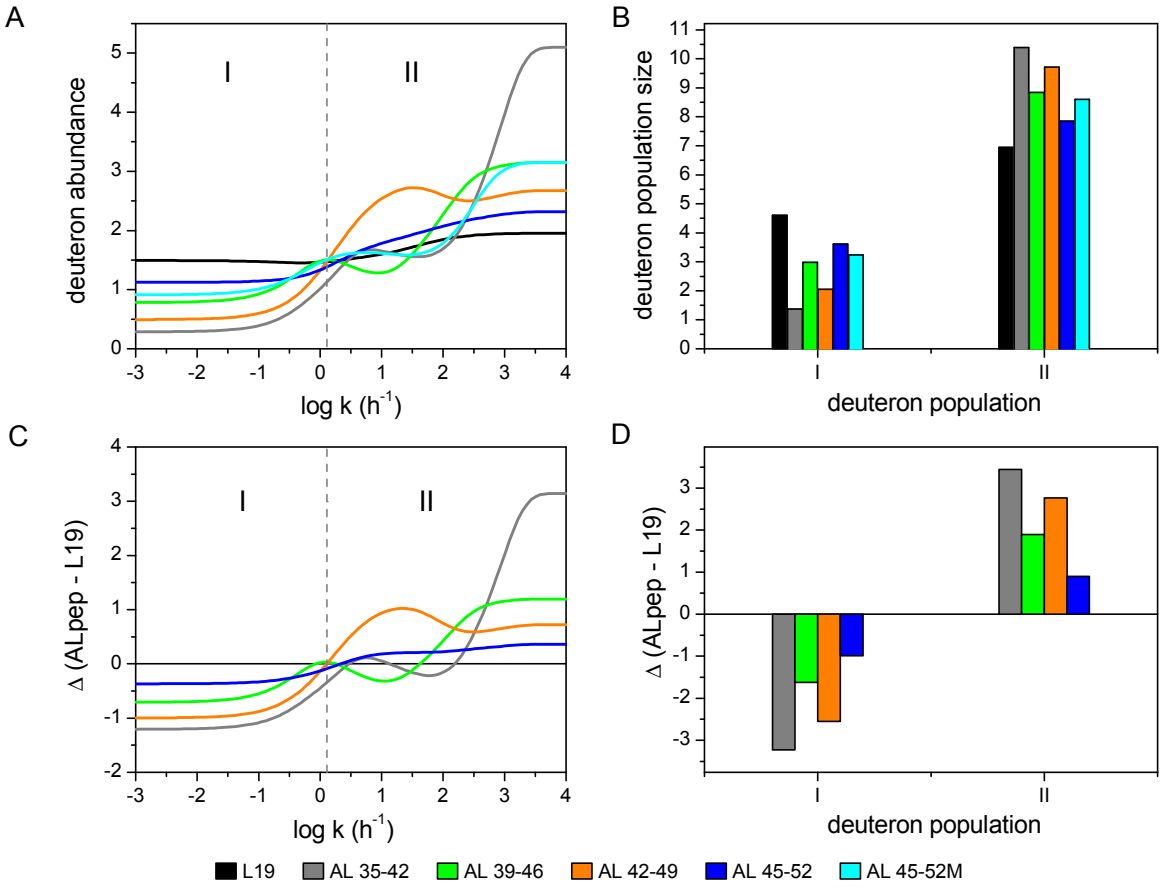

Figure 4.15: Kinetic analysis of AL hybrid peptides. A: Distribution of rate constants by applying the maximum entropy method with conditions mentioned in Figure 4.13. 12 instead of 20 amide deuterons were taken as the maximum for computation. Also the actual measured deuteron count for t=0 was taken. Dashed vertical line signifies the boundary between two amide deuterium populations. B: Amount of amide deuterium atoms within the kinetically distinct populations defined in A. C: Rate constant distribution of Al hybrid peptides corrected by the rate constant distribution of L19. D: Amount of amide deuterium atoms within the kinetically distinct populations defined in C.

C-terminus of AL 45–52 elevated the start of its DHX kinetics by three deuterons, yet a difference of overall exchanging deuterons is only one to two deuterons more than for DHX of AL 45–52. The purpose was to study the effect of C-terminal helix fraying. The terminal LVML motif ought to have deuterons with lower rate constants in AL 45–52M compared to AL 45–52. In the distributions there is a peak shift from log k (h^{-1}) 1.2 to 0.2, but this is not unambiguous as there is also an increase in deuteron abundance for very high rate constants (log k (h^{-1}) = 3-4).

Looking more closely at the DHX fit computed by the MEM method, one notices that the fit does not encompass all data points in the long term range. Also, the input parameters for the MEM analysis were changed. In general to describe the DHX kinetics fully, the number of all H-bonded amide deuterons in an ideal α-helix are given to the programme. Here, it would mean to use 20 exponential terms, each term for

one amide deuteron. Yet, in this case in order to improve the fit, the number was reduced to 12 terms excluding the non-exchangeable deuterons in the kinetic description. Therefore, an alternative to describe the DHX kinetics with a rate constant distribution was to reduce the fit to a triple exponential function in which one term can describe more than one deuteron (see method section 3.2.6 equation 3.7, p. 47). The fitting was performed by Christina Scharnagl. To compare the sizes of deuteron populations, the rate constants were kept constant for all AL peptides. They define three classes of differently fast exchanging deuterons, namely A to C from fast to slow, and class D to which non-exchangeable deuterons were assigned. The used rate constants are summarised in equation 4.2.

$$D(t) = A{\cdot}exp(-27.68\,min^{-1}{\cdot}t)+B{\cdot}exp(-0.86\,min^{-1}{\cdot}t)+C{\cdot}exp(-0.0344\,min^{-1}{\cdot}t)+D \tag{4.2}$$

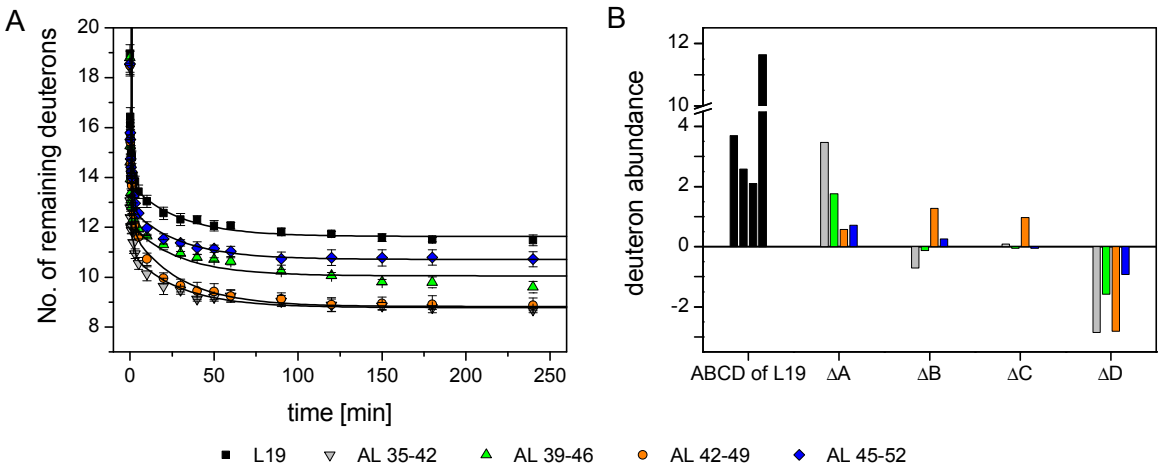

Figure 4.16: Kinetic analysis of AL hybrid peptides with a triple exponential fit. A: Fitting the DHX kinetics of AL peptides with a triple exponential function. The used rate constants represent the average of rate constants for each class and AL peptide in order to have comparable deuteron abundances in each class. B: Deuteron abundances assigned to the kinetically distinct classes A, B, C, and class D which represents deuterons that do not have exchanged within 4 h. Black bars represent numbers found for L19. For comparison reasons, the abundance differences between AL peptides and reference peptide L19 for each class are plotted. The analysis was performed by Christina Scharnagl.

The improved fit of the DHX curves is depicted in Figure 4.16 A. Figure 4.16 B shows the population sizes of L19 for all classes and the respective differences of the AL peptides related to the reference peptide. With this, the order for the class of fast exchanging deuterons (class A) is as follows beginning with the smallest: L19 < AL 45–52 ≈ AL 42–49 < AL 39–46 < AL 35–42. Taking classes B and C together, then AL 42-49 has more deuterons in these populations than AL 39–46. This reflects again that AL 42–49 exchanges in the beginning slower than AL 39–46, yet after 2

min reaction time the order is changed. Comparing both approaches to describe the DHX kinetically, one observes that the sum of deuteron abundances of classes A to C is similar to the deuteron abundance belonging to population II derived from the MEM analysis (Table 4.6). Since the rate constants k_A, k_B and k_C encompass the same range as the rate constant range designated with population II in the MEM analysis, this comparison is legitimate ($\log k_A$ (h^{-1})= 3.2; $\log k_B$ (h^{-1})= 1.7; $\log k_C$ (h^{-1})= 0.3). The deuterons assigned to population I are a subset of class D. This confirms not only the DHX ranking, but also that both approaches complement each other. Where the exponential fit gives a refinement in the deuteron classes, the MEM analysis gives a rate constant distribution for each helix kinetics including the standard deviation in the computation.

Table 4.6: Comparison in deuteron population differences

class/population	L19	AL 35-42	AL 39-46	AL 42-49	AL 45-52
Δ[(A+B+C)$_{AL}$-(A+B+C)$_{L19}$]		2.9	1.6	2.8	0.9
Δ[(PopII)$_{AL}$-(PopII)$_{L19}$]		3.4	1.9	2.8	0.9

Reflecting the results, the experiment's outcome is able to describe the dynamics of the C-terminal fragments defined by the γ-secretase up to 60-80% by using the AL peptides as model. Though a resolution at the level of individual amino acids is not attainable by this experiment, regional differences in dynamics were elucidated. Since fraying is a property of all peptide termini due to 50% H-bond saturation, its extent is determined by absent side chain/ side chain interactions and by the hydrophobicity of the sequence and its resulting solvation. L19, representing the ideal helix, shows the minimum of fraying. In addition, the peptide AL 45-52 which has the endoproteolytic ε-cleavage site in the middle expresses more helix stability than deduced from the kinetics of other AL peptides. The other APP-TMD subsequences have higher dynamics. As already mentionend in section 4.4.1 (p. 71), Thr and its ability to H-bond with the backbone is certainly influencing the termini's dynamics, as well. Save AL 35-42, the AL's guest sequences harbour one or two Thr.

4.5 Structural Comparison of APP-TMD and LV Peptides Representing Non-APP-TMDs

In this experiment the intention was to rank the dynamics of the APP TMD with those of other transmembrane peptides which do not represent substrates for γ-secretase. Therefore, its dynamics was compared with artificial peptides, the LV peptides. Their dynamics were thoroughly investigated by Poschner *et al.* [2009], in isotropic solutions as well as in liposomes. Their helicities in 80 % (v/v) TFE and buffer are with 70-80% [Poschner *et al.*, 2009]. Here, the DHX kinetics of LV peptides were recorded under

conditions as introduced in section 4.2.2 (p. 58) to be comparable to the A peptides with the same length. The LV sequences are enlisted in Table 4.1 (p. 54). L16, LV16 and LV16 G8P9 were the peptides of choice giving a spectrum of dynamics levels from low to very high.

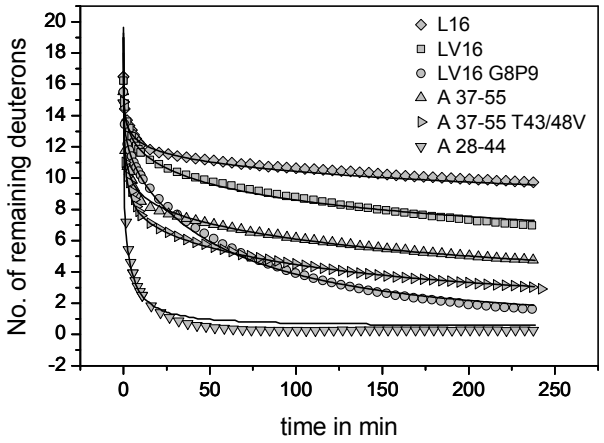

Figure 4.17: D/H exchange kinetics of A 28–44, A 37–55 and its double mutant in comparison to LV peptides. Measurement was performed in 80% (v/v) TFE and 10 mM NH_4Ac, pH 5 at 20°C with a 1:20 dilution and a final peptide concentration of 5 µM. Data points at t=0 min correspond to the numbers of amide deuterium atoms seen after exchange under stop conditions. The data were fitted with a maximum entropy method assuming $D_{(t=0\ min)}$=19 for all peptides apart from LV16 G8P9, this was computed with 18 (continuous lines). All values represent means of 3 independent measurements with an average standard deviation of ± 0.17 D.

As expected, the LV peptides exchange in the following order beginning with the slowest: L16 < LV16 < LV16 G8P9 (see Figure 4.17). Comparing their endpoints, their differences to each other span a window of 8 deuterons. The kinetics of the LV peptides differ from those of the A peptides, their DHX kinetics can be ranked differently regarding the negative exchange slopes before and after 15 min, respectively. After 15 min, the A 37–55 kinetics seems to have a line shape between that of L16 and LV16, and the kinetics of its double mutant seems to resemble that of LV16. Until 25 min, A 37–55 exchanges faster than LV16 G8P9, and until 70 min, its double mutant exchanges even faster than LV16 G8P9.

The β-branched residues Val and Ile occur in LV16 8 times, likewise in A 37–55. Hence, the rest of LV16 core sequence, the 8 Leu, should be responsible for slowing down the dynamics of LV16 compared to LV16 G8P9 which has less Leu and more helix-destabilising residues. If A 37–55 had not exchanged fast in the beginning, its kinetics would have covered that of L16/ LV16 in the long time range. Obviously, the two Gly in A 37–55 can be related to the accelerated exchange kinetics in the beginning due to their stronger helix-destabilising properties. The rest of the core sequence seems to imitate the effect of the Leu in L16/LV16. The results in section 4.3.2 (p. 65) already proved the helix-supporting properties of Thr backbonding in A 37–55.

LV16 G8P9 expresses higher dynamics which is a consequence of the introduced

GP motif in the peptide core. In A 37–55, the two Gly occur close to the N-terminus. Since residues close to termini exchange faster than amide deuterons in the peptide core, A 37–55 exchanges faster in the beginning compared to LV16 G8P9. The two replacements of Thr by Val induce accelerated kinetics in A 37–55 which does not exceed the kinetics of LV16 G8P9 after 15 min exchange. In other words, the Gly-Pro motif induces higher dynamics in a helix core than increasing the amount of Val.

A 28–44 is the fastest exchanging helix in this study set. Though it has a similar amount of Val and Ile as A 37–55, its four Gly distributed in the whole sequence are probably responsible for its kinetics being faster than LV16 G8P9. Pro induces helix kinks and is therefore known for its helix instability. But here, regarding amount and position, the Gly are able to reinforce the helix destabilising effect of the Gly-Pro motif.

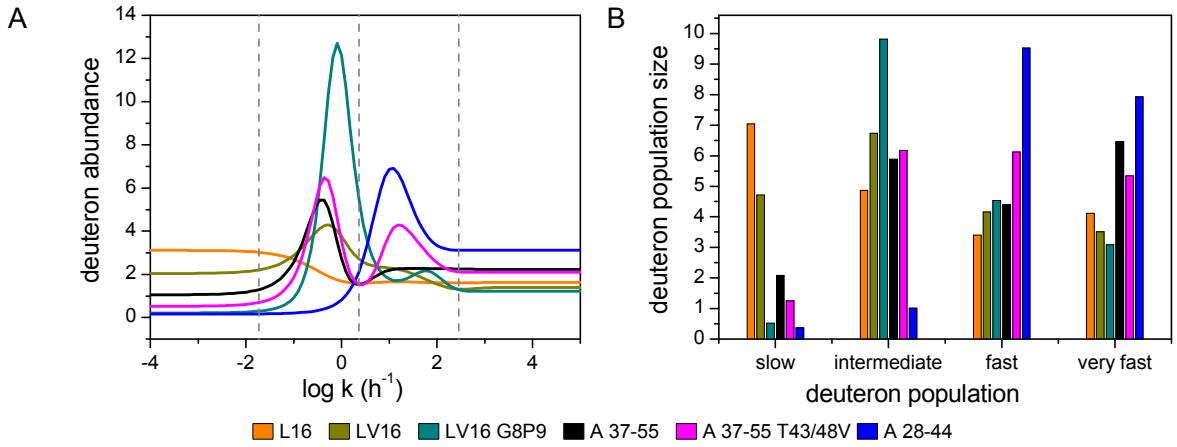

Figure 4.18: Kinetic analysis of A 28–44, A 37–55 and its double mutant in comparison to LV peptides. A: Distribution of rate constants determined by the MEM. The abundance of exchanged deuterons is represented in dependence of the decadic logarithm of rate constants for the exchanged amide deuterons. Dashed vertical lines signify the boundaries between four amide deuterium populations. B: Amount of exchanged deuterons is depicted in bars determined from the integration of the area beneath the distribution curve within the kinetically distinct populations defined in A.

The MEM analysis produces four populations (see Figure 4.18). Two of them, the intermediate and fast population, are distinguished by pronounced peaks. L16 has a rather flat rate constant distribution. Increasing the amount of helix-destabilising residues, the peaks become more pronounced as observed in LV16 and LV16 G8P9. In other words, more amide deuterons exchange with similar rate constants. Further, the two deuteron populations of LV16 are shifted to higher rate constants in LV16 G8P9.

Comparing the LV MEM data with that of the A peptides, the analysis confirms A 37–55 to have a higher amount of deuterons with very high rate constants than the LV peptides. The intermediate deuteron populations of LV16, A 37–55 and its double mutant overlap in size and magnitude reflecting their similar kinetics behaviour in the long time range. The rate constant distribution of A 28–44 gives a deuteron population with high abundance in the fast exchanging range. It has a broader half

width than the intermediate deuteron population of LV16 G8P9 demonstrating that the helix-destabilisers Gly and Pro in LV16 G8P9 and the four Gly in A 28–44 can cause helix dynamics with different rate constants and ranges.

Summarising, the cleavage region represented by A 37–55 exhibits a rather fast kinetics in the beginning due to its Gly in the N-terminal region. Within 15-240 min at 20°C, its kinetics resembles that of LV16. Loosing the backbonding ability by the Thr does not have the same destabilising effect than the Gly-Pro motif. A 28–44 exhibits in this study set the fastest exchange, even faster than LV16 G8P9. This probably originates from the four Gly at certain sequence positions which destabilise the helix.

4.6 Structural Properties of Natural Non-APP-TMDs

To complement the characterisation of APP TMD helix dynamics, naturally occurring transmembrane domains stemming from bitopic membrane proteins were compared with the APP TMD, the KTMD peptides. These peptides have an amino acid composition which occurs in average in TMDs of bitopic membrane proteins and represent non-substrates, save KTMD07 [Anders *et al.*, 2006, Haapasalo and Kovacs, 2011]. For this purpose, TMD sequences were selected with certain requirements (see method section 3.2.8, p. 50). Further, in order to exclude the Gly effect, some of the KTMD sequences were adjusted to the Gly pattern in model peptide A 37–55. The KTMDs' secondary structures were examined with CD spectroscopy, their backbone dynamics with DHX experiments, putting them into the context of the APP TMD model peptides.

4.6.1 Composition Similarity Analysis and Selection of TMDs of Bitopic Membrane Proteins

The initial aim was to find suitable biological TMDs comparing their backbone dynamics with that of the APP TMD with its abundance of β-branched residues. Therefore, sequences should contain ~25% β-branched residues and ~20% Leu. Consequently, sequences had to have similar aa compositions as in average TMDs. The Chair of Genome Oriented Bioinformatics (TUM, Prof. Frishman) provided an average aa composition which was calculated from approximately 20000 bitopic membrane protein annotated in the UniProt Knowledgebase.

In section 3.2.8 (p. 50), the selection process is described. TMDs of bitopic membrane proteins from a PFAM pool were sorted according to the sum of differences between the investigated TMD and the average TMD ΔX_{sum}. The smaller the value was, the closer the TMD was to the average aa occurrence.

The PFAM pool comprised 84 PFAM families with varying member numbers as redundant data set. For each PFAM family, TMDs were extracted and the average of aa occurrence within one PFAM family was computed by Sindy Neumann. With

this, ΔX_{sum} were calculated and compared. 11 PFAM families with ΔX_{sum} values < 40 were chosen for further analysis. Since the PFAM data set was redundant, it was possible to take each slight variation in a TMD into account. Additionally, the chance of missing a single TMD with a ΔX_{sum} value < 40 was low because the set was not homology corrected. For the narrowed PFAM family pool, ΔX_{sum} values for each single TMD were determined. Again, the exclusion criterion was < 40. 37 TMDs were in the final list. Sequences with Pro or charged residues were discarded. Finally, the strictness to average similarity for Gly, Ile, Leu and Val brought out peptides, now termed as KTM01 to 06 and KTMD11 to 13, respectively. KTMDs 07 to 10 are TMDs taken from a pool of human bitopic membrane proteins. These were chosen because of their good agreement in Leu content respectively the [Ile + Val] content compared to the average occurrence. Their residue compositions are compiled in Table 4.7.

Since Gly causes strong helix dynamics, modified KTMD sequences were created which are corrected by the Gly pattern in A 37–55. With this in mind, the β-branched residue rich cleavage region of the APP TMD shall be compared with sequences harbouring an almost average aa composition.

Table 4.7: Residue distribution of KTMDs in comparison to average and APP TMD model peptides. Residues of interest are highlighted in bold with color.

	A	C	F	G	I	L	M	S	T	V	W	Y[a]	UniProtKB accession No.	ΔX_{sum} [b]
A 28–55	2	0	0	**4**	**5**	**3**	2	0	2	**6**	0	0	P05067	80.0[c]
KTMD01	2	0	3	**3**	**4**	**4**	1	1	1	**3**	1	1	Q12LB8	29.9
KTMD02	3	0	5	**1**	**3**	**4**	2	1	1	**3**	0	1	Q1CIP1	38.1
KTMD03	2	1	2	**2**	**4**	**5**	1	0	1	**4**	1	1	Q97FR8	33.6
average[d]	3	1	2	**2**	**3**	**5**	1	1	1	**3**	1	1		
A 28-44	2	0	0	**4**	**3**	**1**	1	0	1	**4**	0	0		84.2[c]
A 37-55	1	0	0	**2**	**3**	**2**	1	0	2	**5**	0	0		88.2[c]
KTMD04	2	0	1	**1**	**2**	**3**	2	1	1	**2**	1	0	Q3XY79	40.6
KTMD05	3	0	1	**2**	**2**	**3**	0	1	0	**2**	1	1	A7HSZ4	37.9
KTMD06	2	0	2	**1**	**3**	**3**	1	1	1	**1**	1	0	A3UU17	35.5
KTMD07[e]	2	0	1	**2**	**3**	**5**	0	1	0	**2**	0	0	Q15262	53.2
KTMD08[f]	2	1	2	**1**	**2**	**4**	0	0	1	**2**	1	0	Q8WVQ1	46.5
KTMD09[e]	0	0	0	**4**	**1**	**4**	0	1	1	**5**	0	0	P01908	89.6
KTMD10[e]	1	1	1	**0**	**0**	**3**	2	2	0	**4**	0	2	Q6ZRP7	82.6
KTMD11	2	0	2	**2**	**2**	**3**	1	0	1	**1**	1	1	Q8DB59	35.3
KTMD12	2	0	1	**1**	**3**	**3**	0	2	1	**2**	0	1	Q0EQ08	38.8
KTMD13	3	0	1	**1**	**3**	**3**	1	1	1	**2**	0	0	Q89EF8	39.3
average[g]	2	0	2	**1**	**2**	**3**	0	1	1	**2**	0	1		
mKTMD04	2	0	1	**2**	**2**	**4**	2	0	0	**2**	1	0		
mKTMD05	2	0	0	**2**	**2**	**5**	0	1	0	**2**	1	1		
mKTMD06	2	0	2	**2**	**3**	**3**	1	1	1	**1**	0	0		
mKTMD08	2	1	2	**2**	**2**	**4**	0	0	1	**1**	1	0		
mKTMD12	2	0	1	**2**	**3**	**3**	0	2	1	**1**	0	1		
mKTMD13	3	0	1	**2**	**3**	**3**	1	1	0	**2**	0	0		

[a] Values for D, E, H, P and R are not shown because they do not occur in the chosen sequences; The residues of the flanking motifs KKWK and KKK are also not enlisted.
[b] Calculation is based on the original TMD of the bitopic membrane protein before it was adjusted to KTMD design.
[c] ΔX_{sum} values were calculated for the 24 aa and 16 aa core sequence, respectively.
[d] Absolute number for a 24 aa long TMD core given, rounded to integral numbers.
[e] These sequences are selected from a TMD clustering of human bitopic membrane proteins done by Jan Kirrbach.
[f] This sequence originates from the pool of TMDs from human bitopic membrane proteins with 16 aa length core sequence given by Jan Kirrbach.
[g] Absolute number for a 16 aa long TMD core given, rounded to integral numbers.

4.6.2 Secondary Structure of Selected Natural TMDs Compared to the APP TMD

Since the backbone dynamics of the KTMD peptides shall be compared with other peptides, their helicities had to be confirmed by analysing their circular dichroism. Hereby, two sets of peptides were assembled. The first set comprises KTMDs with an aa length equalling the full length APP TMD model A 28–55 (Figure 4.19, p. 83). The latter one includes KTMD peptides with 23 aa length like A 37–55 and is subdivided into KTMD04-13 and the modified mKTMD peptides (Figures 4.20 and 4.21, pp. 84 and 85).

All KTMD peptides are shaped dominantly as helices. Their CD spectra exhibit the typical positive band at approx. 190 nm and two negative bands at approx. 206 nm and 222 nm. The diversity in magnitude and position of the CD bands derives from the heterogeneity of the KTMD sequences. Due to their elevated Leu content it was expected that KTMD peptides exhibit in general a higher helix content than the APP TMD models, yet the CDNN/Pepfit evaluation gave a mixture of α-helices, β-sheets and random coil structures. One possible reason may be the overinterpretation of concentration determination and hence the miscalculation of the mean residue ellipticity which is needed for the CDNN/ Pepfit computation. Please note, that the evaluation range is between 200-260 nm instead of 185-260. Since the four secondary structure values (α-helix, β-sheet, β-turn and random coil) of the 185-260 nm evaluation exceeded in sum over 120 %, it gave rise to doubt the correct computation and it was reasonable to choose that evaluation range which gave sums of 100% ± 10%. The following standard procedure was then to cross-multiply values giving in total 100% as done for all the other CD analysises.

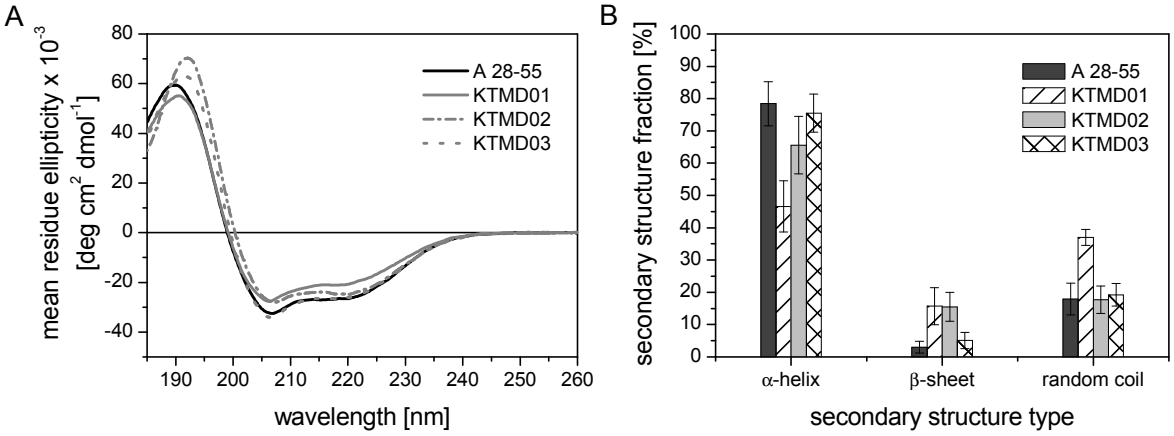

Figure 4.19: Secondary Structure Analysis of 31 aa long KTMD peptides. A: CD average spectra of KTMDs and A 28–55-, 30 µM in 80% (v/v) TFE and 10 mM NH_4Ac, pH 5, path length = 0.5 mm; B: Secondary structure fractions from CDNN/ Pepfit (evaluation range: 200-260 nm). All values represent means of 3 independent measurements.

In the peptide set of the 31 aa long KTMDs, a tentative increase in helicity from KTMD01 to KTMD03 can be observed despite the overlapping standard deviations (Figure 4.19). KTMD03 shares the highest secondary structure similarity to A 28–55.

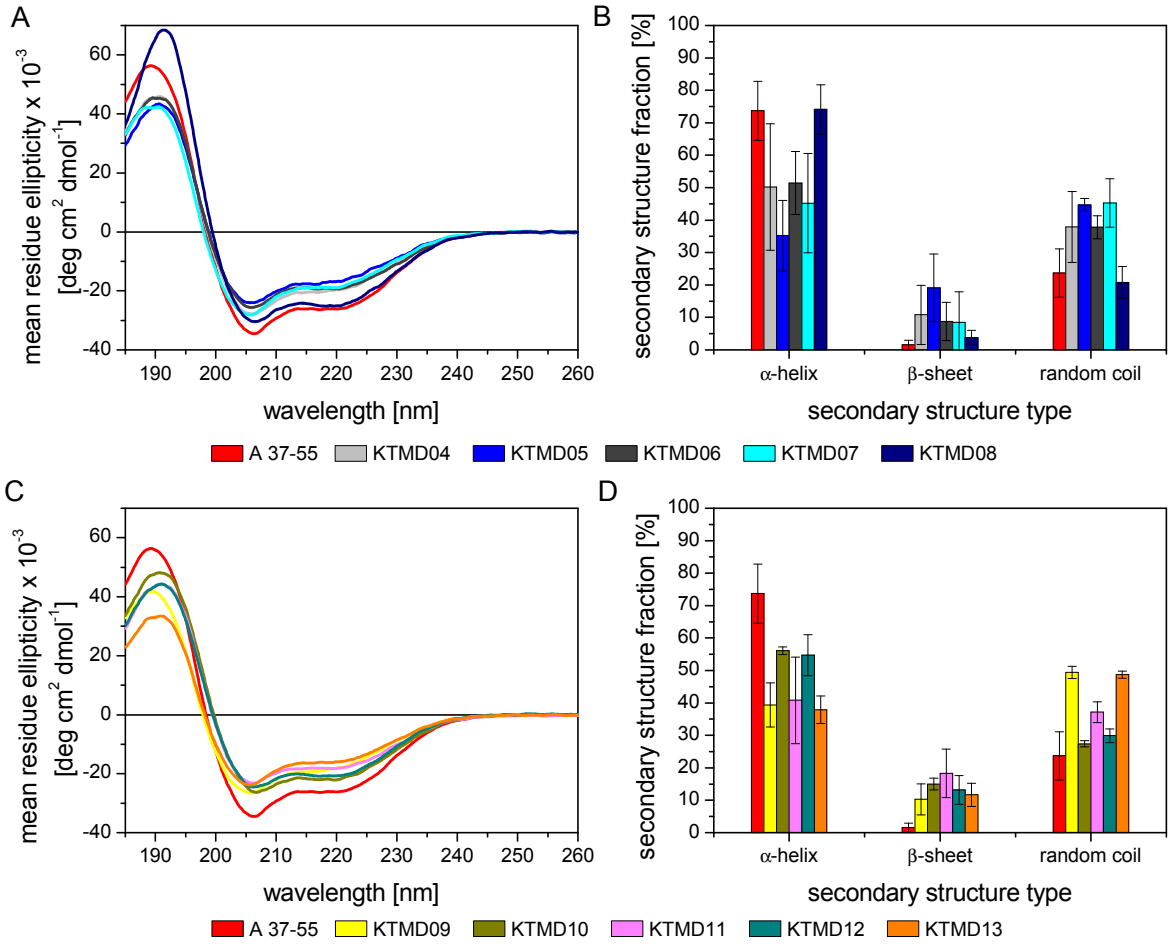

Figure 4.20: Secondary structure analysis of 23 aa long KTMD peptides. A: Circular dichroism average spectra of KTMDs and A 37–55 at 30 µM in 80% (v/v) TFE and 10 mM NH_4Ac, pH 5, path length = 0.5 mm; B: Secondary structure fractions with CDNN/ Pepfit (evaluation range is 200-260 nm). All values represent means of 3-6 independent measurements indicated with standard deviations.

The 23 aa long KTMDs were compared to A 37–55 (Figure 4.20). Here, KTMD08 is cloest to A 37-55. For other peptides, the decrease in helicity is mainly compensated by random coil structure and to a little extent by β-sheet. This supports the idea of α-helix to random coil interconversion, i.e. the folding/unfolding equilibrium. In sum, structural flexibility in comparison to A 37–55 seems to be augmented in the KTMDs. This is surprising in light of their lower [Ile + Val]-contents realtive to A 37–55.

The adjustment to the Gly pattern of A 37–55 in the mKTMD sequences results in the net addition of one Gly for 5 out of 6 peptides. The results show that some mKTMDs exhibit increased helicity as compared to the unmodified one and some exhibit decreased helicity (Figure 4.21). A correlation of Gly amount and position to the secondary structure shift between KTMD and corresponding mKTMD cannot be

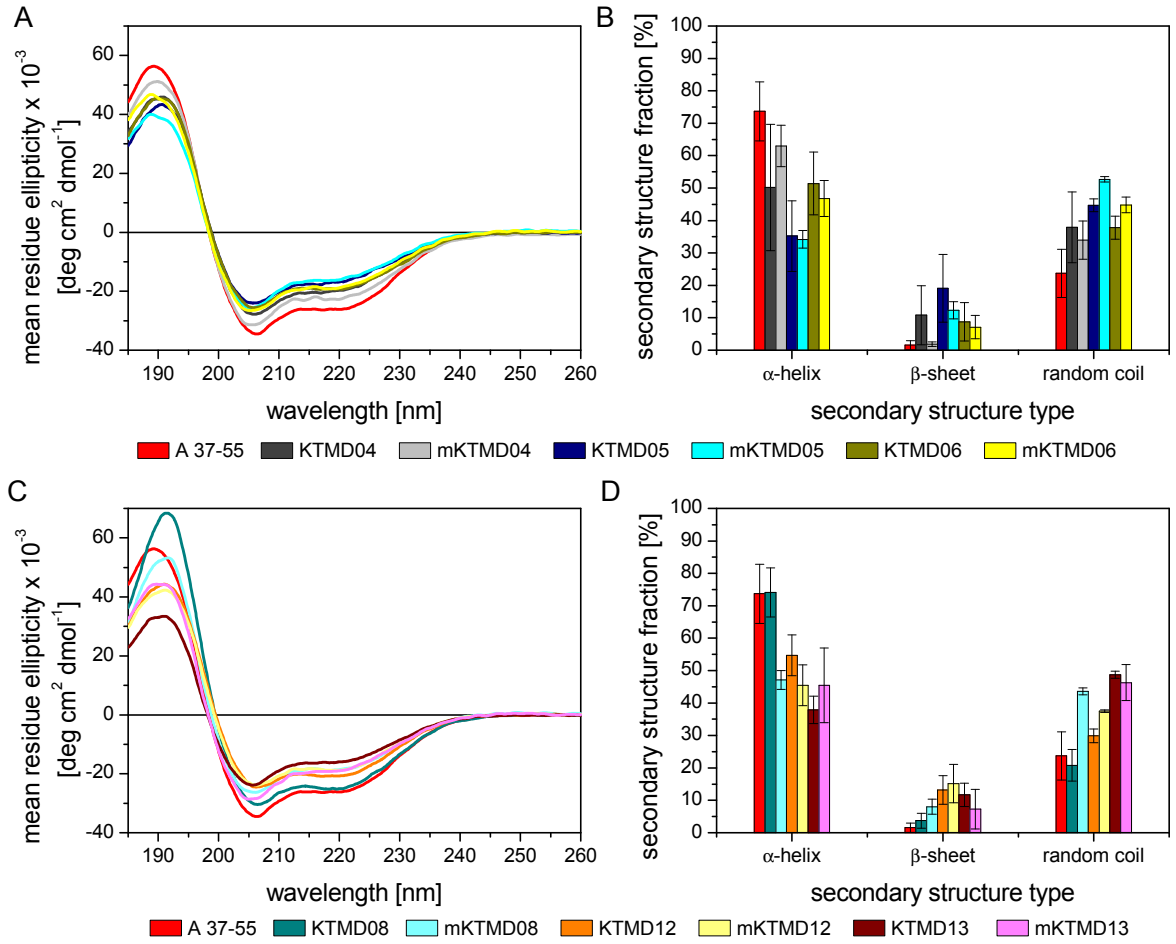

Figure 4.21: Secondary structure analysis of modified KTMD peptides in comparison with their KTMD analogues and A 37–55. A: Circular dichroism average spectra of mKTMDs, KTMDs and A 37–55 at 30 µM in 80% (v/v) TFE and 10 mM NH_4Ac, pH 5, path length = 0.5 mm; B: Secondary structure content determined by CDNN/ Pepfit (evaluation range is 200-260 nm). All values represent means of 3-6 independent measurements indicated with standard deviations.

found.

4.6.3 Comparison of D/H Exchange and Backbone Dynamics of Natural TMDs and the APP-TMD

Subsequent to the CD analysis in the previous section, backbone dynamics of the full length APP TMD model peptide shall be evaluated with those of the KTMD peptides of the same length. Comparing only the KTMD peptides amongst each other, the following order of DHX kinetics is seen beginning with the slowest: KTMD03 < KTMD02 < KTMD01 (Figure 4.22). The same order is observed for their helicity. Since the kinetics of A 28–55 shows a different line shape compared to that of the KTMD peptides, a ranking is not possible.

In the study set, it was anticipated that model peptide A 28-55 should be the fastest

in D/H exchange, yet this did not come true. The kinetics of A 28–55 behaves similar to that of KTMD02 in the first 20 min. Afterwards, it slows down. At approx. 125 min, KTMD03 possesses the same number of protected deuterons as A 28–55. Afterwards, KTMD03 exchanges more deuterons than A 28–55. These different kinetics behaviours indicate that A 28–55 has different sequence motifs inducing helix dynamics respectively stability. Since helix dynamics depends on sequence, it may be possible that Phe, which occurs in the KTMD but not in the A 28–55 sequences, plays a certain role in the dynamics of KTMDs (compare Table 4.7, p. 82). Further, KTMD01 and KTMD03 have two to three Gly in close proximity in the sequence centre. This is a property A 28–55 harbours, too (see Table 4.1, p. 54). Likely, KTMD03 and A 28–55 but not KTMD01 possess subsequences which are able to compensate these instabilities resulting in decelerated kinetics.

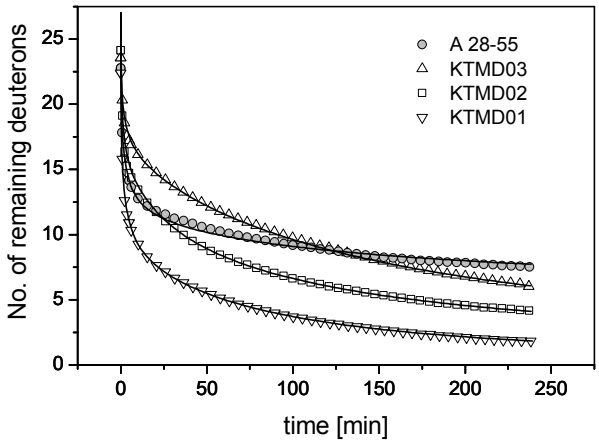

Figure 4.22: D/H exchange kinetics of A 28–55 in comparison to KTMD peptides of 31 aa length in 80% (v/v) TFE and 10 mM NH_4Ac, pH 5 at 20°C with a 1:20 dilution and 5 µM final peptide concentration. Data points at t=0 min correspond to the numbers of amide deuterium atoms seen after exchange under stop conditions. The data were fit with MEM assuming $D_{(t=0\ min)}$=27 for all peptides (continuous lines). All values represent means of 3 independent measurements with an average standard deviation of ± 0.19 D.

In the kinetic analysis by MEM (Figure 4.23), four populations characterise the rate constant distribution. The deuteron abundances of the intermediate and fast population confirm the DHX order of KTMD peptides. Interestingly, the population of fast exchanging deuterons of A 28–55 coincides almost with that of KTMD01, whereas KTMD02 has its population shifted towards higher rate constants. Further, A 28–55 has the least amount of deuterons in the intermediate population compared to the KTMDs, but has in each rate constant class a significant deuteron abundance, whereas the KTMD peptides have their deuterons concentrated in the fast and intermediately fast exchanging region.

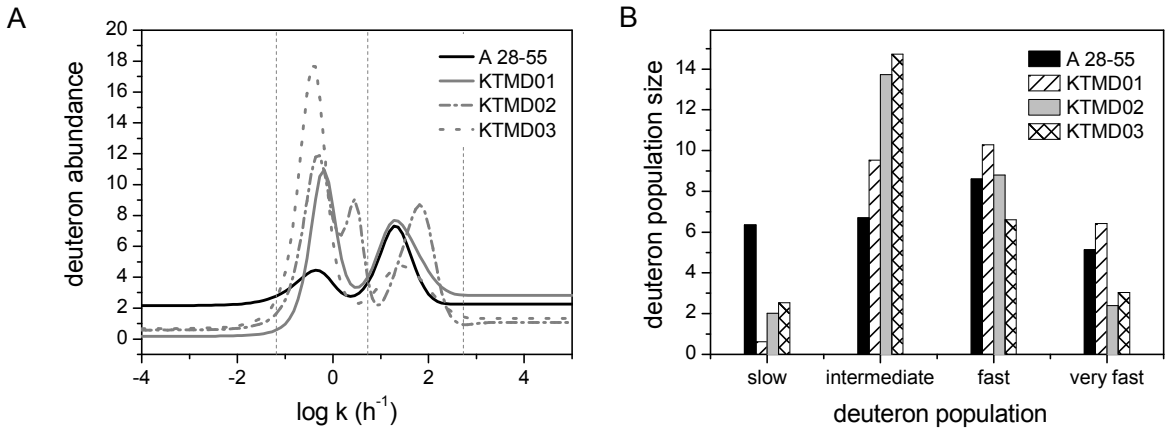

Figure 4.23: Kinetic analysis of A 28–55 in comparison to KTMD peptides of 31 aa length. A: Distribution of rate constants determined by MEM. The abundance of exchanged deuterons is represented in dependence of the decadic logarithm of rate constants for the exchanged amide deuterons. Dashed vertical lines signify the boundaries between four amide deuterium populations. B: Amount of exchanged deuterons is depicted in bars determined from the integration of the area beneath the distribution curve within the kinetically distinct populations defined in A.

4.6.4 Comparison of D/H Exchange and Backbone Dynamics of Natural TMDs and the APP TMD Cleavage Region

Since the cleavage region of the APP TMD is of interest for the etiology of Alzheimer's Disease, this section evaluates the backbone dynamics of KTMDs with the same aa length as the A 37–55 model peptide. D/H exchange kinetics were recorded and assembled in Figure 4.24.

From that, one can observe a broad spectrum of kinetics. A 37–55 and A 28–44 seem to be at the limits of this spectrum. In the first 15 min, KTMD08, KTMD10 and KTMD13 exchange with comparable velocity. Afterwards, their kinetics drift apart. It seems that the course of subsequent exchange kinetics is laid by how much KTMD peptides have already exchanged up to 25 min. Above all, it is surprising that none of the Leu enriched and (Val + Ile) reduced KTMDs exchange more slowly than A 37–55.

A better comparison between A 37–55 and the KTMDs is possible from the MEM analysis (Figure 4.27, p. 91). Their rate constant distributions are categorised in four populations. The population of deuterons with intermediate kinetics of A 37-55 coincides with those of KTMD04, KTMD06, KTMD07, KTMD10, KTMD12 and KTMD13. The intermediate peaks of KTMD08 and KTMD11 overlap only partly with it. The most similar rate constant distribution to A 37–55 is representing KTMD07 which was confirmed as a γ-secretase substrate with *in vivo* experiments [Anders *et al.*, 2006]. KTMD07 possesses three Leu more and has three Val and two Thr less than A 37–55 (see Table 4.7, p. 82). It seems, that the two Thr of A 37–55 are able to compensate the other helix-destabilising residues by additional H-bonds, whereas KTMD07 is compensating

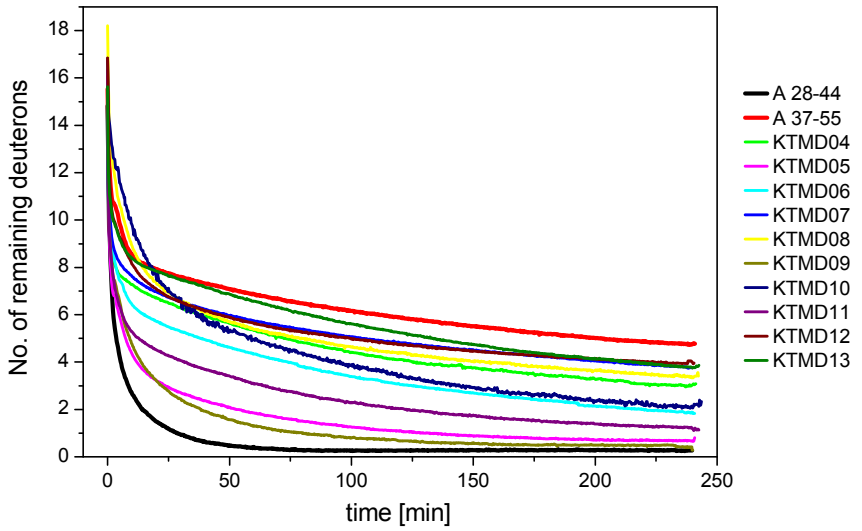

Figure 4.24: DHX of 23aa long KTMDs. D/H exchange kinetics of A 28–44 and A 37–55 in comparison to KTMD peptides of 23 aa length. Measurement was performed in 80% (v/v) TFE and 10 mM NH_4Ac, pH 5 at 20°C with a 1:20 dilution and a final peptide concentration of 5 µM. Data points at t = 0 min correspond to the numbers of amide deuterium atoms seen after exchange under stop conditions. All values represent means of 3 independent measurements with an average standard deviation of ± 0.19 D.

this by an L_4 motif known to induce helix stability (sequences are compiled in Table 4.1, p. 54).

KTMD05, KTMD09 and KTMD11, that display DHX kinetics most similar to A 28–44, have deuteron populations with rate constants in the fast region as A 28–44 has. Especially KTMD09 which possesses two GxxxG motifs, like A 28–44, has a large overlapping part to the rate constant distribution of A 28–44. Yet, KTMD07 with one

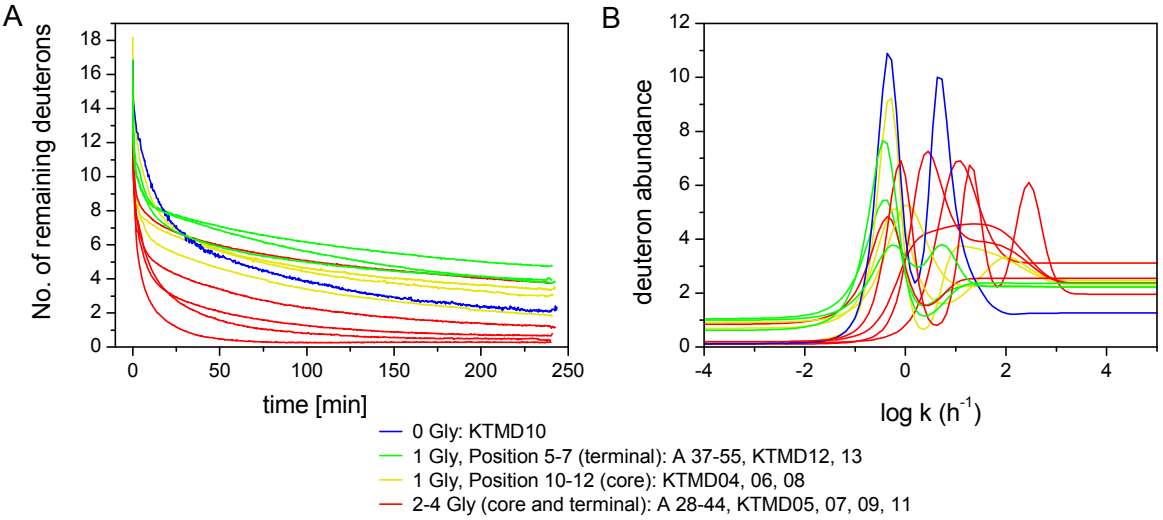

Figure 4.25: Heat Map indicating Gly position dependence in DHX kinetics (A) and MEM analysis (B). Backbone dynamics increase is marked from green over yellow to red. KTMD07 makes an exception.

GxxxG motif is able to exchange more slowly than KTMD09. KTMD05 and KTMD11 have their Gly close to the sequence centre. Hence, a tandem GxxxG motif and/or single Gly positioned in the sequence centre correlate with increased backbone dynamics in the helix (Figure 4.25). This might indicate that amount and position of Gly are partly responsible for helix dynamics.

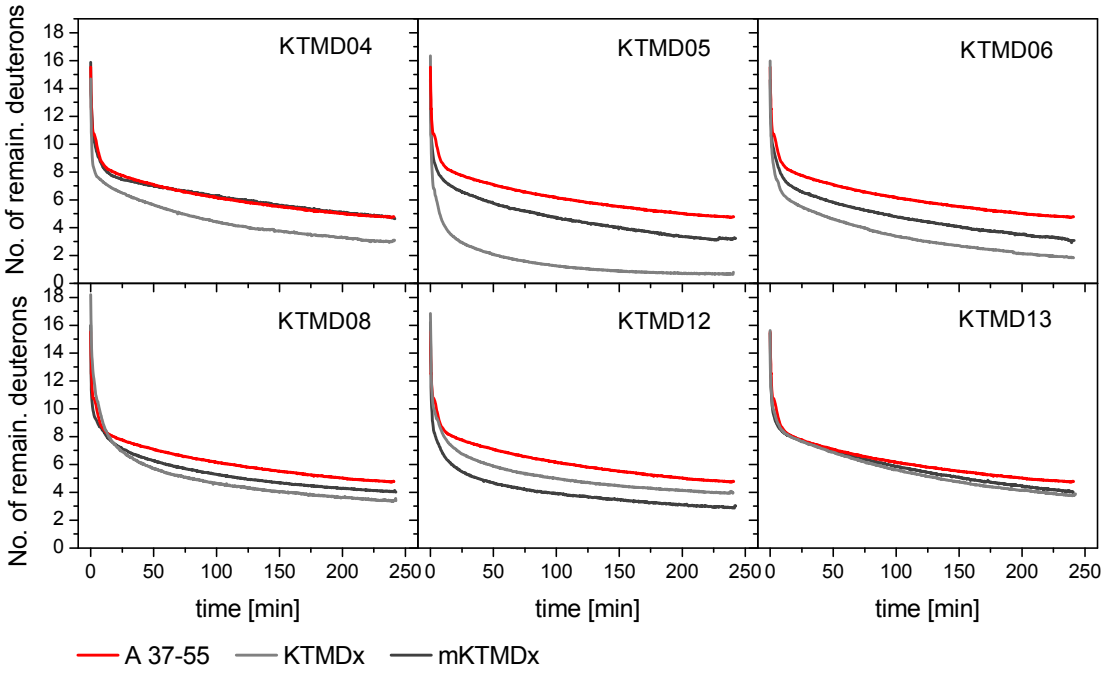

Figure 4.26: D/H exchange kinetics of A 37–55 in comparison to glycine modified KTMD peptides of 23 aa length. Measurement was performed in 80% (v/v) TFE and 10 mM NH_4Ac, pH 5 at 20°C with a 1:20 dilution and a final peptide concentration of 5 µM. Data points at t = 0 min correspond to the numbers of amide deuterium atoms seen after exchange under stop conditions. All values represent means of 3 independent measurements with an average standard deviation of ± 0.19 D.

Because Gly impairs the comparison to the cleavage region of the APP TMD in terms of sequence specific helix dynamics, a set of modified KTMDs was created. Gly positions were mutated, so that the sequence remains close to the original residue composition of the KTMD. The 5th and 6th position, counting from the N-terminus of the KTMDs, were replaced by Gly to match the Gly pattern of A 37–55.

The recorded DHX kinetics are compiled in Figure 4.26.

Strikingly, the Gly modifications generally reduce DHX kinetics. Strong kinetics decreases were obtained with mKTMD04, mKTMD05 and mKTMD06. Slight decreases in velocities were observed for mKTMD08 and mKTMD13. For the peptides mKTMD04, mKTMD05 and mKTMD06, this was expected because the Gly occurred in the original sequence in the centre and their replacements were Leu and Ala for KTMD04 and KTMD05. In KTMD06, the substitution by Val caused an increase in remaining deuterons of one deuteron. In KTMD08, the replacement was Ile, and here the increase was by 0.5 deuterons. So insertion of one β-branched residue does not change necessarily

kinetics in an extreme way as Gly at certain position does. KTMD12 and KTMD13 had their Gly originally close to the N-terminus and since Gly modifications were small, exchange kinetics were altered only little and KTMD12 exchanged even with increased velocity.

From the MEM analysis (Figure 4.27, p. 91), one can conclude that the rate constant distribution of KTMD04 in its modified form resembles strongly that of A 37–55, such as KTMD07 does. A strong approximation to the peak in the A 37–55 intermediate population is observed for all mKTMDs apart from mKTMD12. This infers that Gly in the sequence centre indeed modulate amide deuterons from other residues in such a way that their amide deuterons exchange with higher rate constants. An extreme example represents KTMD05. In KTMD06, the peak in the fast population is sharpened by the Gly modification. In this case variety of different rate constants is reduced.

It is apparent that there is an interplay between Gly, Leu and the β-branched residues Ile, Val and Thr whose effects are different and eventually oppositional. This results in the final H-bond stability in helices and therefore in helix dynamics. A comparison of DHX kinetics and MEM analysis between the LV and KTMD peptides can be found in the appended Figures A.3 and A.4 (p. 146).

4.6.5 Comparison of Backbone Dynamics of KTMDs with Thr APP TMD Mutants

Here, the question is addressed whether replacing the Thr residues in A 37–55 to Val will make its backbone dynamics faster than that of Gly modified KTMDs.

In Figure 4.28 A (p. 92) the DHX kinetics of mKTMDs, A 37–55 and A 37–55 T43V T48V are compared. The double mutant exchanges faster or with comparable velocity compared to mKTMDs, except for mKTMD12. This would account for the stabilisation strength of Thr by additional backbone H-bonding overcoming the high abundance of helix destabilising Val and Ile residues. Thus, a natural TMD does not necessarily have to have an average aa composition to exhibit low backbone dynamics. For comparison with unmodified KTMDs, please view Figure A.5 in the appendix (p. 148).

Figure 4.28 B shows the rate constant distribution. The deuteron population of A 37–55 T43/48V in the fast range overlaps partly with that of mKTMD06 and mKTMD12, whereas other mKTMDs have only "intermediate" deuteron populations confirming the comparison of DHX kinetics between KTMDs and A 37–55 T43/48V.

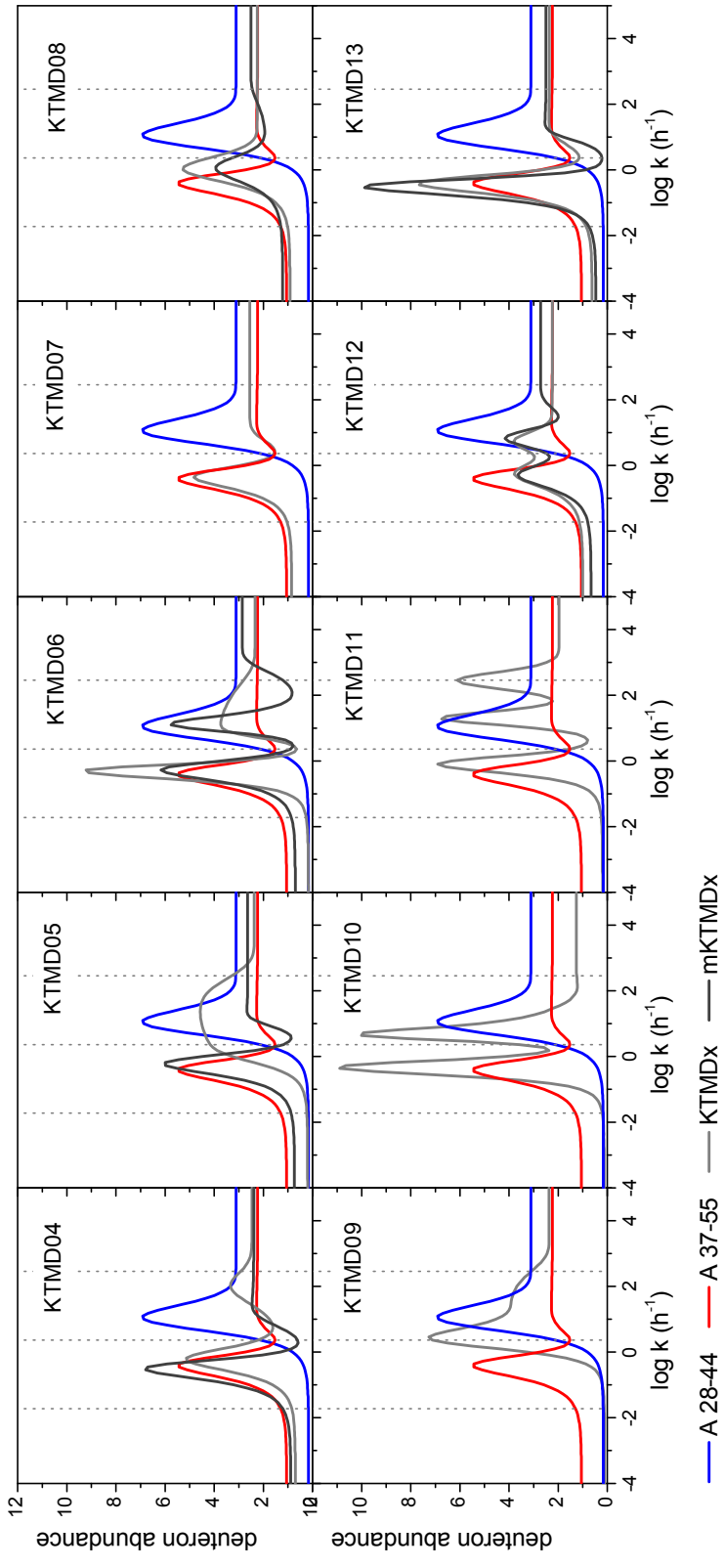

Figure 4.27: Rate constant distribution of A 28–44 and A 37–55 in comparison to KTMD and mKTMD peptides of 23 aa length. The abundance of exchanged deuterons is represented in dependence of the decadic logarithm of rate constants for the exchanged amide deuterons. For running the algorithm, D = 19 is assumed, the maximum number of hydrogen bonded amide deuterons in an ideal α-helix. Dashed lines separate the rate constant distribution into slow, intermediate, fast and very fast exchange regions beginning from the left.

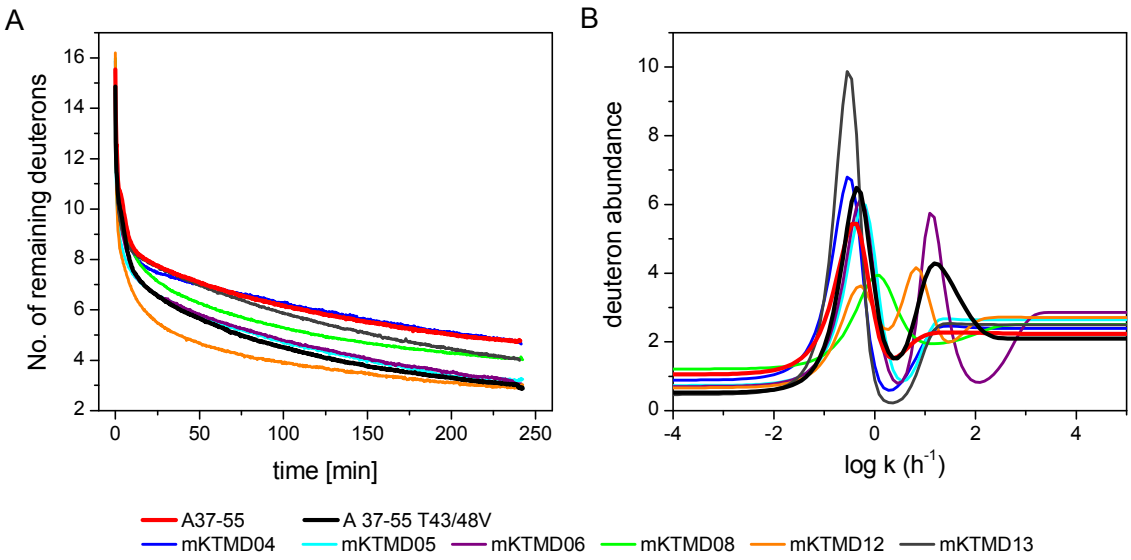

Figure 4.28: D/H exchange kinetics and MEM analysis of A 37–55 T43/48V in comparison to glycine modified KTMD peptides. A: D/H exchange kinetics in 80% (v/v) TFE and 10 mM NH_4Ac, pH 5 at 20°C with a 1:20 dilution and 5 µM final peptide concentration. $D_{t\,=\,0min}$ correspond to the numbers of amide deuterium atoms seen after exchange under stop conditions. Values represent means of 3 independent measurements with an average standard deviation of ± 0.19 D. B: Rate constant distribution of A 37–55 T43/48V in comparison to glycine modified KTMD peptides. The abundance of exchanged deuterons is represented in dependence of the decadic logarithm of rate constants for the exchanged amide deuterons. For running MEM, D = 19 is assumed, the maximum number of H-bonded amide deuterons in an ideal α-helix.

5 Discussion

The thesis was motivated by the attempt to understand one key factor in the etiology of Alzheimer's Disease, the γ-secretase mediated proteolysis of the transmembrane domain of the C99 fragment derived from the amyloid precursor protein at the level of substrate dynamics. Recent research by Beel and Sanders [2008], Miyashita *et al.* [2009], Sato *et al.* [2009] and Lu *et al.* [2011] had indicated that helix dynamics of the APP TMD substrate is linked in some way to proteolysis.

In this chapter, the results from conformational analysis of the APP TMD obtained by CD spectroscopy and DHX experiments are discussed and its implications for γ-secretase proteolysis are derived. In detail, it deals with APP TMD helix dynamics (sections 5.1 and 5.2, pp. 93 and 97), followed by the influence of potent therapeutic NSAIDs (section 5.3, p. 100). Since the APP TMD contains two Thr with strong backbinding ability [Gray and Matthews, 1984], their impact on helix dynamics and implications for proteolysis are evaluated (section 5.4, p. 101). With the help of overlapping APP TMD fragments, regional differences of backbone dynamics are addressed (section 5.5, p. 104). Completing the picture of backbone dynamics, the APP TMD is compared to artificial and biological non-APP TMDs (section 5.6, p. 107).

5.1 Mapping the Conformational Properties of the APP Transmembrane Domain

To map the APP TMD structure in a cleavage environment, three model peptides which mimic different parts of the APP TMD were investigated in 80% (v/v) TFE (equaling 50 mol–%) and 10 mM NH_4Ac solution. TFE supports helicity of hydrophobic peptides by mimicking the membranous environment. Similar to the lipid bilayer, it has a low dielectric constant and is also a poor H-bond partner (for details see section 1.1.4, p. 14). Hence, compared to water, it is not competing with the intramolecular H-bonds of the polypeptide. Moreover, it is of interest to choose a solvent system which not only mimics the lipid bilayer environment but also the hydrophobic environment of the surrounding transmembrane segments of presenilin. Further, the solvent system should contain water reflecting the situation in the lumen of presenilin harbouring the catalytic Asp. The hydrolysis of a peptide bond without water is not feasible. Since the electron microscopic works of Lazarov *et al.* [2006], Osenkowski *et al.* [2009] and Renzi *et al.*

[2011] reveal an aqueous intramembrane chamber and cysteine-scanning mutagenesis based accessibility studies by Sato *et al.* [2006] and Tolia *et al.* [2006] support the idea that the TMDs 6 and 7 of presenilin form a cavity to capture water molecules, water was added to the solvent system which was here 50 mol-% . Note that a low water molarity does not necessarily exclude proteolysis. The molecular dynamics simulation of a Rhomboid protease, a serine membrane protease, shows that the enzyme harbours a water-retention site close to the active site and captures via H-bonds a cluster of three water molecules supplying the active site [Zhou *et al.*, 2012]. A low water concentration could limit the proteolysis speed of the substrate TMD.

It should be mentioned that the experimental design examined monomeric peptides at 5 µM. At the Chair of Biopolymer Chemistry (Prof. Langosch), FRET based assays were applied to nitrobenzoxadiazole (NBD) (donor)- and Dabcyl (acceptor)-labeled Aβ 26-55. As their NBD fluorescence decreased little in presence of the respective Dabcyl peptide up to 50 µM, no interactions between the APP TMD model peptides occurred in 80% (v/v) TFE and 10 mM NH_4Ac [Kutzner, 2011].

CD (section 4.2, p. 55) reveals a pronounced helix for A 28–55 modelling the full length APP TMD. This is in line with previous work. A solution NMR structure of the C99 fragment in detergent micelles of LMPG at 45°C revealed a helix in the region between K28 and L52 without any interruption [Beel and Sanders, 2008]. Polarised ATR-IR spectroscopy in pelleted DMPC:DMPG membrane bilayers confirms helicity of a model similar to A 28–55 but with approx. 10 aa long juxtamembrane additions on each terminus [Sato *et al.*, 2009]. Further, A 37–55, which represents the cleavage region, expresses similar helicity as A 28–55. The helicity of A 28–44 is decreased by 13% and compensated by an increase of random coil. This underlines the increased structural flexibility in the dimerisation region. Its folding/ unfolding equilibrium is reflected by the ratio of α-helix to random coil and is shifted towards unfolding explaining the increased random coil portion. This infers that the Gibbs free energy difference between folded and unfolded state is lowered. As explained in section 1.1.4 (p. 11), the propensity to be in a folded state is influenced by the side chain effects [Creamer and Rose, 1995]. Folding of a TMD depends in general on the enthalpic and entropic contributions. The enthalpic one derives from intramolecular H-bonding of the polypeptide which has to overcome the breakage of intermolecular H-bonds between peptide and solvent, from van der Waals interactions between side chain atoms and with the backbone, from side chain packing and, if existing, from ionic and polar interactions. The entropic contribution is based on the interplay between the increase of freely moving solvent molecules and the loss of side chain rotation freedom and side chain translation freedom.

The resulting helix instability in model peptide A 28–44 is likely related to its Gly rich sequence occurring as tandem GxxxG motif (for residue composition see Figure 4.1, p. 56). The Gly side chain constitutes only a single atom. As a consequence, packing is inefficient in an α-helical conformation because the interaction between the C_β-atom of

a side chain and the helix backbone is missing which would give an additional enthalpic gain in helix formation [Go *et al.*, 1968, Luque *et al.*, 1996, Yang and Honig, 1995]. Yet, the Gibbs free energy difference is not only driven by this enthalpic contribution but also by an entropic effect. The Φ and Ψ dihedral angles are able to engage a larger space around the Gly positions in a random coil than helical structure. The presence of a Thr in A 28–44 has a helix-stabilising effect since it is able to form a H-bond to the backbone, details follow in section 5.4 (p. 101), compensating more or less the effects of Gly.

CD results indicate a better helix stability for the cleavage region than for the dimerisation region in the APP TMD. When one considers the high content in β-branched residues such as Val and Ile in both regions, it is rather unusual that the sequence of the cleavage region still is helix-supporting. A general reason is their hydrophobicity. Liu *et al.* [1996] have shown with model peptides replacing three residues with increasing hydrophobicity such as Ser, Gly, Thr, Ala, Val and Phe in a poly-Ala sequence without any possibility in side chain interaction between the guest positions that helicity was increased with hydrophobicity in a hydrophobic environment. In addition, the packing of the hydrophobic side chains is based on mainly van der Waals interactions. Depending on residue and rotamer type, this results in a favourable enthalpic effect making thus the energy barrier for unfolding higher. So the hydrophobicity of the residue contributes to the helicity of a TMD. Nevertheless, Val and Ile induce backbone dynamics in transmembrane helices due to their restricted side chain rotation leading to an increased entropy loss and/or due to unfavourable side chain side chain interactions (see introductory section 1.1.4, p. 13) [Creamer and Rose, 1992, Poschner *et al.*, 2009, Quint *et al.*, 2010, Stelzer *et al.*, 2008]. In sum, the results from CD spectroscopy can be explained by thermodynamic aspects concerning the helix stability of the APP TMD which may also influence β-sheet formation once Aβ fragments are released from the lipid bilayer and/or lumen of the γ-secretase.

DHX experiments provide information on helix stability as well as dynamics because H-bond stability in an α-helix is probed by deuterium/ hydrogen isotope exchange occurring only at transiently opened H-bonds (see section 1.2.2, p. 18). Based on the DHX kinetics of model peptides A 28–44 and A 37–55, one can distinguish a pronounced dynamic dimerisation domain and relative to it a more moderately dynamic cleavage domain in the APP TMD (see section 4.2.2, p. 58). As the isotopic exchange proceeds in an EX2 mechanism reflected by the continuous shift of the mass over charge ratio of the investigated peptides over time (compare Figure 4.3, p. 58) combined with the distribution of different rate constants, the exchange takes place only at open H-bonds resulting here from local unfolding. Only the starting point of DHX is lowered by the random coil proportion as described in the results section 4.2.2 on p. 59.

For comparison, the DHX kinetics of an unfolded A 28–55 can be determined by calculating the intrinsic rate constants k_{int} ($k_{int} = k_{ch}$, see equation 1.17, p. 22), which

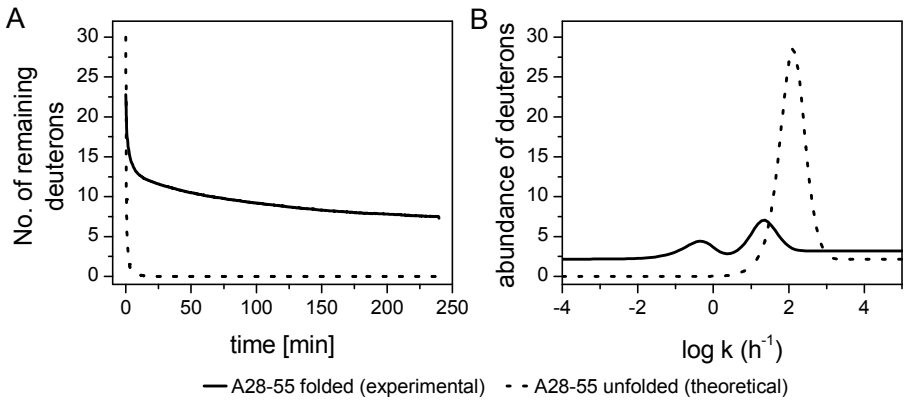

Figure 5.1: Comparison between simulated DHX of unfolded A 28-55 and experimental DHX of folded A 28–55. A: Respective kinetics for folded and unfolded A 28–55 are shown. For the folded one, data from the DHX experiment at pH 5 are depicted as seen in Figure 4.4 (p. 60). For the unfolded one, intrinsic rate constants were calculated on the basis of acid-, base- and water-catalysed isotope exchange and for the respective residue pairs with the web server program Sphere for an exchange against water at pH 5 (http://www.fccc.edu/research/labs/roder/sphere, visited on 02.02.2012) [Bai *et al.*, 1993, Zhang, 1995]. The DHX kinetics are thus generated from a 30 term exponential function in which for each amide deuteron the respective calculated rate constant was taken ($D(t) = \sum_{i=1}^{30} exp(-k_i \cdot t)$). B: Rate constant distributions for unfolded and folded A 28–55. Both distribution were determined on the number of amide deuterons in A 28–55 ($D = 30$), irrespective of the helix structure, and on $D_{t=0} = 0$. The MEM rate constants for the unfolded peptide were calculated with a fictive standard deviation of 0.1 D. The distribution corresponds to the rate constant distribution calculated from Sphere.

is done by using the web server program Sphere based on the PDLA peptide references [Bai *et al.*, 1993, Zhang, 1995] (see Figure 5.1). The simulated isotope exchange for the unfolded full length APP TMD clearly ends after 3 min. Because each amide deuteron exchanges in a single reaction of pseudo-first order, their half lifes can be determined with $t_{1/2} = \frac{ln2}{k}$. The average half life for amide-hydrogens in the unstructured A 28–55 is 0.34 min, whereas it is 1.8 min and 96.1 min for the helical A 28–55 (converted from the average $log\ k$ of peaks seen in Figure 5.1 B). In other words, an α-helical structure is indeed able to protect its amide hydrogens against isotope exchange. Only when an intrahelical H-bond opens, it allows the isotope exchange. Since the DHX in EX2 mechanism is described by equation 1.12 (p. 20), the thermodynamic equilibrium constant K_{unfold} with regard to unfolding is influenced by the ratio of the exchange rate constant over chemical rate constants for each amide hydrogen involved in a H-bond. Because the chemical rate constants are higher than the exchange rate constants, K_{unfold} is low which agrees with the fact that a transmembrane model peptide is populated more or less in the native state. In which way the equilibrium constants K_{op} of each amide hydrogen bond contribute to the overall K_{unfold} of a transmembrane helix cannot be described easily because some H-bond openings may have an cooperative effect and some are independent from each other, this means the two-state model (α-helix $\rightleftharpoons$

random coil) would not reflect the complex local unfolding reactions. Beside the H-bond formation contributing to K_{fold}, the contribution from the side chain - side chain and side chain - backbone interactions need to be included for determining K_{fold}.

When considering all this, the question arises whether it is possible to distinguish between local and global unfolding when in both cases the closing rate is higher than the intrinsic exchange rate. In the case of global unfolding, it would mean firstly that the equilibrium constant K_{op} would be the same for each exchanging amide deuteron and has a small value. Secondly, global unfolding would arise from a cooperative effect, in other words, events of H-bond opening depend on each other. Thirdly, more than one unfolding event is needed for exchange. And finally, since all rate constants k_{ex} depend on K_{op} and k_{ch}, each k_{ex} of an amide deuteron will not differ very much and the rate distribution would yield only one peak similar to that describing exchange in completely unstructured peptides yet with a lower peak value.

5.2 How Does APP TMD Backbone Dynamics Influence γ-Secretase Mediated Cleavage

Beside the analysis of the helix dynamics, the biological significance shall be addressed, as well. Our results show that the dimerisation domain exhibits a highly dynamic region, whereas the cleavage region is restrained in its backbone dynamics compared to the tandem GxxxG region. Sato *et al.* identified further structural instabilities in the APP TMD by solid state NMR at -68°C in DMPC:DMPG membranes at residues Val50 and Leu52 which are near the ε-cleavage site and assigned to random coil structure [2009]. Also, Lu *et al.* report on solid state NMR experiments of a model peptide Aβ 28-55 where the APP TMD in membranes of neuronal lipid composition and at physiological temperatures (37°C) show destabilisation at the N- and C-termini at Ala30 and Val50 and in the APP TMD centre at Gly38 and Val40 [2011]. These findings suggest that Gly37, Gly38 and Val40 in model peptide A 28–44 are mainly responsible for the pronounced dynamics. Because these residues in model peptide A 37–55 are close to the N-terminus, one can conclude that at these positions the residues do not influence the overall backbone dynamics of A 37–55 in spite its great effect in A 28–44. Here, it becomes clear that backbone dynamics is position dependent. In line with the works of Lu *et al.* [2011], molecular dynamics simulation done by Widmaier [2009], Hornburg [2010], and Proebstle [2012] show that the APP TMD is a helix exhibiting elevated C_α-RMSF values at the N- and C-termini and in the centre between Leu34 and Ala42. In addition, their respective standard deviations are greater for the tandem GxxxG region than for the cleavage region (see Figure 5.2). C_α-RMSF values are a measure for the deviation from the average structure sampled from a simulation, implying increased backbone dynamics at the named sites. The destabilisation at the termini of a helix

polypeptide is a property which is called fraying. For example, the N-terminal helix of cytochrome c was investigated with hydrogen exchange by ^{1}H-NMR and revealed the consequence of 50% H-bond coverage at the termini because the respective H-bond partners are lacking, at the N-terminus the carbonyl oxygens and at the C-terminus the amide hydrogens [Milne *et al.*, 1999].

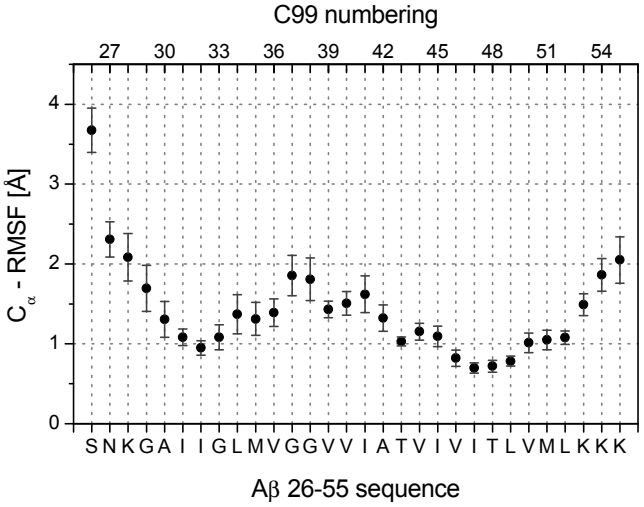

Figure 5.2: C_α-RMSF of Aβ 26-55 monomer model with amidated C-terminus from 190 ns MD simulations in 80% (v/v) TFE in water performed by Daniel Hornburg [2010] and analysed by Rasmus Proebstle [2012]. Modelling is based on the CHARMM force field, and parallelised on NAMD.

In order to get information for the APP TMD cleavage by γ-secretase, one should notice that the C_α-atoms investigated by MD simulation and the H-bonded amide hydrogens studied by DHX experiments are indirect probes for carbonyl accessibility. The decisive reaction centre is the carbonyl when it approximates the two catalytic Asp of presenilin. One Asp of presenilin is protonated and forms a complex with the carbonyl oxygen via a H-bond which requires prior transient openinig of the intrahelical H-bond to amide hydrogen of $i + 4$. The second Asp, which is charged, acidifies the water molecule in order to facilitate the nucleophilic attack of the water to the carbonyl carbon atom (C_1-atom). A tetrahedral intermediate evolves and forms back into a carbonyl by breaking the peptide bond between the carbonyl carbon and the amide nitrogen [Singh *et al.*, 2009] (see also section 1.3.3, p. 29). For this, the carbonyl carbon C_1 of residue i needs to be exposed to water. This can be achieved by the deviation from the helical geometry via H-bond opening to amide hydrogen of $i + 4$.

Though CD and DHX results from this work are not able to give site-resolved information and to explain γ-secretase mediated cleavage, the combination with molecular dynamics complements this. Therefore, in the group of Christina Scharnagl, a model was developed in order to simulate a DHX experiment from a MD simulation of model peptide A 28–55 in 80% (v/v) TFE and water [Hornburg, 2010, Widmaier, 2009]. Figure 5.3 shows the comparison between experimental exchange kinetics and the calculated

one. Computation of the deuteron count is based on equation $D(t) = \sum_{i=1}^{N} exp(-k_i \cdot t)$ where N respresents the number of amide hydrogens and k_i the exchange rate constant for each amide hydrogen. As the EX2 type is the underlying mechanism, k_i results from the product of K_{op} and k_{ch} (see equation 1.12, p. 20). The chemical rate constant k_{ch} is calculated with equation 1.17 (p. 22). The ratio of opened to closed states over the simulation time for each residue was determined and gave K_{op}. For this, the distance criterion to find an amide hydrogen in a closed H-bond was set to < 3 Å for the duration of more than one picosecond.

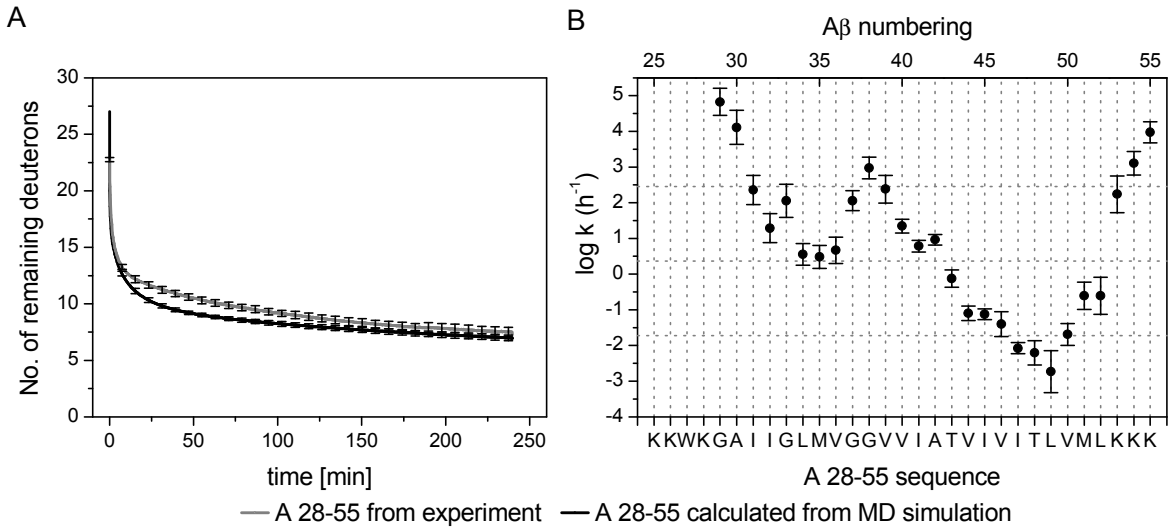

Figure 5.3: Comparison of calculated and experimental exchange kinetics of A 28–55. A: DHX kinetics; the good agreement between experimental and modeled kinetics is described by χ^2 (exp-calc)=0.840 B: Rate constants assigned to the sequence. Data from MD modelling are provided by Christina Scharnagl. Horizontal dashed lines signify borders, the same as in Fig. 4.5 (p. 61).

With the MD simulation, it is now possible to assign rate constants to single amide deuterons. A first glance at Figure 5.3 A reveals a good agreement between calculated and experimental DHX which validates the rate constants in Figure 5.3 B. In agreement with the DHX results obtained with A 28–44 and A 37–55, the dimerisation domain has amide deuterons with higher rate constants than the cleavage region (see Figure 4.5, p. 61). The absolute counts of amide deuterons within $log\,(k\,/h^{-1})$ boundaries defined in Figure 4.5 (p. 61) do not deviate very much from the counts derived from MD simulation. Only for the fast exchanging region, the MD simulation gives two deuterons more explaining the small difference between the DHX curves.

The lowest rate constant from MD simulation is assigned to the amide deuteron of residue Leu49, whereas further C-terminal amide deuterons exchange with higher rate constants. The biggest rate constant difference is between Leu52 and Lys53. Applying the thought that the carbonyl at $i-4$ is influenced by the H-bond opening, then one can conclude that the carbonyl of residue Leu49 is less protected than the one of Thr48. As their chemical rate constants are comparable to each other ($log\,(k_{ch,Leu52}\,/h^{-1}) = 2.1$,

$log\,(k_{ch,Lys53}\,/h^{-1}) = 2.3$), the probability of an opened H-bond at carbonyl of Leu49 is higher than for Thr48 ($K_{op,Leu49} > K_{op,Thr48}$), which might explain why more Aβ40 than Aβ42 is found with the wild type APP [Suzuki *et al.*, 1994, Younkin, 1998] (see also section 1.3.2, p. 26). In line with the observation of Sato *et al.* [2009], a particular helix unraveling at position Leu52 and Lys53 might be required for the initial cleavage event. Beside this, of course substrate recognition, lateral movement of the substrate, substrate anchorage by presenilin, enzymatic efficiency and substrate dimerisation are important key factors in the process [Beel *et al.*, 2008, Beel and Sanders, 2008].

Further questions arise from the overall helix dynamics of the APP TMD. How can backbone dynamics be modulated with small molecules such as NSAIDs? Or which key residues are important for the moderate dynamics of the cleavage region? How is backbone dynamics at the C-terminus altered, once the initial cut at the ε-site is performed. These and other questions shall be addressed in the following sections.

5.3 NSAIDs Do Not Impair Backbone Dynamics of Lys-Flanked APP TMD in 80% (v/v) TFE in Water

NSAIDs are promising therapeutics modulating the Aβ peptide production in Alzheimer's Disease [Weggen *et al.*, 2001]. It is discussed whether NSAIDs target the γ-secretase [Barrett *et al.*, 2011, Beel *et al.*, 2009, Gamerdinger *et al.*, 2008, Lleo *et al.*, 2004, Weggen *et al.*, 2003] and/ or the APP TMD respectively the Aβ peptides [Kukar *et al.*, 2008, Richter *et al.*, 2010, Sagi *et al.*, 2011]. Surface plasmon resonance spectroscopy and ^{1}H-^{15}N-NMR spectroscopy reveal a binding between the Ile32-Val39 region of Aβ42 and sulindac sulfide, probably in a 1:1 molarity ratio [Richter *et al.*, 2010]. Molecular docking simulations identify the binding site between a flat region constituted by the helical $G_{29}xxxG_{33}$ region and the NSAID (structures are assembled in Figure 4.6, p. 63) [Richter *et al.*, 2010]. Their binding nature results from an amide-π-interaction between the quadrupole moment of the aromatic backbone of the NSAID [Dougherty, 1996] and the electrostatic surface of the $G_{29}xxxG_{33}$ APP TMD region and from H-bonds between the NSAID's carboxy-group and the amide hydrogen of Gly29 or the amino group of Lys28 in case of sulindac sulfide [Hughes and Waters, 2006, Ma and Dougherty, 1997, Richter *et al.*, 2010]. It is suggested that the NSAIDs' binding to this motif reduces dimerisation of the APP TMD as the interface between both monomers is occupied by NSAID binding. This could affect Aβ production since the mutation of Gly33 against Ala leads to shorter and less aggregation prone Aβ peptides [Munter *et al.*, 2007, Richter *et al.*, 2010].

Therefore, to shine more light into the mechanistic way of action, NSAIDs were also tested for its impact on helix dynamics (see structures in section 4.2.3, p. 62). However, the results reveal no difference in DHX kinetics compared with A 28–55 in absence

of NSAIDs. Here, it is unclear whether NSAID had bound to A 28–5 at all, and if, the nature of binding would have been unspecific. It is likely that TFE molecules surround the hydrophobic NSAIDs with their fluorinated methyl groups like they do with a hydrophobic peptide [Roccatano *et al.*, 2002]. Since there is less need in burying hydrophobic surfaces like it would occur in pure water solutions, it would not make a binding of an NSAID to the peptide favourable.

Though weak hydrophobic effects, van der Waals and dipole-like forces are not excluded in TFE [Buck, 1998, Roccatano *et al.*, 2002] leading to another explanation. This would be the binding to other sites than the reported $G_{29}xxxG_{33}$ motif. The Lys side chains of A 28–55 could interact in two ways with the NSAIDs, either in a cation-π-interaction between the charged amino group of Lys and the aromatic system of the NSAIDs [Dougherty, 1996] or in an ionic interaction between positively charged amino group of Lys and the negatively charged carboxylic group of the NSAID. In a hydrophobic environment, an ionic interaction seems more likely by the reason that its strength is increasing with a decreasing dielectric constant [Elston *et al.*, 1998, Jiang *et al.*, 2002, Subczynski *et al.*, 1994, White *et al.*, 1981]. Consequently, the amount of Lys side chains, the variety of other binding sites and the better accessibility of the polypeptide's termini account for a high binding competition. Additionally, a π-π-interaction between the indol ring of Trp in A 28–55 and the aromatic system of NSAIDs is another binding possibility. Therefore, it is unlikely that the aromatic moiety of the NSAIDs shall interact with the GxxxG motif in a preferential way and protect the APP TMD from DHX as a consequence.

In order to find out any NSAID impact, the model peptide should exclude Lys and Trp side chains or any other positively charged residues and aromatic based side chains.

5.4 Thr Backbonding In the APP TMD Increases Helix Stability - Implications For γ-Secretase Proteolysis

Here, the impact of Thr on helix dynamics shall be evaluated and the question will be discussed why they are able to increase helix stability in the cleavage region (see Figure 4.1, p. 56).

The APP TMD incorporates two Thr on position 43 and 48 (Aβ numbering). These were changed into Val as single and double mutants in order to replace the polar hydroxy group of Thr. Another mutant was created with Ile at Thr43 which is the Austrian FAD mutant [Kumar-Singh *et al.*, 2000, van Broeck *et al.*, 2008].

The secondary structure results revealed attenuated helix-levels in favour of increased random coil fractions accompanied by little β-sheet content in the following order: A 37–55 > A 37–55 T43V ≈ A 37–55 T43I ≈ A 37–55 T48V > A 37–55 T43V T48V. Already in 1984, it was discovered that a Thr residue at position i forms a H-bond

to the backbone carbonyl oxygen of residue $i-4$ in TM helices of membrane-bound proteins [Baker and Hubbard, 1984, Ballesteros *et al.*, 2000, Gray and Matthews, 1984] and thus allows polar residues to be in hydrophobic environments [Gray and Matthews, 1984]. H-bond backbinding by Thr is confirmed for Aβ 26–55 and A 37–55 wild type by MD simulations [Hornburg, 2010, 2011] (see Figure 5.4). Here, the helicity extent is represented by their different H-bond occupancies.

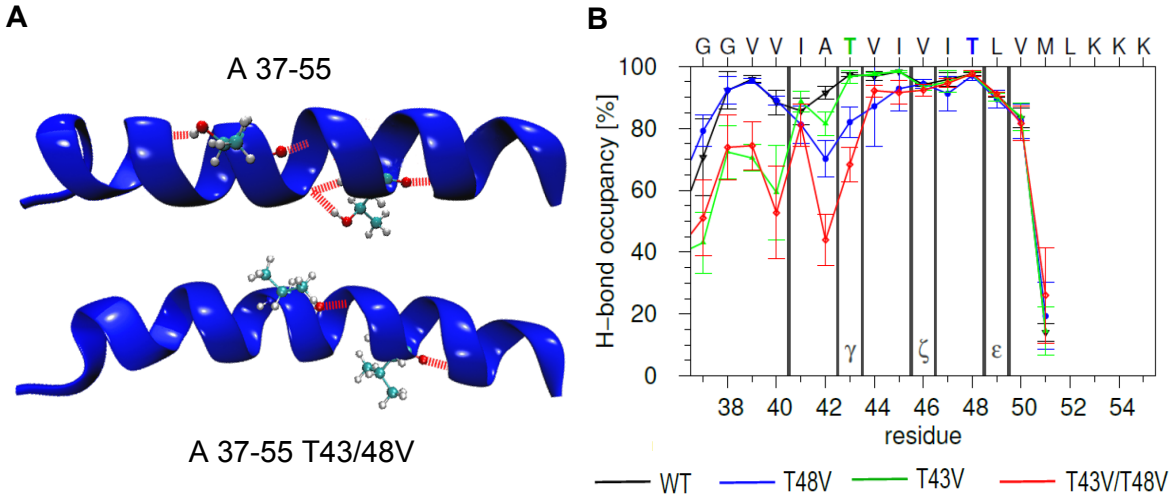

Figure 5.4: Hydrogen bond pattern of A 37–55 peptides from MD simulations. A: One snap shot of A 37–55 and its double mutant T43V T48V from 190 ns MD simulations emphasizing residues on position 43 and 48 and depicting the involved, in red dashed H-bonds. Oxygens are in red, carbons in turquoise and hydrogens in white. N-terminus is on the left. B: H-bond occupancy of the residue CO(i) to NH($i+4$, α) and NH($i+3$, 3_{10}). Figures are provided by Hornburg [2011] and by Christina Scharnagl.

In DHX, the slowest kinetic is represented by A 37-55 wild type, followed by A 37-55 T43V, A 37-55 T43I, A 37-55 T48V and A 37-55 T43/48V. Thr43 mutants showed slightly elevated backbone dynamics in the very fast exchanging range (first 3 min) and have in addition more deuterons with intermediate rate constants. Kinetics of both T48V mutant and the double mutant accelerated with higher rate constants assigned to very fast and fast deuterons. This is in line with MD simulations, from which the stabilities of H-bonds expressed as H-bond occupancy probabilities for carbonyl oxygens are computed and provided by Philipp Hornburg and Christina Scharnagl (Figure 5.4 B) [Hornburg, 2011]. Note, for partnering amide hydrogens, one has to read the 3rd (3_{10}-helix) and 4th (α-helix) next residue. Based on MD data, all mutants show less H-bond occupancy than the wild type. In detail, T43V has less amide hydrogen-bond occupancies in the region between residue 40 and 44 and T48V in the region from 46 to 49. Since the region between 40 and 49 is affected for the double mutant, the effects of the single mutations seem to be additive. Consequently, one may assume that amide deuterons with very fast exchange velocities probably lie between region 40 and 44. Deuterons which are fast in the T48V mutant can be probably assigned to the region between 46 and 49, whereas the increase of intermediate deuterons in the T43V mutant

can be explained by the slight decrease of H-bond occupancy in the same region.

What does Thr backbonding in the APP TMD imply for the γ-secretase cleavage? To address this questions, the influence of mutations at positions 43 and 48 on Aβ production shall be compared. With specific anti-Aβ ELISA assays, endogenous Aβ peptides from cells producing APP mutants are quantified. Mutations of Thr43 against Phe, also deficient of an H-bond donor, led to a 30% Aβ40 reduction and a 15% Aβ42 and 10% Aβ38 augmentation, yet total Aβ amount was decreased by 40% compared to wild type [Tan *et al.*, 2008]. Similar, but smaller differences were detected for a T48F mutation [Tan *et al.*, 2008]. In an earlier study of Lichtenthaler *et al.*, Aβ42 levels were elevated too. Indeed, the T43F mutation caused a double increase compared to wild type, Aβ40 and total Aβ level remained the same as for wild type. For T48F, the increase in Aβ42 was about 50% [Lichtenthaler *et al.*, 1999]. The Austrian mutation T714I (T43I) was investigated by Munter *et al.* [2010]. They noticed an increase for Aβ42 by 150% and for Aβ38 by 40% and a decrease in Aβ40 by 75% compared to wild type. The total level in Aβ was comparable to wild type. Cell-free based assays by Chavez-Gutierrez *et al.* [2012] confirm the results by Munter *et al.*, though they observe a decrease in ε-site cleavage efficiency. Similar results were gained for the T43V mutation in the same lab (personal communication with Lisa Muenter, FU Berlin, lab of Prof. Gerd Multhaup). Thus, the abolishment of a side chain backbone H-bond influences the Aβ product pattern.

To explain the outcome of the T43V and T43I mutation, two scenarios could possibly take place. First is that the T43 mutation induces a preference to cut at position 48 instead at 49. The latter is that a switch from the Aβ40 to the Aβ42 product line occurs at ζ- or γ-cleavage sites. To test these hypotheses one needs to measure the Aβ peptide profile by mass spectrometry. It could be also possible that cleavage pattern is in general altered and does not behave according to the established product lines in a 3 to 4aa wise pattern. Yet, this seems not likely. The research by Kukar *et al.* [2011] showed that a K28A mutation extended the product pattern to Aβ33 and Aβ34 but did not induce necessarily random subsequent cleavage, though by this mutation the binding site to presenilin at the height of the lipid head groups was lost. In addition, recent research of Chavez-Gutierrez *et al.* [2012] supports the first scenario to be possible. They discovered by AICD concentration determination that more $AICD_{49-99}$ was produced than $AICD_{50-99}$ with a T43 mutation indicating the preference to cut at ε-site 48 than 49. From this, the enhancement of backbone dynamics in the region between G37 and V44 may infer a long distance effect at the ε-site. This might be a slight helix rotation (about 100°) making cleavage site 48 more accessible to the Asp-H_2O-Asp^- complex. This rotation might be caused by loosing not only an intramolecular H-bonding possibility by Thr43 but also an intermolecular one and thus loosing anchorage. A H-bond between Thr of one monomer to a backbone carbonyl oxygen of the other monomer has been discovered for a glycophorin dimer [Smith *et al.*,

2002] and this principle could apply also to the APP TMD interacting with a TMD of presenilin, most likely either TMD6 or TMD7 in which the catalytically active Asp are located.

In addition, it was described in the computational studies of Singh *et al.* [2009] that the rate limiting formation of the geminal diol had a transition state of lower energy for the peptide bond between Val40 and Ile41 than for Ala42 and Thr43 explaining an energetic preference for the V40I41 peptide bond cleavage. A H-bond between the Thr side chain and the negatively charged Asp residue of the catalytic site was observed deterring the Asp from abstracting the proton of the water molecule. So the mutation at site 43 into Val or Ile would present another electronic microenvironment probably making the cut between residue 42 and 43 energetically more favourable.

From personal communication with Lisa Muenter (FU Berlin, lab of Prof. Gerd Multhaup), a T48V mutant caused in her ELISA experiments of the cell culture supernatant (derived from SH-SY5Y cells including full-length APP) a 20% elevation of Aβ40 and a 50% relegation of Aβ42 compared to wild type. It seems that the general preference of the Aβ40 product line over Aβ42 in wild type is reinforced by this mutation. To exclude whether there might by a change in the product line after initial cleavage at postion 48, a mass spectrometric profile needs to be recorded from the supernatant of the cell cultures. Explanation might be the loss of a possible intermolecular H-bond between Thr48 and one of the residues of presenilin's TMDs reorientating the helix towards the active site including the absence of possible interactions to one of the catalytic Asp [Singh *et al.*, 2009].

All in all, the key residues Thr at position 43 and 48 play a crucial role in defining the Aβ product pattern. The lack of H-bonding of the Thr side chain to the backbone alters the dynamics of the substrate helix. From this point, it seems that ε-cleavage is more or less influenced by the dynamics induced by the T43 and T48 mutations. Nevertheless, one should keep in mind that proteolysis is also influenced by the alteration of the electronic microenvironment and by the orientation to the active site due to presence/absence of potential interaction between the APP TMD and the cleaving enzyme.

5.5 Analysis of APP TMD Fragments Gives Site-Resolved Information on Backbone Dynamics

So far, the DHX experiments and MD simulations (see Figure 5.2 and 5.3 on p. 98) suggest that local dynamics at position 53 in the C99 sequence defines the preference in ε-cleavage 49 over 48 since position 49 is less protected by a backbone H-bond which leads to higher Aβ40 levels than Aβ42. Further, we see increased stability in the cleavage region caused by additional H-bonds between the Thr side chains and the

$i-4$-carbonyls defining the Aβ product pattern.

Because the first possible H-bond occurs between the NH of the last C-terminal residue to the $i-4$ CO group and protects it from the catalytic diad, it is also of interest how backbone dynamics of the C-terminal region is modulated once the initial cleavage by γ-secretase took place.

For this purpose, AL model peptides were created which have a variable APP TMD octasequence with a C-terminal residue representing a cleavage site and an invariable Leu_{11} sequence flanked with a K_4W tag on the N-terminus (sequences can be viewed in section 4.4 on p. 69). CD analysis of the AL peptides reconstituted in DLPC:DLPS:DLPE liposomes revealed in general a helical conformation. Within the peptide set, the reference peptide L19 exhibited the highest helicity. This is followed by AL 45-52, AL 42-49 and AL 39-46 with similar helix contents (approx. 60%) and AL 35-42 with the lowest helix content with approx. 40%. The low helicity in the latter peptide results from the two Gly in the guest sequence.

DHX experiments were performed also in liposomes with an acyl chain length of C12 at 70°C and pH 7.5 (pH adjusted at room temperature), the same conditions as in CD experiments. As expected, L19 exhibited the slowest kinetics revealing low backbone dynamics. The most elevated one was observed for AL 35-42. This is followed by AL 39-46, then AL 42-49 and AL 45-52. The order between AL 42-49 and AL 39-46 is reversed after the first 3 min exchange. With the assignment of the non-exchangeable, exchanged and, due to their rapidity, not detected deuterons, a rough assignment of the three groups to the sequence of L19 was possible (see Figure 4.14, p. 74). Based on this, assignment to the C-terminus of the hybrid APP TMD peptides was refined. Approx. 60% to 80% coverage was possible and a difference of three deuterons between the lowest and the highest exchanging guest sequence is seen. Comparing dynamics of the guest sequences, AL 42-49 with its two Thr belongs to those peptides which exchanged slowly given the low abundance of class A (fast) and higher abundance of class B (intermediate) and C (slow) deuterons (derived from triple exponential fitting). Yet, one may ask why it was not the most rigid helix since a double Thr backbonding in A 37–55 had such a high stabilising effect. In a liposomal membrane, the polar hydroxy group of Thr has a higher preference to interact with the polar backbone since the environment is more hydrophobic than TFE. Despite that, high temperature leads to increased rotational and vibrational movements of the side chains. Therefore, Thr's H-bonds could open and close more frequently. Further, competition to form H-bonds with water could occur. Under these extreme conditions a water penetration into the lipid bilayer is possible. Since the CD results report more or less a helical conformation for AL 42-49 at 70°C, it supports the idea that DHX experiments sense a high frequency in opening and closing thus increasing isotope exchange. This effect may not contribute to conditions modelling exact backbone dynamics in a cleavage environment. But in order to increase penetration depth for the DHX catalyst, both membrane fluidity was

increased and membrane thickness was decreased.

L19 as the most hydrophobic sequence exhibits the slowest exchange. Hence, another perspective on DHX is the correlation between the sequence hydrophobicity and the accessibility of the polar hydroxide ion mimicking the cleavage situation (see Figure 5.5). The polar Asp-H_2O-Asp$^-$ triad as catalytic centre and the interaction with the hydrophobic cleavage sites may give information for the cleavage efficiency. Since the octasequence of AL 45-52 is more hydrophobic than the other ones, ε-cleavage in general would need more time to form the tetrahedral intermediate as this is the rate-limiting step [Singh *et al.*, 2009]. In that order, the more hydrophilic a subsequence becomes, the deeper the penetration by the catalyst and the faster the cleavage would occur. In this experiment not only backbone dynamics comes into account for DHX kinetics but most probably also the hydrophobicity of the C-terminal octasequences.

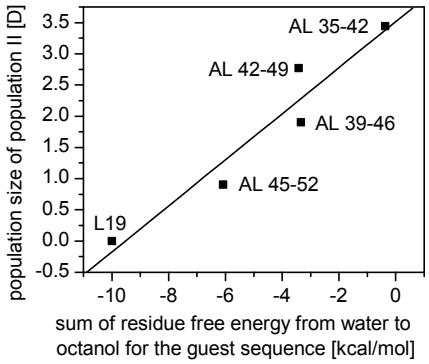

Figure 5.5: Correlation of subsequence hydrophobicity with rate constant population II. Hydrophobicity of the octapeptide in AL peptides was determined with the sum of free residue energies computed from the MPEx programm provided by Steven White [Snider *et al.*, 2009] and correlated to the population size of the rate constant population II (see Figure 4.15 on p. 75). Regression function: y=0.369x+3.513, Pearson correlation coeffcient: R^2=0.92

Applying this new hypothesis that cleavage efficiency would depend on sequence hydrophobicity and follow the order $\varepsilon < \zeta < \gamma$, would be though only one view on this. Singh *et al.* discovered that scissile bond of $V_{40}I_{41}$ needs less activation energy to form the tetrahedral intermediate than the more hydrophilic $A_{42}T_{43}$ pair due to their electronic microenvironment and steric allowances [2009]. This means a preference to form Aβ40 over Aβ42 peptides. Here, the hydrophobicity, i.e. the probability to be solvated, is not the only factor influencing cleavage.

It is plausible once the initial cut at the ε-site has taken place, sequential processing is eased due to fraying at the C-terminus by the reason that the AL backbone dynamics order is influenced by the extent of fraying. Since fraying is a property of all peptide termini due to 50% H-bond saturation and less side chain/ side chain interactions, its extent is determined by the degree of existing side chain/ side chain interactions and by the hydrophobicity of the sequence and its resulting solvation.

Since the 3 to 4 aa stepwise cleavage is proven by Fukumori *et al.* [2010], one may

ask how cleavage sidedness does not conflict with C-terminal helix fraying. First, the next cleavage occurs at the 3rd/ 4th residue upstream from where H-bonds start to be formed, second timescales of subsequent cleavage and fraying may probably oppose each other and third the "electronic nature of the cleavage site" is important [Singh *et al.*, 2009].

Another perspective is the backbone dynamics of TMD 6 and 7 of presenilin. Could the backbone dynamics of both TMDs play a role in the proteolysis? Their hydrophobic sequences are: TMD6 (LILAVISVYDLVAVL) and TMD7 (GVKLGLGDFIFYSVLVG) (UniProt-Accession number for presenilin: P49768). With 4 Leu and 3 Ala it is likely that TMD6 exhibits a stable α-helix, whereas TMD7 contains 4 Gly inferring higher backbone dynamics than TMD6. Compared to the amino acid distribution of the APP TMD, the APP TMD is longer (24aa hydrophobic length) and has in addition to 4 Gly a higher Val/Ile content. A TMD length mismatch could occur with a possible hydrophobic mismatch with the respective membrane and/or perhaps in the lumen of presenilin. The PS-TMDs have their Asp quite in the middle of the sequence. Related to the cleavage mechanism, it is imaginable that the APP TMD is tilted due to the hydrophobic mismatch. Further, its curvature at around Gly37 and Gly38 has been revealed by MD simulations [Widmaier, 2009] and by NMR and electron spin resonance spectroscopy (EPR) with double electron electron resonance (DEER) determining a length of 33.5 $\pm$ 1.0 Å instead 36 Å [Barrett *et al.*, 2012]. Thus, a positioning of the ε-site to the middle of the membrane respectively to the active site is possible. Once the initial cleavage took place, the shortened helix curve could move step by step back to the membrane normal explaining the fact that the APP TMD is cleaved in a range of ca. 10 amino acids since an up- and downward movement along the membrane normal is not likely because Lys28 was proved to act as an anchor in the height of the lipid head group region of the membrane [Kukar *et al.*, 2011].

5.6 Comparing Backbone Dynamics of the APP TMD with that of Non-APP-TMDs

The transmembrane domain of the APP shall be compared with other artificial (LV peptides) or natural (TMDs with an average residue composition) TMDs. If backbone dynamics has an impact on the cleavage processes by γ-secretase, the question will arise how the backbone dynamics of non-APP-TMD is distinguished from APP TMD helix dynamics.

5.6.1 Helix Dynamics of Artificial Non-APP-TMDs

The LV peptides were used because the ratio of Leu (α-helix former) and Val (α-helix destabiliser) determines the helix backbone dynamics [Poschner *et al.*, 2009]. Here, L16, LV16 and LV16 G8P9 were chosen.

The DHX kinetics of A 37–55 is similar to that of LV16 except that A 37–55 has a fast exchange behaviour in the first minutes exceeding the kinetics even of LV16 G8P9. In A 37-55, two Gly are close to the N-terminus and could therefore account for the rapidity at the beginning of isotope exchange. Positioning the Gly close to the N-terminus will affect the already fast exchanging region. In section 5.6.2 further examples shall be discussed when Gly are located in the core of a helical peptide. Peptide A 28-44 has four Gly well distributed along the sequence, therefore also the core which is thought to elicit fast and/or intermediate exchange is affected by Gly.

5.6.2 Helix Dynamics of Natural Non-APP-TMDs

Backbone dynamics of a TM helix is dependent on its sequence. The high content in β-branched residues of the APP TMD compared to the average occurrence in TMD helices suggested strong backbone dynamics which could be important for membrane protease mediated cleavage. Here, we compared backbone dynamics of the APP-TMD to that of non-APP-TMDs.

Selecting the transmembrane domains for their residue composition resulted in a pool of TMDs which are enlisted with their sequences and residue compositions in Tables 4.1 (p. 54) and 4.7 (p. 82). None of the selected TMDs had the exact residue composition as computed for the average. KTMD01-06 and KTMD11-13 were the sequences of choice as they had a difference sum between 29% and 40% which reflects differences to the average. Further, we focused on good agreements for the Gly, Leu, Ile and Val contents. Therefore, also KTMD07-10 were considered which are of human origin. KTMD07 represents a γ-secretase-substrate [Anders *et al.*, 2006, Haapasalo and Kovacs, 2011].

In order to compare the backbone dynamics of the KTMDs with that of the APP-TMD models, CD analysis was performed to test helicity. Although the line shapes of the spectra hinted good helicity, quantitative evaluation suggests substantial random coil structure, too.

The DHX of the 31aa long peptides indicated that TM helices with average residue composition can also exhibit pronounced backbone dynamics and that the APP TMD was not more dynamic than the KTMDs. Thus, similarity to the Leu content in average TMDs does not confer strong rigidity. This supports the fact that amino acid composition can predict roughly backbone dynamics, but the order how the residues are arranged to each other needs to be considered, as well. Based on the order, specific influences on backbone dynamics derive such as side chain - side chain interactions [Fisinger *et al.*, 2001], side chain packing [Cornish *et al.*, 1994, Quint *et al.*, 2010],

hydrophobicity [Liu *et al.*, 1996], side chain rotation freedom [Creamer and Rose, 1992] and side chain - backbone interactions [Gray and Matthews, 1984].

As A 37–55 models the cleavage domain, KTMDs of 23 aa length were chosen for comparison. KTMDs exhibited great variety in DHX kinetics in between that of A 37–55 and A 28–44. That was surprising, as none of the KTMDs showed slower kinetics than A 37–55. In fact, Gly were found to affect the backbone dynamics of the KTMDs. The more they were located in the centre of the sequence, the faster the DHX kinetics. But even the Gly deficient KTMD10 peptide had kinetics with higher rate constants than A 37–55. Introducing other types of residues can apparently also enhance backbone dynamics. As a consequence, natural TM helices display strong average backbone dynamics. Here, the question arises whether the high content in Val and Ile (in sum 8 for A 37–55) would confer exceptional backbone dynamics to the APP cleavage region. As Thr were identified in MD and DHX to stabilise the A 37–55 helix via an additional H-bond between the Thr's hydroxyl group and the $i-4$ carbonyl oxygen, mutations of Thr into Val enhanced backbone dynamics in A 37–55 such that it was similar to that of KTMD04, KTMD08 and KTMD10. To eliminate the Gly effect, several KTMDs were selected and adjusted to the Gly pattern of A 37–55 which lacks a central Gly. Here, the backbone dynamics of the mKTMDs indeed decelerated. Compared to the backbone dynamics of A 37–55 T43V T48V, a high content of β-branched Val and Ile may indeed cause elevated backbone dynamics and hence elevated DHX kinetics. In principle, a sequence close to the average aa composition can form a more stable helix than a Thr mutated APP TMD cleavage region.

Another exceptional TMD is KTMD07 since this represents a γ-secretase-substrate [Anders *et al.*, 2006, Haapasalo and Kovacs, 2011]. However, cleavage efficiency, its exact cleavage sites and whether the substrate is cleaved multiple times is not known to my knowledge. The DHX and MEM results state that it has a similar rate constant distribution compared to A 37–55. The N-terminal half of the KTMD07 sequence has mainly helix-destabilising residues (sequences are compiled in Table 4.1, p. 54). It is likely, that the C-terminal L_4 motif stabilises its helical backbone and thus governs the overall backbone dynamics of KTMD07. Since a dynamic helix is required for cleavage by γ-secretase, cleavage may possibly occur at the N-terminal half of the KTMD07 sequence.

Above all, the cleavage region of the APP TMD does not exhibit higher backbone dynamics than average TMDs do. Since local unfolding is a requirement of the proteolytic cleavage by γ-secretase and the APP TMD cleavage region has more than 50% of helix-destabilising β-branched residues, one asks then how γ-secretase can distinguish the APP TMD from a non-APP-TMD. It has been proved for the APP-TMD that local dynamics downstream of the ε-site is required for endoproteolysis and represents a key factor [Sato *et al.*, 2009]. Further, it has been shown for other membrane protease classes that helix-destabilising residues are prerequisite [Urban and Shi, 2008]. For

example, a study showed that the insertion of the helix-kink inducing Pro in the APP TMD made its cleavage by a Rhomboid protease feasible demonstrating the need of exceptional high backbone dynamics in Rhomboid substrates [Moin and Urban, 2012]. The research by Fluhrer *et al.* uncovered the importance of a certain Gly in the cleavage of the Bri2 TMD substrate by the signal peptide peptidase [2012]. In sum, membrane based proteolysis needs substrates with specific backbone dynamics.

5.7 Conclusions and Outlook

Overall, this thesis aims to give an understanding how helix dynamics of the transmembrane domain of the amyloid precursor protein is characterised and how its intrinsic molecular properties influence the ability to be processed by the γ-secretase.

The major conclusions drawn from the experiments are that the β-branched residue rich cleavage region is less dynamic than the dimerisation domain harbouring a tandem GxxxG motif. This is confirmed by the results of the MD simulation done by the group of Christina Scharnagl [Hornburg, 2010, Proebstle, 2012]. Further, threonine side chains were found to stabilise the APP TMD helix by its ability to H-bond to the next turn of the backbone in N-terminal direction. Since Thr mutations in the APP TMD are linked with the alteration of the Aβ product pattern, it is believed that Thr may play a role in it. This might be the modulation of the backbone dynamics and/or the possibility of additional H-bonding to the presenilin's TMDs functioning as a potential molecular switch. Studying model peptides imitating the C-termini of the processed APP TMD suggest that once the ε-cut took place, further cleavages become more facile due to helix fraying and decreased intrinsic hydrophobicity. In addition, non-APP-TMDs were compared with the cleavage region of the APP TMD. Due to a double threonine backbonding and the lack of glycine in the core sequence, the cleavage region is a less dynamic helix than TM helices with an amino acid composition close to the average. In other words an average leucine and/or alanine content do not guarantee for a very stable helix.

It is assumed that local unraveling of the TM helix is prerequisite for the initial cleavage. The accessibility of a C1-atom is thought to be a consequence of local transient H-bond opening. When an amide hydrogen of residue i is not H-bonding to the carbonyl oxygen of residue $i-4$, then the C1-atom of residue $i-4$ is believed to be more prone to a nucleophilic attack. MD simulations done by the group of Christina Scharnagl show a decreased H-bond occupancy between the amide H of residue i (Leu52/ Lys53) and the carbonyl O of residue $i-4$ (Thr48/Leu49), where lower H-bond occupancy was seen with Lys53-Leu49 [Hornburg, 2010, Proebstle, 2012]. This helix destabilisation is in line with the findings of Sato *et al.* [2009]. They determined with solid state NMR an unraveling downstream of the ε-site, a feature which has been suggested for other

γ-secretase substrates according to a bioinformatic analysis, as well [Beel and Sanders, 2008]. With this residue resolved picture it becomes clear that nuances in backbone dynamics play a role in the initial cleavage, the preference of the product line Aβ40 over that of Aβ42, and also in the cleavage pattern. Since the cleavage region of the APP TMD is found to form a moderately dynamic helix, it is obvious that the key for the first cut lies in the destabilisation of the C-terminal residues of the TM helix, where fraying and the transition from a rather hydrophilic environment represented by the lipid head group of the membrane and presenilin's edge domains seem logic. The local helix destabilisation in the unprocessed APP TMD vs. the frayed termini of the fragments infer that the endoproteolytic event has to overcome a higher energy barrier than for the subsequent cleavages.

Helix dynamics is not the only important factor for the cleavage efficiency of presenilin, dimerisation plays a role, as well [Munter, 2007]. In fact, it is thought that both dimerisation and backbone dynamics influence each other. Several evidences such as the ToxR assay prove that the dimer interface of the APP TMD is a tandem GxxxG motif [Munter, 2007]. Though others argue it is the $G_{38}xxxA_{42}$ motif [Gorman *et al.*, 2008, Nadezhdin *et al.*, 2012]. Here it comes to the question whether the TMD of the C99 fragment is cleaved both as monomer and dimer or solely as monomer or solely as dimer. Therefore, helix dynamics of the dimer is worth to study further. An approach via MD simulations showed that the APP TMD helix dimer in a TFE/water environment had increased backbone dynamics at the C-termini which may hint for increased cleavage [Proebstle, 2012].

Another aspect not covered by the answered questions of this thesis is the role of lipids and other membrane members influencing the cleavage process. For example the binding of cholesterol to the GxxxG motif of the APP TMD was discovered [Barrett *et al.*, 2012]. This is discussed to enhance the preference of the APP-TMD to be in a lipid raft like locus in which γ-secretase is enriched [Ehehalt *et al.*, 2003, Simons *et al.*, 1998, van Meer *et al.*, 2008]. The cholesterol binding to the GxxxG motif could additionally explain why the successive processing ends with Aβ37 when cholesterol is seen as a kind of a plug and would push water away due to its hydrophobicity. In addition, Holmes *et al.* describe that membrane lipid chain length, saturation grade, double bond isomerisation and type of lipid headgroups alter the activity and processivity of γ-secretase in terms of AICD and Aβ peptide concentration [2012]. Studying the effect of lipids and cholesterol with respect to backbone dynamics of the APP TM helix monomer and dimer respectively would increase the understanding of the molecular mechanism. Specific interactions between lipid, substrate helix and to selected TMDs of the γ-secretase might play a role.

In summary, circular dichroism spectroscopy and deuterium hydrogen exchange coupled to mass spectrometry represent powerful tools to complement results gained from other methods such as molecular dynamic simulations. It completes the picture

of the intrinsic properties of the TMD of the C99 fragment and may give explanation possibilities for the proteolysis events of the APP TMD.

List of Abbreviations

aa	amino acid
AcN	Acetonitril
ADH-1	anterior pharynx-defective-1
APP	amyloid precursor protein
CD	circular dichroism
Fmoc	9-fluorenylmethyloxycarbonyl
$CHCl_3$	chloroform
CID	collision induced dissociation
D	deuteron
DEER	double electron electron resonance
DHX	deuterium hydrogen exchange
DLPC	1,2-dilauroyl-sn-glycero-3-phosphocholine
DLPE	1,2-dilauroyl-sn-glycero-3-phosphoethanolamin
DLPS	1,2-dilauroyl-sn-glycero-3-phospho-L-serine
DMPC	1,2-dimyristoyl-sn-glycero-3-phosphocholine
DMSO	dimethylsulfoxid
DOPE	1,2-dioleoyl-sn-glycero-3-phosphoethanolamin
DOPS	1,2-dioleoyl-sn-glycero-3-phospho-L-serine
ELISA	enzyme-linked immunosorbent assay
EPR	electron spin resonance
ESI	electron spray ionisation
ETD	electron transfer dissociation
FA	formic acid
FAD	familial Alzheimer's Disease
HFIP	hexafluoroisopropanol
H	hydrogen
KTMD	lysine flanked transmembrane domain
LMPG	lysomyristoylphosphatidylglycerol
MD	molecular dynamics
MEM	maximum entropy method
MP	membrane protein
MS	mass spectrometry

NCT	nicastrin
NH_4Ac	ammonium acetate
NMR	nuclear magnetic resonance
NBD	nitrobenzoxadiazole
NSAID	non-steroidal anti-inflammatory drugs
p.	page
PDLA	poly-DL-alanine
PEN-2	presenilin enhancer-2
P/L	peptide/ lipid
POPC	1-palmitoyl-2-oleoyl-sn-glycero-3-phosphocholine
PS	presenlin
Q-ToF	quadrupol time-of-flight
RIP	regulated intramembrane proteolysis
RMSD	root mean square deviation
RMSF	root mean square fluctuation
SDS	sodium dodecyl sulfate
SUV	small unilamellar vesicle
TFE	trifluoroethanol
TM	transmembrane
TMD	transmembrane domain
TMS	transmembrane segment
ToF	time of flight
UniProtKB	UniProt Knowledgebase
UV	ultraviolet

amino acids:

A (Ala)	alanine	M (Met)	methionine
C (Cys)	cysteine	N (Asn)	asparagine
D (Asp)	aspartate	P (Pro)	proline
E (Glu)	glutamate	Q (Gln)	glutamine
F (Phe)	phenylalanine	R (Arg)	arginine
G (Gly)	glycine	S (Ser)	serine
H (His)	histidine	T (Thr)	threonine
I (Ile)	isoleucine	V (Val)	valine
K (Lys)	lysine	W (Trp)	tryptophane
L (Leu)	leucine	Y (Tyr)	tyrosine

List of Figures

List of Tables

Bibliography

Alston RW, Lausagna M, Grimsley GR, Scholz JM, Reinhart GD, and Pace CN (2008) Peptide Sequence and Conformation strongly influence Tryptophan Fluorescence. *Biophysical Journal*, **94**, 2280–2287.

Alzheimer A (1907) Über eine eigenartige Erkrankung der Hirnrinde. *Allgemeine Zeitschrift für Psychiatrie und Psychisch-Gerichtliche Medizin*, **64**, 146–148.

Anders L, Mertins P, Lammich S, Murgia M, Hartmann D, Saftig P, Haass C, and Ullrich A (2006) Furin-, ADAM 10-, and γ-secretase-mediated cleavage of a receptor tyrosine phosphatase and regulation of β-catenin's transcriptional activity. *Molecular and Cellular Biology*, **26**, 3917–3934.

Annaert W and De Strooper B (2002) A cell biological perspective on Alzheimer's Disease. *Annual Review of Cell and Developmental Biology*, **18**, 25–51.

Arkin IT and Brunger AT (1998) Statistical analysis of predicted transmembrane α-helices. *Biochimica Et Biophysica Acta-Protein Structure and Molecular Enzymology*, **1429**, 113–128.

Arribas J and Borroto A (2002) Protein ectodomain shedding. *Chemical Reviews*, **102**, 4627–4637. Arribas, J Borroto, A.

Arvinte T and Drake AF (1993) Comparative study of human and salmon calcitonin secondary structure in solutions with low dielectric constants. *J Biol Chem*, **268**, 6408–14.

Asai M, Hattori C, Szabo B, Sasagawa N, Maruyama K, Tanuma S, and Ishiura S (2003) Putative function of ADAM9, ADAM10, and ADAM17 as APP α-secretase. *Biochem Biophys Res Commun*, **301**, 231–5.

Bai YW, Milne JS, Mayne L, and Englander SW (1993) Primary Structure Effects on Peptide Group Hydrogen-Exchange. *Proteins-Structure Function and Genetics*, **17**, 75–86.

Baker EN and Hubbard RE (1984) Hydrogen bonding in globular proteins. *Prog Biophys Mol Biol*, **44**, 97–179.

Ballesteros JA, Deupi X, Olivella M, Haaksma EEJ, and Pardo L (2000) Serine and threonine residues bend α-helices in the chi(1) = g(-) conformation. *Biophysical Journal*, **79**, 2754–2760.

Barlow DJ and Thornton JM (1988) Helix geometry in proteins. *J Mol Biol*, **201**, 601–619.

Barrett AJ and McDonald JK (1986) Nomenclature: protease, proteinase and peptidase. *Biochem J*, **237**, 935.

Barrett PJ, Sanders CR, Kaufman SA, Michelsen K, and Jordan JB (2011) NSAID-based γ-secretase modulators do not bind to the amyloid-β polypeptide. *Biochemistry*, **50**, 10328–42.

Barrett PJ, Song Y, Van Horn WD, Hustedt EJ, Schafer JM, Hadziselimovic A, Beel AJ, and Sanders CR (2012) The amyloid precursor protein has a flexible transmembrane domain and binds cholesterol. *Science*, **336**, 1168–71.

Bartolini M, Bertucci C, Bolognesi ML, Cavalli A, Melchiorre C, and Andrisano V (2007) Insight Into the Kinetic of Amyloid β (1–42) Peptide Self-Aggregation: Elucidation of Inhibitors' Mechanism of Action. *ChemBioChem*, **8**, 2152–2161.

Beel AJ, Barrett P, Schnier PD, Hitchcock SA, Bagal D, Sanders CR, and Jordan JB (2009) Nonspecificity of Binding of γ-Secretase Modulators to the Amyloid Precursor Protein. *Biochemistry*, **48**, 11837–11839.

Beel AJ, Mobley CK, Kim HJ, Tian F, Hadziselimovic A, Jap B, Prestegard JH, and Sanders CR (2008) Structural Studies of the Transmembrane C-Terminal Domain of the Amyloid Precursor Protein (APP): Does APP Function as a Cholesterol Sensor? *Biochemistry*, **47**, 9428–9446.

Beel AJ and Sanders C (2008) Substrate specificity of γ-secretase and other intramembrane proteases. *Cell Mol Life Sci*, **65**, 1311–1334.

Beher D, Hesse L, Masters CL, and Multhaup G (1996) Regulation of Amyloid Protein Precursor (APP) Binding to Collagen and Mapping of the Binding Sites on APP and Collagen Type I. *J Biol Chem*, **271**, 1613–1620.

Bella J and Berman HM (1996) Crystallographic evidence for C-α-H center dot center dot center dot O=C hydrogen bonds in a collagen triple helix. *J Mol Biol*, **264**, 734–742.

Ben-Tal N, Sitkoff D, Topol IA, Yang AS, Burt SK, and Honig B (1997) Free Energy of Amide Hydrogen Bond Formation in Vacuum, in Water, and in Liquid Alkane Solution. *J Phys Chem B*, **101**, 450–457.

Bergmann M and Niemann C (1937) On proteolytic enzymes. *J Biol Chem*, **118**, 781–788.

Bernstein SL, Dupuis NF, Lazo ND, Wyttenbach T, Condron MM, Bitan G, Teplow DB, Shea JE, Ruotolo BT, Robinson CV, and Bowers MT (2009) Amyloid-β protein oligomerization and the importance of tetramers and dodecamers in the aetiology of Alzheimer's disease. *Nature Chemistry*, **1**, 326–331.

Bickel H (2010) Das Wichtigste 1 - Epidemiologie der Demenz, Deutsche Alzheimer Gesellschaft e.V. Selbsthilfe Demenz.

Bigelow HR, Petrey DS, Liu J, Przybylski D, and Rost B (2004) Predicting transmembrane β-barrels in proteomes. *Nucleic Acids Research*, **32**, 2566–2577.

Bitan G, Kirkitadze MD, Lomakin A, Vollers SS, Benedek GB, and Teplow DB (2003) Amyloid β-protein (A β) assembly: A β 40 and A β 42 oligomerize through distinct pathways. *PNAS*, **100**, 330–335.

Blaber M, Zhang XJ, and Matthews BW (1993) Structural basis of amino acid α helix propensity. *Science*, **260**, 1637–1640.

Bowie JU (2005) Solving the membrane protein folding problem. *Nature*, **438**, 581–589.

Bowie JU (2011) Membrane protein folding: how important are hydrogen bonds? *Current Opinion in Structural Biology*, **21**, 42–49.

Brandl M, Weiss MS, Jabs A, Suhnel J, and Hilgenfeld R (2001) C-H center dot center dot center dot pi-interactions in proteins. *J Mol Biol*, **307**, 357–377.

Brier S and Engen JR (2008) Mass Specrometry Analysis for Protein-Protein Interactions and Dynamics, chap. Hydrogen Exchange Mass Spectrometry: Principles and Capabilities. John Wiley & Sons, Hoboken, New Jersey, 1st edn., 1–43.

Brown MS, Ye J, Rawson RB, and Goldstein JL (2000) Regulated intramembrane proteolysis: A control mechanism conserved from bacteria to humans. *Cell*, **100**, 391–398.

Brown RS, Bennet AJ, and Slebockatilk H (1992) Recent pespectives concerning the mechanism of H_3O^+-promoted and OH^--promoted amide hydrolysis. *Accounts of Chemical Research*, **25**, 481–488.

Brown WH, Foote CS, and Iverson BL (2010) Organic Chemistry: Enhanced. Brooks Cole Pub Co, enhanced edn.

Bryson JW, Betz SF, Lu HS, Suich DJ, Zhou HX, O'Neil KT, and DeGrado WF (1995) Protein Design: A Hierarchic Approach. *Science*, **270**, 935–941.

Buck M (1998) Trifluoroethanol and colleagues: cosolvents come of age. Recent studies with peptides and proteins. *Quarterly Reviews of Biophysics*, **31**, 297–355.

Bush AI, Beyreuther K, and Masters CL (1992) β A4 amyloid protein and its precursor in Alzheimer's disease. *Pharmacol Ther*, **56**, 97–117.

Cai J, Jiang WG, Grant MB, and Boulton M (2006) Pigment epithelium-derived factor inhibits angiogenesis via regulated intracellular proteolysis of vascular endothelial growth factor receptor 1. *J Biol Chem*, **281**, 3604–13.

Cao XW and Sudhof TC (2001) A transcriptively active complex of APP with Fe65 and histone acetyltransferase Tip60. *Science*, **293**, 115–120.

Capell A, Grunberg J, Pesold B, Diehlmann A, Citron M, Nixon R, Beyreuther K, Selkoe DJ, and Haass C (1998) The Proteolytic Fragments of the Alzheimer's Disease-associated Presenilin-1 Form Heterodimers and Occur as a 100-150-kDa Molecular Mass Complex. *J Biol Chem*, **273**, 3205–3211.

Chamberlain AK and Bowie JU (2004) Analysis of Side-Chain Rotamers in Transmembrane Proteins. *Biophysical Journal*, **87**, 3460–3469.

Chavez-Gutierrez L, Bammens L, Benilova I, Vandersteen A, Benurwar M, Borgers M, Lismont S, Zhou L, Van Cleynenbreugel S, Esselmann H, Wiltfang J, Serneels L, Karran E, Gijsen H, Schymkowitz J, Rousseau F, Broersen K, and De Strooper B (2012) The mechanism of γ-Secretase dysfunction in familial Alzheimer disease. *EMBO J*, **31**, 2261–2274.

Chiti F and Dobson CM (2006) Protein Misfolding, Functional Amyloid, and Human Disease. *Annual Review of Biochemistry*, **75**, 333–366.

Chou PY and Fasman GD (1974) Conformational parameters for amino acids in helical, b-sheet, and random coil regions calculated from proteins. *Biochemistry*, **13**, 211–222.

Coates L, Erskine PT, Mall S, Gill R, Wood SP, Myles DAA, and Cooper JB (2006) X-ray, neutron and NMR studies of the catalytic mechanism of aspartic proteinases. *European Biophysics Journal with Biophysics Letters*, **35**, 559–566.

Coates L, Tuan HF, Tomanicek S, Kovalevsky A, Mustyakimov M, Erskine P, and Cooper J (2008) The catalytic mechanism of an aspartic proteinase explored with neutron and X-ray diffraction. *JACS*, **130**, 7235–7237.

Coen K and Annaert W (2010) Presenilins: how much more than γ-secretase?! *Biochemical Society Transactions*, **038**, 1474–1478.

Cole SL and Vassar R (2008) The Role of Amyloid Precursor Protein Processing by BACE1, the {β}-Secretase, in Alzheimer Disease Pathophysiology. *J Biol Chem*, **283**, 29621–29625.

Compton LA and Johnson WC (1986) Analysis of Protein Circular-Dichroism Spectra for Secondary Structure Using a Simple Matrix Multiplication. *Analytical Biochemistry*, **155**, 155–167.

Cordes FS, Bright JN, and Sansom MS (2002) Proline-induced distortions of transmembrane helices. *J Mol Biol*, **323**, 951–60.

Cornish VW, Kaplan MI, Veenstra DL, Kollman PA, and Schultz PG (1994) Stabilizing and Destabilizing Effects of Placing β-Branched Amino-Acids in Protein α-Helices. *Biochemistry*, **33**, 12022–12031.

Creamer TP and Rose GD (1992) Side-chain entropy opposes α-helix formation but rationalizes experimentally determined helix-forming propensities. *Proceedings of the National Academy of Sciences of the United States of America*, **89**, 5937–5941.

Creamer TP and Rose GD (1994) α-helix-forming propensities in peptides and proteins. *Proteins-Structure Function and Genetics*, **19**, 85–97.

Creamer TP and Rose GD (1995) Interactions between hydrophobic side-chains within α-helices. *Protein Science*, **4**, 1305–1314.

Creighton TE (1993) Proteins - Structures and Molecular Properties. W. H. Freeman and Company, New York, 2nd edn., 171–325.

Czirr E, Cottrell BA, Leuchtenberger S, Kukar T, Ladd TB, Esselmann H, Paul S, Schubenel R, Torpey JW, Pietrzik CU, Golde TE, Wiltfang J, Baumann K, Koo EH, and Weggen S (2008) Independent generation of A β 42 and A β 38 peptide species by γ-secretase. *J Biol Chem*, **283**, 17049–17054.

Darocha-Souto B, Scotton TC, Coma M, Serrano-Pozo A, Hashimoto T, Sereno L, Rodriguez M, Sanchez B, Hyman BT, and Gomez-Isla T (2011) Brain Oligomeric β-Amyloid but Not Total Amyloid Plaque Burden Correlates With Neuronal Loss and Astrocyte Inflammatory Response in Amyloid Precursor Protein/Tau Transgenic Mice. *J Neuropathol Exp Neurol*, **70**, 360–376.

de Planque MRR and Killian JA (2003) Protein-lipid interactions studied with designed transmembrane peptides: role of hydrophobic matching and interfacial anchoring (Review). *Molecular Membrane Biology*, **20**, 271–284.

de Strooper B (2010) Proteases and Proteolysis in Alzheimer Disease: A Multifactorial View on the Disease Process. *Physiological Reviews*, **90**, 465–494.

Deber CM and Li SC (1995) Peptides in membranes: Helicity and hydrophobicity. *Biopolymers*, **37**, 295–318.

Dempsey CE (1986) pH Dependence of hydrogen exchange from backbone peptide amides in apamin. *Biochemistry*, **25**, 3904–3911.

Dempsey CE (2001) Hydrogen exchange in peptides and proteins using NMR-spectroscopy. *Progress in Nuclear Magnetic Resonance Spectroscopy*, **39**, 135–170.

Dilger JP, Fisher LR, and Haydon DA (1982) A critical comparison of electrical and optical methods for bilayer thickness determination. *Chemistry and Physics of Lipids*, **30**, 159–176.

Doig AJ, Errington N, and Iqbalsyah TM (2005) Handbook of Protein Folding, chap. Stability and design of α-helices. Wiley, Weinheim, 247–313.

Dougherty DA (1996) Cation-π interactions in chemistry and biology: A new view of benzene, Phe, Tyr, and Trp. *Science*, **271**, 163–168.

Dries DR and Yu G (2008) Assembly, Maturation, and Trafficking of the γ-Secretase Complex in Alzheimer's Disease. *Current Alzheimer Research*, **5**, 132–146.

Dunbrack RLJ and Karplus M (1994) Conformational analysis of the backbone-dependent rotamer preferences of protein side chains. *Nat Struct Biol*, **1**, 334–40.

Dürrbaum M (2010) Sequenzspezifische Dynamik und Sekundärstruktur der Transmembrandomäne des Amyloid Vorläuferproteins. Bachelor Thesis. München. Technische Universität München, Lehrstuhl fÃ¼r Chemie der Biopolymere.

Eckstrom HC, Berger JE, and Dawson LR (1960) Intermolecular effects in solutions of methyl isobutyl ketone in alcohols and fluoroalcohols. *The Journal of Physical Chemistry*, **64**, 1458–1461.

Edbauer D, Winkler E, Regula JT, Pesold B, Steiner H, and Haass C (2003) Reconstitution of γ-secretase activity. *Nature Cell Biology*, **5**, 486–488.

Ehehalt R, Keller P, Haass C, Thiele C, and Simons K (2003) Amyloidogenic processing of the Alzheimer β-amyloid precursor protein depends on lipid rafts. *Journal of Cell Biology*, **160**, 113–123.

Eigen M (1964) Proton Transfer, Acid-Base Catalysis, and Enzymatic Hydrolysis. Part I: Elementary Processes. *Angewandte Chemie International Edition in English*, **3**, 1–19.

Eilers M, Shekar SC, Shieh T, Smith SO, and Fleming PJ (2000) Internal packing of helical membrane proteins. *Proceedings of the National Academy of Sciences*, **97**, 5796–5801.

Elston T, Wang HY, and Oster G (1998) Energy transduction in ATP synthase. *Nature*, **391**, 510–513.

Englander SW (2006) Hydrogen Exchange and Mass Spectrometry: A Historical Perspective. *Journal of the American Society for Mass Spectrometry*, **17**, 1481–1489.

Englander SW, Downer NW, and Teitelbaum H (1972) Hydrogen-Exchange. *Annual Review of Biochemistry*, **41**, 903–924.

Englander SW and Kallenbach NR (1984) Hydrogen exchange and structural dynamics of proteins and nucleic acids. *Quarterly Reviews of Biophysics*, **16**, 521–655.

Englander SW and Poulsen A (1969) Hydrogen-tritium exchange of the random chain polypeptide. *Biopolymers*, **7**, 379–393.

Erez E, Fass D, and Bibi E (2009) How intramembrane proteases bury hydrolytic reactions in the membrane. *Nature*, **459**, 371–378.

Eriksson MA, Hard T, and Nilsson L (1995) On the pH dependence of amide proton exchange rates in proteins. *Biophys J*, **69**, 329–339.

Espinosa E, Molins E, and Lecomte C (1998) Hydrogen bond strengths revealed by topological analyses of experimentally observed electron densities. *Chemical Physics Letters*, **285**, 170–173.

Farrens DL, Altenbach C, Yang K, Hubbell WL, and Khorana HG (1996) Requirement of rigid-body motion of transmembrane helices for light activation of rhodopsin. *Science*, **274**, 768–770.

Fersht AR (1971) Acyl-transfer reactions of amides and esters with alcohols and thiols. Reference system for the serine and cysteine proteinases. Nitrogen protonation of amides and amide-imidate equilibriums. *JACS*, **93**, 3504–3515.

Fersht AR, Shi JP, Knill-Jones J, Lowe DM, Wilkinson AJ, Blow DM, Brick P, Carter P, Waye MMY, and Winter G (1985) Hydrogen bonding and biological specificity analysed by protein engineering. *Nature*, **314**, 235–238.

Finn RD, Mistry J, Tate J, Coggill P, Heger A, Pollington JE, Gavin OL, Gunasekaran P, Ceric G, Forslund K, Holm L, Sonnhammer ELL, Eddy SR, and Bateman A (2010) The Pfam protein families database. *Nucleic Acids Research*, **38**, D211–D222.

Fisinger S, Serrano L, and Lacroix E (2001) Computational estimation of specific side chain interaction energies in α helices. *Protein Sci*, **10**, 809–18.

Fiske CH and Subbarow Y (1925) The Colorimetric Determination of Phosphorus. *J Biol Chem*, **66**, 375–400.

Fluhrer R, Martin L, Klier B, Haug-Kroeper M, Grammer G, Nuscher B, and Haass C (2012) The α-helical content of the transmembrane domain of the British dementia protein-2 (Bri2) determines its processing by signal peptide peptidase-like 2b (SPPL2b). *J Biol Chem*, **287**, 5156–5163.

Fukumori A, Fluhrer R, Steiner H, and Haass C (2010) Three-Amino Acid Spacing of Presenilin Endoproteolysis Suggests a General Stepwise Cleavage of γ-Secretase-Mediated Intramembrane Proteolysis. *Journal of Neuroscience*, **30**, 7853–7862.

Gamerdinger M, Clement AB, and Behl C (2008) Effects of sulindac sulfide on the membrane architecture and the activity of γ-secretase. *Neuropharmacology*, **54**, 998–1005.

Gast K, Zirwer D, Müller-Frohne M, and Damaschun G (1999) Trifluoroethanol-induced conformational transitions of proteins: Insights gained from the differences between α-lactalbumin and ribonuclease A. *Protein Science*, **8**, 625–634.

Gente G and La Mesa C (2000) Water—Trifluoroethanol Mixtures: Some Physicochemical Properties. *Journal of Solution Chemistry*, **29**, 1159–1172.

Glenner GG and Wong CW (1984) Alzheimer's disease: Initial report of the purification and characterization of a novel cerebrovascular amyloid protein. *Biochemical and Biophysical Research Communications*, **120**, 885–890.

Go N, Go M, and Scheraga HA (1968) Molecular theory of the helix-coil transition in polyamino acids, I. Formulation. *PNAS*, **59**, 1030–7.

Goedert M and Spillantini MG (2006) A Century of Alzheimer's Disease. *Science*, **314**, 777–781.

Goldgaber D, Lerman MI, McBride OW, Saffiotti U, and Gajdusek DC (1987) Characterization and chromosomal localization of a cDNA encoding brain amyloid of Alzheimer's disease. *Science*, **235**, 877–80.

Gorman PM, Kim S, Guo M, Melnyk RA, McLaurin J, Fraser PE, Bowie JU, and Chakrabartty A (2008) Dimerization of the transmembrane domain of amyloid precursor proteins and familial Alzheimer's disease mutants. *BMC Neuroscience*, **9**, 17.

Gray TM and Matthews BW (1984) Intrahelical hydrogen-bonding of serine, threonine and cysteine residues within α-helices and its relevance to membrane-bound proteins. *J Mol Biol*, **175**, 75–81.

Greenfield NJ (2007) Using circular dichroism spectra to estimate protein secondary structure. *Nat Protocols*, **1**, 2876–2890.

Gregory RB, Crabo L, Percy AJ, and Rosenberg A (1983) Water catalysis of peptide hydrogen isotope exchange. *Biochemistry*, **22**, 910–917.

Groemer TW, Thiel CS, Holt M, Riedel D, Hua YF, Huve J, Wilhelm BG, and Klingauf J (2011) Amyloid Precursor Protein Is Trafficked and Secreted via Synaptic Vesicles. *Plos One*, **6**.

Haapasalo A and Kovacs DM (2011) The many substrates of presenilin/γ-secretase. *J Alzheimers Dis*, **25**, 3–28.

Haass C, Hung AY, and Selkoe DJ (1991) Processing of β-amyloid precursor protein in microglia and astrocytes favors an internal localization over constitutive secretion. *The Journal of Neuroscience*, **11**, 3783–3793.

Haass C and Selkoe DJ (2007) Soluble protein oligomers in neurodegeneration: lessons from the Alzheimer's amyloid β-peptide. *Nature Reviews Molecular Cell Biology*, **8**, 101–112.

Hansen DF and Kay LE (2011) Determining Valine Side-Chain Rotamer Conformations in Proteins from Methyl 13C Chemical Shifts: Application to the 360 kDa Half-Proteasome. *JACS*, **133**, 8272–8281.

Heijne G (1986) The distribution of positively charged residues in bacterial inner membrane proteins correlates with the trans-membrane topology. *EMBO J*, **5**, 3021–7.

Hemming ML, Elias JE, Gygi SP, and Selkoe DJ (2008) Proteomic profiling of γ-secretase substrates and mapping of substrate requirements. *PLoS Biol*, **6**, e257.

Henzler-Wildman K and Kern D (2007) Dynamic personalities of proteins. *Nature*, **450**, 964–972.

Hermans J, Anderson AG, and Yun RH (1992) Differential helix propensity of small apolar side chains studied by molecular dynamics simulations. *Biochemistry*, **31**, 5646–5653.

Herrmann JR, Fuchs A, Panitz JC, Eckert T, Unterreitmeier S, Frishman D, and Langosch D (2010) Ionic Interactions Promote Transmembrane Helix-Helix Association Depending on Sequence Context. *J Mol Biol*, **396**, 452–461.

Hildebrand PW, Preissner R, and Frömmel C (2004) Structural features of transmembrane helices. *FEBS Letters*, **559**, 145–151.

Hildebrand PW, Rother K, Goede A, Preissner R, and Frommel C (2005) Molecular packing and packing defects in helical membrane proteins. *Biophysical Journal*, **88**, 1970–1977.

Hirota N, Mizuno K, and Goto Y (1997) Cooperative α-helix formation of β-lactoglobulin and melittin induced by hexafluoroisopropanol. *Protein Sci*, **6**, 416–21.

Hirota N, Mizuno K, and Goto Y (1998) Group additive contributions to the alcohol-induced α-helix formation of melittin: implication for the mechanism of the alcohol effects on proteins. *J Mol Biol*, **275**, 365–78.

Hobza P and Havlas Z (2000) Blue-shifting hydrogen bonds. *Chemical Reviews*, **100**, 4253–4264.

Hol WGJ, van Duijnen PT, and Berendsen HJC (1978) The [α]-helix dipole and the properties of proteins. *Nature*, **273**, 443–446.

Holmes O, Paturi S, Ye W, Wolfe MS, and Selkoe DJ (2012) Effects of Membrane Lipids on the Activity and Processivity of Purified γ-Secretase. *Biochemistry*, **51**, 3565–3575.

Hong DP, Hoshino M, Kuboi R, and Goto Y (1999) Clustering of Fluorine-Substituted Alcohols as a Factor Responsible for Their Marked Effects on Proteins and Peptides. *J Am Chem Soc*, **121**, 8427–8433.

Hornburg D (2010) Investigation of the Structural Flexibility of the APP Transmembrane Domain and Its Mutant Aβ 26-55 G33I With Molecular Biological Methods and Molecular Methods. Master Thesis. München. Technische Universität München, Lehrstuhl fÃ¼r Chemie der Biopolymere.

Hornburg P (2011) Comparative Molecular Dynamics Analysis of Thr-to-Val Mutants in the Transmembrane Domain of the Alzheimer Precuror Protein. Bachelor Thesis. München. Technische Universität München, Lehrstuhl fÃ¼r Chemie der Biopolymere.

Hughes RM and Waters ML (2006) Effects of lysine acetylation in a β-hairpin peptide: Comparison of an amide-pi and a cation-pi interaction. *JACS*, **128**, 13586–13591.

Huovila AP, Turner AJ, Pelto-Huikko M, Karkkainen I, and Ortiz RM (2005) Shedding light on ADAM metalloproteinases. *Trends Biochem Sci*, **30**, 413–22.

Jennings ML (1989) Topography of membrane proteins. *Annual Review of Biochemistry*, **58**, 999–1027.

Jiang YX, Lee A, Chen JY, Cadene M, Chait BT, and MacKinnon R (2002) The open pore conformation of potassium channels. *Nature*, **417**, 523–526.

Johannsen J (2003) Molecular determinants for amyloid fibril formation: lessons from lung surfactant protein C. *Swiss Medical Weekly*, **133**, 275–282.

Johnson WCJ (1985) Circular dichroism and its empirical application to biopolymers. *Methods Biochem Anal*, **31**, 61–163.

Kaden D, Munter LM, Joshi M, Treiber C, Weise C, Bethge T, Voigt P, Schaefer M, Beyermann M, Reif B, and Multhaup G (2008) Homophilic interactions of the APP ectodomain are regulated by the loop region and affect β-secretase cleavage of APP. *J Biol Chem*, **283**, 7271–7279.

Kaden D, Munter LM, Reif B, and Multhaup G (2011) The amyloid precursor protein and its homologues: Structural and functional aspects of native and pathogenic oligomerization. *Eur J Cell Biol*, **91**, 234–239.

Kaether C, Haass C, and Steiner H (2006) Assembly, trafficking and function of γ-secretase. *Neurodegener Dis*, **3**, 275–83.

Kall L, Krogh A, and Sonnhammer EL (2004) A combined transmembrane topology and signal peptide prediction method. *J Mol Biol*, **338**, 1027–36.

Kaltashov IA and Eyles SJ (2005) Mass Spectrometry in Biophysics: Conformation and Dynamics of Biomolecules, chap. Mass Spectrometry-based approaches to study biomolecular dynamics: equilibrium intermediates. Wiley-Interscience, Series on Mass Spectrometry, John Wiley & Sons, Hoboken, New Jersey, 183–223.

Kang J, Lemaire HG, Unterbeck A, Salbaum JM, Masters CL, Grzeschik KH, Multhaup G, Beyreuther K, and Muller-Hill B (1987) The precursor of Alzheimer's disease amyloid A4 protein resembles a cell-surface receptor. *Nature*, **325**, 733–6.

Kim S and Cross TA (2002) Uniformity, ideality, and hydrogen bonds in transmembrane α-helices. *Biophysical Journal*, **83**, 2084–2095. Kim, S Cross, TA.

Kim SH and Sisodia SS (2005a) Evidence that the "NF" motif in transmembrane domain 4 of presenilin 1 is critical for binding with PEN-2. *J Biol Chem*, **280**, 41953–66.

Kim SH and Sisodia SS (2005b) A sequence within the first transmembrane domain of PEN-2 is critical for PEN-2-mediated endoproteolysis of presenilin 1. *J Biol Chem*, **280**, 1992–2001.

Kitaguchi N, Takahashi Y, Tokushima Y, Shiojiri S, and Ito H (1988) Novel precursor of Alzheimer's disease amyloid protein shows protease inhibitory activity. *Nature*, **331**, 530–2.

Klein WL, Krafft GA, and Finch CE (2001) Targeting small Aβ oligomers: the solution to an Alzheimer's disease conundrum? *Trends in Neurosciences*, **24**, 219–224.

Kopan R and Ilagan MX (2004) γ-secretase: proteasome of the membrane? *Nat Rev Mol Cell Biol*, **5**, 499–504.

Kornilova AY, Bihel F, Das C, and Wolfe MS (2005) The initial substrate-binding site of γ-secretase is located on presenilin near the active site. *PNAS*, **102**, 3230–3235.

Kukar T and Golde TE (2008) Possible mechanisms of action of NSAIDs and related compounds that modulate γ-secretase cleavage. *Current Topics in Medicinal Chemistry*, **8**, 47–53.

Kukar TL, Ladd TB, Bann MA, Fraering PC, Narlawar R, Maharvi GM, Healy B, Chapman R, Welzel AT, Price RW, Moore B, Rangachari V, Cusack B, Eriksen J, Jansen-West K, Verbeeck C, Yager D, Eckman C, Ye WJ, Sagi S, Cottrell BA, Torpey J, Rosenberry TL, Fauq A, Wolfe MS, Schmidt B, Walsh DM, Koo EH, and Golde TE (2008) Substrate-targeting γ-secretase modulators. *Nature*, **453**, 925–930.

Kukar TL, Ladd TB, Robertson P, Pintchovski SA, Moore B, Bann MA, Ren Z, Jansen-West K, Malphrus K, Eggert S, Maruyama H, Cottrell BA, Das P, Basi GS, Koo EH, and Golde TE (2011) Lysine 624 of the Amyloid Precursor Protein (APP) Is a Critical Determinant of Amyloid β Peptide Length: Support for a sequential model of γ-secretase intramembrane proteolysis and regulation by the amyloid β precursor protein (APP) juxtamembrane region. *J Biol Chem*, **286**, 39804–12.

Kumar-Singh S, De Jonghe C, Cruts M, Kleinert R, Wang R, Mercken M, De Strooper B, Vanderstichele H, Loefgren A, Vanderhoeven I, Backhovens H, Vanmechelen E, Kroisel PM, and Van Broeckhoven C (2000) Nonfibrillar diffuse amyloid deposition due to a γ 42-secretase site mutation points to an essential role for N-truncated Aβ42 in Alzheimer's disease. *Human Molecular Genetics*, **9**, 2589–2598.

Kuprin S, Graslund A, Ehrenberg A, and Koch MHJ (1995) Nonideality of Water-Hexafluoropropanol Mixtures as Studied by X-Ray Small Angle Scattering. *Biochemical and Biophysical Research Communications*, **217**, 1151–1156.

Kutzner C (2011) Establishing a FRET Dimerization Assay for Aβ 26-55 in liposomes. Master Thesis. München. Technische Universität München, Lehrstuhl fÃ¼r Chemie der Biopolymere.

Lambert MP, Barlow AK, Chromy BA, Edwards C, Freed R, Liosatos M, Morgan TE, Rozovsky I, Trommer B, Viola KL, Wals P, Zhang C, Finch CE, Krafft GA, and Klein WL (1998) Diffusible, nonfibrillar ligands derived from Aβ1–42 are potent central nervous system neurotoxins. *PNAS*, **95**, 6448–6453.

Langosch D and Arkin IT (2009) Interaction and conformational dynamics of membrane-spanning protein helices. *Protein Science*, **18**, 1343–1358.

Langosch D, Crane JM, Brosig B, Hellwig A, Tamm LK, and Reed J (2001) Peptide mimics of SNARE transmembrane segments drive membrane fusion depending on their conformational plasticity. *J Mol Biol*, **311**, 709–721.

Laudon H, Hansson EM, Melen K, Bergman A, Farmery MR, Winblad B, Lendahl U, von Heijne G, and Naeslund J (2005) A Nine-transmembrane Domain Topology for Presenilin 1. *J Biol Chem*, **280**, 35352–35360.

LaVoie MJ, Fraering PC, Ostaszewski BL, Ye W, Kimberly WT, Wolfe MS, and Selkoe DJ (2003) Assembly of the γ-Secretase Complex Involves Early Formation of an Intermediate Subcomplex of Aph-1 and Nicastrin. *J Biol Chem*, **278**, 37213–37222.

Lazarov VK, Fraering PC, Ye W, Wolfe MS, Selkoe DJ, and Li H (2006) From the Cover: Electron microscopic structure of purified, active γ-secretase reveals an aqueous intramembrane chamber and two pores. *PNAS*, **103**, 6889–6894.

Lazo ND, Maji SK, Fradinger EA, Bitan G, and Teplow DB (2008) Amyloid Proteins, chap. The Amyloid β Protein. Wiley-VCH Verlag GmbH, 384–491.

Lee SF, Shah S, Li H, Yu C, Han W, and Yu G (2002) Mammalian APH-1 Interacts with Presenilin and Nicastrin and Is Required for Intramembrane Proteolysis of Amyloid-β Precursor Protein and Notch. *J Biol Chem*, **277**, 45013–45019.

Lee SF, Shah S, Yu C, Wigley WC, Li H, Lim M, Pedersen K, Han W, Thomas P, Lundkvist J, Hao YH, and Yu G (2004) A Conserved GXXXG Motif in APH-1 Is Critical for Assembly and Activity of the Î³-Secretase Complex. *J Biol Chem*, **279**, 4144–4152.

Leichtling BH and Klotz IM (1966) Catalysis of Hydrogen-Deuterium Exchange in Polypeptides. *Biochemistry*, **5**, 4026–4037.

Lemberg MK (2011) Intramembrane Proteolysis in Regulated Protein Trafficking. *Traffic*, **12**, 1109–1118.

Lemberg MK and Martoglio B (2002) Requirements for signal peptide peptidase-catalyzed intramembrane proteolysis. *Molecular Cell*, **10**, 735–744.

Lesne S, Koh MT, Kotilinek L, Kayed R, Glabe CG, Yang A, Gallagher M, and Ashe KH (2006) A specific amyloid-[β] protein assembly in the brain impairs memory. *Nature*, **440**, 352–357.

Levitt M and Greer J (1977) Automatic identification of secondary structure in globular proteins. *J Mol Biol*, **114**, 181–239.

Lichtenthaler SF, Haass C, and Steiner H (2011) Regulated intramembrane proteolysis – lessons from amyloid precursor protein processing. *Journal of Neurochemistry*, **117**, 779–796. 1471-4159.

Lichtenthaler SF, Wang R, Grimm H, Uljon SN, Masters CL, and Beyreuther K (1999) Mechanism of the cleavage specificity of Alzheimer's disease γ-secretase identified by phenylalanine-scanning mutagenesis of the transmembrane domain of the amyloid precursor protein. *PNAS*, **96**, 3053–3058.

Liu LP and Deber CM (1998) Uncoupling hydrophobicity and helicity in transmembrane segments - α-helical propensities of the amino acids in non-polar environments. *J Biol Chem*, **273**, 23645–23648.

Liu LP, Li SC, Goto NK, and Deber CM (1996) Threshold hydrophobicity dictates helical conformations of peptides in membrane environments. *Biopolymers*, **39**, 465–470.

Lleo A, Berezovska O, Herl L, Raju S, Deng A, Bacskai BJ, Frosch MP, Irizarry M, and Hyman BT (2004) Nonsteroidal anti-inflammatory drugs lower A β(42) and change presenilin 1 conformation. *Nature Medicine*, **10**, 1065–1066.

Llinas M and Klein MP (1975) Solution conformation of ferrichrome. 6. Charge relay at peptide-bond – proton magnetic resonance study of solvation effects on amide electron-density distribution. *JACS*, **97**, 4731–4737.

Lovell SC, Word JM, Richardson JS, and Richardson DC (2000) The penultimate rotamer library. *Proteins*, **40**, 389–408.

Lu JX, Yau WM, and Tycko R (2011) Evidence from Solid-State NMR for Nonhelical Conformations in the Transmembrane Domain of the Amyloid Precursor Protein. *Biophysical Journal*, **100**, 711–719.

Luchsinger JA and Mayeux R (2004) Dietary factors and Alzheimer's disease. *Lancet Neurology*, **3**, 579–587.

Lue LF, Kuo YM, Roher AE, Brachova L, Shen Y, Sue L, Beach T, Kurth JH, Rydel RE, and Rogers J (1999) Soluble Amyloid β Peptide Concentration as a Predictor of Synaptic Change in Alzheimer's Disease. *The American Journal of Pathology*, **155**, 853–862.

Luo P and Baldwin RL (1997) Mechanism of helix induction by trifluoroethanol: a framework for extrapolating the helix-forming properties of peptides from trifluoroethanol/water mixtures back to water. *Biochemistry*, **36**, 8413–21.

Luque I, Mayorga OL, and Freire E (1996) Structure-Based Thermodynamic Scale of α-Helix Propensities in Amino Acids†. *Biochemistry*, **35**, 13681–13688.

Ma JC and Dougherty DA (1997) The cation-pi interaction. *Chemical Reviews*, **97**, 1303–1324.

Marambaud P, Shioi J, Serban G, Georgakopoulos A, Sarner S, Nagy V, Baki L, Wen P, Efthimiopoulos S, Shao Z, Wisniewski T, and Robakis NK (2002) A presenilin-1/γ-secretase cleavage releases the E-cadherin intracellular domain and regulates disassembly of adherens junctions. *Embo J*, **21**, 1948–56.

Masters CL, Simms G, Weinman NA, Multhaup G, McDonald BL, and Beyreuther K (1985) Amyloid plaque core protein in Alzheimer disease and Down syndrome. *Proc Natl Acad Sci U S A*, **82**, 4245–9.

McCloskey MA and Poo MM (1986) Rates of membrane-associated reactions: reduction of dimensionality revisited. *The Journal of Cell Biology*, **102**, 88–96.

McLean CA, Cherny RA, Fraser FW, Fuller SJ, Smith MJ, Konrad V, Bush AI, and Masters CL (1999) Soluble pool of Aβ amyloid as a determinant of severity of neurodegeneration in Alzheimer's disease. *Annals of Neurology*, **46**, 860–866.

Menendez-Gonzalez M, Perez-Pinera P, Martinez-Rivera M, Calatayud MT, and Blazquez Menes B (2005) APP processing and the APP-KPI domain involvement in the amyloid cascade. *Neurodegener Dis*, **2**, 277–83.

Milne JS, Xu Y, Mayne LC, and Englander SW (1999) Experimental study of the protein folding landscape: unfolding reactions in cytochrome c. *J Mol Biol*, **290**, 811–822.

Miura S, Zhang JL, Boros J, and Karnik SS (2003) TM2-TM7 interaction in coupling movement of transmembrane helices to activation of the angiotensin II type-1 receptor. *J Biol Chem*, **278**, 3720–3725.

Miyashita N, Straub JE, Thirumalai D, and Sugita Y (2009) Transmembrane Structures of Amyloid Precursor Protein Dimer Predicted by Replica-Exchange Molecular Dynamics Simulations. *JACS*, **131**, 3438–3439.

Moghekar A, Rao S, Li M, Ruben D, Mammen A, Tang XP, and O'Brien RJ (2011) Large Quantities of A β Peptide Are Constitutively Released during Amyloid Precursor Protein Metabolism in Vivo and in Vitro. *J Biol Chem*, **286**.

Moin SM and Urban S (2012) Membrane immersion allows rhomboid proteases to achieve specificity by reading transmembrane segment dynamics. *Elife*, **1**, e00173.

Molday RS and Kallen RG (1972) Substituent Effects on Amide Hydrogen-Exchange Rates in Aqueous-Solution. *JACS*, **94**, 6739–&.

Morokuma K (1977) Why do molecules interact - origin of electron donor-acceptor complexes, hydrogen-bonding, and proton affinity. *Accounts of Chemical Research*, **10**, 294–300.

Morris JC (1999) Is Alzheimer's disease inevitable with age?: Lessons from clinico-pathologic studies of healthy aging and very mild alzheimer's disease. *J Clin Invest*, **104**, 1171–3.

Muga A, Neugebauer W, Hirama T, and Surewicz WK (1994) Membrane interaction and conformational properties of the putative fusion peptide PH-30, a protein active in sperm-egg fusion. *Biochemistry*, **33**, 4444–4448.

Mukherjee P, Kass I, Arkin IT, and Zanni MT (2006) Picosecond dynamics of a membrane protein revealed by 2D IR. *PNAS*, **103**, 3528–3533.

Multhaup G (2006) Amyloid precursor protein and BACE function as oligomers. *Neurodegenerative Diseases*, **3**, 270–274.

Munter LM (2007) Charakterisierung eines Dimerisierungsmotivs in der Aß-Region des Amyloid-Vorläuferproteins: Mechanismus der Aß-Entstehung. Ph.D. thesis, Berlin.

Munter LM, Botev A, Richter L, Hildebrand PW, Althoff V, Weise C, Kaden D, and Multhaup G (2010) Aberrant amyloid precursor protein (APP) processing in hereditary forms of Alzheimer disease caused by APP familial Alzheimer disease mutations can be rescued by mutations in the APP GxxxG motif. *J Biol Chem*, **285**, 21636–43.

Munter LM, Voigt P, Harmeier A, Kaden D, Gottschalk KE, Weise C, Pipkorn R, Schaefer M, Langosch D, and Multhaup G (2007) GxxxG motifs within the amyloid precursor protein transmembrane sequence are critical for the etiology of A β 42. *EMBO Journal*, **26**, 1702–1712.

Nadezhdin KD, Bocharova OV, Bocharov EV, and Arseniev AS (2012) Dimeric structure of transmembrane domain of amyloid precursor protein in micellar environment. *FEBS Lett*, **586**, 1687–1692.

Niimura M, Isoo N, Takasugi N, Tsuruoka M, Ui-Tei K, Saigo K, Morohashi Y, Tomita T, and Iwatsubo T (2005) Aph-1 Contributes to the Stabilization and Trafficking of the γ-Secretase Complex through Mechanisms Involving Intermolecular and Intramolecular Interactions. *J Biol Chem*, **280**, 12967–12975.

Nyborg AC, Jansen K, Ladd TB, Fauq A, and Golde TE (2004) A signal peptide peptidase (SPP) reporter activity assay based on the cleavage of type II membrane protein substrates provides further evidence for an inverted orientation of the SPP active site relative to presenilin. *J Biol Chem*, **279**, 43148–56.

Osenkowski P, Li H, Ye W, Li D, Aeschbach L, Fraering PC, Wolfe MS, Selkoe DJ, and Li H (2009) Cryoelectron Microscopy Structure of Purified [γ]-Secretase at 12?Å Resolution. *J Mol Biol*, **385**, 642–652.

Pace CN (1990) Conformational stability of globular proteins. *Trends in Biochemical Sciences*, **15**, 14–17.

Page RM, Baumann K, Tomioka M, Perez-Revuelta BI, Fukumori A, Jacobsen H, Flohr A, Luebbers T, Ozmen L, Steiner H, and Haass C (2008) Generation of Ab 38 and Ab42 Is Independently and Differentially Affected by Familial Alzheimer Disease-associated Presenilin Mutations and γ-Secretase Modulation. *J Biol Chem*, **283**, 677–683.

Park K, Perczel A, and Fasman GD (1992) Differentiation between Transmembrane Helices and Peripheral Helices by the Deconvolution of Circular-Dichroism Spectra of Membrane-Proteins. *Protein Science*, **1**, 1032–1049.

Pearl L and Blundell T (1984) The active-site of aspartic proteinases. *FEBS Letters*, **174**, 96–101.

Pearson RG (1963) Hard and soft acids and bases. *JACS*, **85**, 3533–&. Pearson, rg.

Perrin CL (1989) Proton exchange in amides: Surprises from simple systems. *Accounts of Chemical Research*, **22**, 268–275.

Poirier J, Davignon J, Bouthillier D, Kogan S, Bertrand P, and Gauthier S (1993) Apolipoprotein-E polymorphism and Alzheimer's Disease. *Lancet*, **342**, 697–699.

Poschner BC, Quint S, Hofmann MW, and Langosch D (2009) Sequence-Specific Conformational Dynamics of Model Transmembrane Domains Determines Their Membrane Fusogenic Function. *J Mol Biol*, **386**, 733–741.

Poschner BC, Reed J, Langosch D, and Hofmann MW (2007) An automated application for deconvolution of circular dichroism spectra of small peptides. *Analytical Biochemistry*, **363**, 306–308.

Proebstle R (2012) Influence of Dimerization on Helix Dynamics of Alzheimer's Precursor Protein's Transmembrane Domain. Master Thesis. München. Technische Universität München, Lehrstuhl fÃ¼r Chemie der Biopolymere.

Prokop S, Shirotani K, Edbauer D, Haass C, and Steiner H (2004) Requirement of PEN-2 for stabilization of the presenilin N-/C-terminal fragment heterodimer within the γ-secretase complex. *J Biol Chem*, **279**, 23255–61.

Qi-Takahara Y, Morishima-Kawashima M, Tanimura Y, Dolios G, Hirotani N, Horikoshi Y, Kametani F, Maeda M, Saido TC, Wang R, and Ihara Y (2005) Longer Forms of Amyloid $\{\beta\}$ Protein: Implications for the Mechanism of Intramembrane Cleavage by $\{\gamma\}$-Secretase. *J Neurosci*, **25**, 436–445.

Quint S, Widmaier S, Minde D, Hornburg D, Langosch D, and Scharnagl C (2010) Residue-specific side-chain packing determines the backbone dynamics of transmembrane model helices. *Biophysical Journal*, **99**, 2541–9.

Rajamani R and Reynolds CH (2004) Modeling the protonation states of the catalytic aspartates in β-secretase. *Journal of Medicinal Chemistry*, **47**, 5159–5166.

Rattei T, Tischler P, Gotz S, Jehl MA, Hoser J, Arnold R, Conesa A, and Mewes HW (2010) SIMAP–a comprehensive database of pre-calculated protein sequence similarities, domains, annotations and clusters. *Nucleic Acids Res*, **38**, D223–6.

Reiersen H and Rees AR (2000) Trifluoroethanol may form a solvent matrix for assisted hydrophobic interactions between peptide side chains. *Protein Engineering*, **13**, 739–743.

Renfrew PD, Butterfoss GL, and Kuhlman B (2008) Using quantum mechanics to improve estimates of amino acid side chain rotamer energies. *Proteins: Structure, Function, and Bioinformatics*, **71**, 1637–1646.

Renzi F, Zhang X, Rice WJ, Torres-Arancivia C, Gomez-Llorente Y, Diaz R, Ahn K, Yu C, Li YM, Sisodia SS, and Ubarretxena-Belandia I (2011) Structure of γ-Secretase and Its Trimeric Pre-activation Intermediate by Single-particle Electron Microscopy. *J Biol Chem*, **286**, 21440–21449.

Richardson JS (1981) The anatomy and taxonomy of protein structure. *Advances in Protein Chemistry*, **34**, 167–339.

Richter L, Munter LM, Ness J, Hildebrand PW, Dasari M, Unterreitmeier S, Bulic B, Beyermann M, Gust R, Reif B, Weggen S, Langosch D, and Multhaup G (2010) Amyloid β 42 peptide (A β 42)-lowering compounds directly bind to A β and interfere with amyloid precursor protein (APP) transmembrane dimerization. *PNAS*, **107**, 14597–14602.

Roccatano D, Colombo G, Fioroni M, and Mark AE (2002) Mechanism by which 2,2,2-trifluoroethanol/water mixtures stabilize secondary-structure formation in peptides: a molecular dynamics study. *PNAS*, **99**, 12179–84.

Rodriguez EJ, Angeles TS, and Meek TD (1993) Use of 15N kinetic isotope effects to elucidate details of the chemical mechanism of human immundefienciency virus-1 protease. *Biochemistry*, **32**, 12380–12385.

Rohl CA and Baldwin RL (1994) Exchange Kinetics of Individual Amide Protons in 15N-Labeled Helical Peptides Measured by Isotope-Edited NMR. *Biochemistry*, **33**, 7760–7767.

Sagi SA, Lessard CB, Winden KD, Maruyama H, Koo JC, Weggen S, Kukar TL, Golde TE, and Koo EH (2011) Substrate Sequence Influences γ-Secretase Modulator Activity, Role of the Transmembrane Domain of the Amyloid Precursor Protein. *J Biol Chem*, **286**, 39794–803.

Sanders CR and Myers JK (2004) Disease-related misassembly of membrane proteins. *Annual Review of Biophysics and Biomolecular Structure*, **33**, 25–51.

Sato C, Morohashi Y, Tomita T, and Iwatsubo T (2006) Structure of the Catalytic Pore of γ-Secretase Probed by the Accessibility of Substituted Cysteines. *J Neurosci*, **26**, 12081–12088.

Sato T, Dohmae N, Qi Y, Kakuda N, Misonou H, Mitsumori R, Maruyama H, Koo EH, Haass C, Takio K, Morishima-Kawashima M, Ishiura S, and Ihara Y (2003) Potential Link between Amyloid b-Protein 42 and C-terminal Fragment g 49-99 of b-Amyloid Precursor Protein. *J Biol Chem*, **278**, 24294–24301.

Sato T, Tang Tc, Reubins G, Fei JZ, Fujimoto T, Kienlen-Campard P, Constantinescu SN, Octave JN, Aimoto S, and Smith SO (2009) A helix-to-coil transition at the Îμ-cut site in the transmembrane dimer of the amyloid precursor protein is required for proteolysis. *PNAS*, **106**, 1421–1426.

Saunders AM, Strittmatter WJ, Schmechel D, Georgehyslop PHS, Pericakvance MA, Joo SH, Rosi BL, Gusella JF, Crappermaclachlan DR, Alberts MJ, Hulette C, Crain B, Goldgaber D, and Roses AD (1993) Association of apolipoprotein-E allele epsilon-4 with late-onset familial and sporadic Alzheimer's Disease. *Neurology*, **43**, 1467–1472.

Scholtz JM, Marqusee S, Baldwin RL, York EJ, Stewart JM, Santoro M, and Bolen DW (1991) Calorimetric determination of the enthalpy change for α-helix to coil transition of an alanine peptide in water. *PNAS*, **88**, 2854–2858.

Selkoe D and Kopan R (2003) Notch and presenilin: Regulated intramembrane proteolysis links development and degeneration. *Annual Review of Neuroscience*, **26**, 565–597.

Senes A, Engel DE, and DeGrado WF (2004) Folding of helical membrane proteins: the role of polar, GxxxG-like and proline motifs. *Current Opinion in Structural Biology*, **14**, 465–479.

Senes A, Gerstein M, and Engelman DM (2000) Statistical analysis of amino acid patterns in transmembrane helices: The GxxxG motif occurs frequently and in association with β-branched residues at neighboring positions. *J Mol Biol*, **296**, 921–936.

Seubert P, Vigo-Pelfrey C, Esch F, Lee M, Dovey H, Davis D, Sinha S, Schiossmacher M, Whaley J, Swindlehurst C, McCormack R, Wolfert R, Selkoe D, Lieberburg I, and Schenk D (1992) Isolation and quantification of soluble Alzheimer's [β]-peptide from biological fluids. *Nature*, **359**, 325–327.

Shah S, Lee SF, Tabuchi K, Hao YH, Yu C, LaPlant Q, Ball H, Dann CEr, Sudhof T, and Yu G (2005) Nicastrin functions as a γ-secretase-substrate receptor. *Cell*, **122**, 435–47.

Shiraishi H, Sai X, Wang HQ, Maeda Y, Kurono Y, Nishimura M, Yanagisawa K, and Komano H (2004) PEN-2 enhances γ-cleavage after presenilin heterodimer formation. *J Neurochem*, **90**, 1402–13.

Shiraki K, Nishikawa K, and Goto Y (1995) Trifluoroethanol-induced Stabilization of the α-Helical Structure of β-Lactoglobulin: Implication for Non-hierarchical Protein Folding. *J Mol Biol*, **245**, 180–194.

Shoji M, Golde TE, Ghiso J, Cheung TT, Estus S, Shaffer LM, Cai XD, McKay DM, Tintner R, Frangione B, and et a (1992) Production of the Alzheimer amyloid β protein by normal proteolytic processing. *Science*, **258**, 126–129.

Sigel H and Martin RB (1982) Coordinating properties of the amide bond - stability and structure of metal-ion complexes of peptides and related ligands. *Chemical Reviews*, **82**, 385–426.

Simons M, Keller P, De Strooper B, Beyreuther K, Dotti CG, and Simons K (1998) Cholesterol depletion inhibits the generation of β-amyloid in hippocampal neurons. *Proceedings of the National Academy of Sciences of the United States of America*, **95**, 6460–6464.

Singh R, Barman A, and Prabhakar R (2009) Computational Insights into Aspartyl Protease Activity of Presenilin 1 (PS1) Generating Alzheimer Amyloid b-Peptides (AÎ²b40 and Ab42). *J Phys Chem B*, **113**, 2990–2999.

Sisodia SS (1999) Alzheimer's disease: perspectives for the new millennium. *J Clin Invest*, **104**, 1169–70.

Skilling J and Bryan RK (1984) Maximum Entropy Image Reconstruction - General Algorithm. *Royal Astronomical Society Monthly Notices*, **211**, 111.

Smith SO, Eilers M, Song D, Crocker E, Ying WW, Groesbeek M, Metz G, Ziliox M, and Aimoto S (2002) Implications of threonine hydrogen bonding in the glycophorin A transmembrane helix dimer. *Biophysical Journal*, **82**, 2476–2486.

Snatzke G (1981) Chiroptische Methoden in der Stereochemie, Teil I. *Chemie in unserer Zeit*, **15**, 78–87. 1521-3781.

Snider C, Jayasinghe S, Hristova K, and White SH (2009) MPEx: a tool for exploring membrane proteins. *Protein Sci*, **18**, 2624–8.

Sobhanifar S, Schneider B, Lohr F, Gottstein D, Ikeya T, Mlynarczyk K, Pulawski W, Ghoshdastider U, Kolinski M, Filipek S, Guntert P, Bernhard F, and Dotsch V (2010) Structural investigation of the C-terminal catalytic fragment of presenilin 1. *PNAS*, **107**, 9644–9.

Sreerama N and Woody RW (1994) Protein Secondary Structure from Circular Dichroism Spectroscopy: Combining Variable Selection Principle and Cluster Analysis with Neural Network, Ridge Regression and Self-consistent Methods. *J Mol Biol*, **242**, 497–507.

Steiner H, Fluhrer R, and Haass C (2008) Intramembrane Proteolysis by γ-Secretase. *J Biol Chem*, **283**, 29627–29631.

Steiner H, Winkler E, Edbauer D, Prokop S, Basset G, Yamasaki A, Kostka M, and Haass C (2002) PEN-2 is an integral component of the γ-secretase complex required for coordinated expression of presenilin and nicastrin. *J Biol Chem*, **277**, 39062–5.

Steiner T (2002) Die Wasserstoffbrücke im Festkörper. *Angewandte Chemie*, **114**, 50–80.

Stelzer W, Poschner B, Stalz H, Heck A, and Langosch D (2008) Sequence-specific conformational flexibility of SNARE transmembrane helices probed by hydrogen/deuterium exchange. *Biophys J*, **95**, 1326–1335.

Storrs RW, Truckses D, and Wemmer DE (1992) Helix propagation in trifluoroethanol solutions. *Biopolymers*, **32**, 1695–702.

Straub JE and Thirumalai D (2011) Toward a Molecular Theory of Early and Late Events in Monomer to Amyloid Fibril Formation. *Annu Rev Phys Chem*, **62**, 437–463.

Subczynski WK, Wisniewska A, Yin JJ, Hyde JS, and Kusumi A (1994) Hydrophobic Barriers of Lipid Bilayer-Membranes Formed by Reduction of Water Penetration by Alkyl Chain Unsaturation and Cholesterol. *Biochemistry*, **33**, 7670–7681.

Suguna K, Padlan EA, Smith CW, Carlson WD, and Davies DR (1987) Binding of a reduced peptide inhibitor to the aspartic proteinase from rhizopus-chinensis - implications for a mechanism of action. *PNAS*, **84**, 7009–7013.

Suzuki N, Cheung TT, Cai XD, Odaka A, Otvos L, Eckman C, Golde TE, and Younkin SG (1994) An increased percentage of long amyloid β protein secreted by familial amyloid β protein precursor (β APP717) mutants. *Science*, **264**, 1336–1340.

Suzuki T, Araki Y, Yamamoto T, and Nakaya T (2006) Trafficking of Alzheimer's Disease–Related Membrane Proteins and Its Participation in Disease Pathogenesis. *Journal of Biochemistry*, **139**, 949–955.

Takagi S, Tominaga A, Sato C, Tomita T, and Iwatsubo T (2010) Participation of Transmembrane Domain 1 of Presenilin 1 in the Catalytic Pore Structure of the $\{\gamma\}$-Secretase. *J Neurosci*, **30**, 15943–15950.

Takami M, Nagashima Y, Sano Y, Ishihara S, Morishima-Kawashima M, Funamoto S, and Ihara Y (2009) γ-Secretase: Successive Tripeptide and Tetrapeptide Release from the Transmembrane Domain of b-Carboxyl Terminal Fragment. *J Neurosci*, **29**, 13042–13052.

Tan JX, Mao GZ, Cui MZ, Kang SC, Lamb B, Wong BS, Sy MS, and Xu XM (2008) Effects of γ-secretase cleavage-region mutations on APP processing and A β formation: interpretation with sequential cleavage and α-helical model. *Journal of Neurochemistry*, **107**, 722–733.

Tanaka Y, Xiao YF, and Matsuo S (2000) Relative permittivity of fluoroalcohols at temperatures from 293 to 323 K and pressures up to 50 MPa. *Fluid Phase Equilibria*, **170**, 139–149.

Tang K, Wang C, Shen C, Sheng S, Ravid R, and Jing N (2003) Identification of a novel alternative splicing isoform of human amyloid precursor protein gene, APP639. *European Journal of Neuroscience*, **18**, 102–108.

Tanzi RE, McClatchey AI, Lamperti ED, Villa-Komaroff L, Gusella JF, and Neve RL (1988) Protease inhibitor domain encoded by an amyloid protein precursor mRNA associated with Alzheimer's disease. *Nature*, **331**, 528–30.

Thinakaran G, Borchelt DR, Lee MK, Slunt HH, Spitzer L, Kim G, Ratovitsky T, Davenport F, Nordstedt C, Seeger M, Hardy J, Levey AI, Gandy SE, Jenkins NA, Copeland NG, Price DL, and Sisodia SS (1996) Endoproteolysis of presenilin 1 and accumulation of processed derivatives in vivo. *Neuron*, **17**, 181–90.

Thinakaran G and Koo EH (2008) Amyloid Precursor Protein Trafficking, Processing, and Function. *J Biol Chem*, **283**, 29615–29619.

Thinakaran G, Regard JB, Bouton CM, Harris CL, Price DL, Borchelt DR, and Sisodia SS (1998) Stable association of presenilin derivatives and absence of presenilin interactions with APP. *Neurobiol Dis*, **4**, 438–53.

Thomas PD and Dill KA (1993) Local and nonlocal interactions in globular-proteins and mechanisms of alcohol denaturation. *Protein Science*, **2**, 2050–2065.

Tolia A, Chavez-Gutierrez L, and De Strooper B (2006) Contribution of Presenilin Transmembrane Domains 6 and 7 to a Water-containing Cavity in the γ-Secretase Complex. *J Biol Chem*, **281**, 27633–27642.

Tolia A, Horre K, and De Strooper B (2008) Transmembrane Domain 9 of Presenilin Determines the Dynamic Conformation of the Catalytic Site of $\{\gamma\}$-Secretase. *J Biol Chem*, **283**, 19793–19803.

Ulmschneider MB, Sansom MS, and Di Nola A (2005) Properties of integral membrane protein structures: derivation of an implicit membrane potential. *Proteins*, **59**, 252–65.

Unterreitmeier S, Fuchs A, Schäffler T, Heym RG, Frishman D, and Langosch D (2007) Phenylalanine Promotes Interaction of Transmembrane Domains via GxxxG Motifs. *J Mol Biol*, **374**, 705–718.

Unwin N and Henderson R (1984) The structure of proteins in biological membranes. *Scientific American*, **250**, 78–&.

Urban S and Freeman M (2003) Substrate Specificity of Rhomboid Intramembrane Proteases Is Governed by Helix-Breaking Residues in the Substrate Transmembrane Domain. *Molecular Cell*, **11**, 1425–1434.

Urban S and Shi Y (2008) Core principles of intramembrane proteolysis: comparison of rhomboid and site-2 family proteases. *Current Opinion in Structural Biology*, **18**, 432–441.

van Broeck B, Vanhoutte G, Pirici D, van Dam D, Wils H, Cuijt I, Vennekens K, Zabielski M, Michalik A, Theuns J, De Deyn PP, Van der Linden A, Van Broeckhoven C, and Kumar-Singh S (2008) Intraneuronal amyloid β and reduced brain volume in a novel APP T714I mouse model for Alzheimer's disease. *Neurobiol Aging*, **29**, 241–52.

van Meer G, Voelker DR, and Feigenson GW (2008) Membrane lipids: where they are and how they behave. *Nature Reviews Molecular Cell Biology*, **9**, 112–124.

Vassar R (2004) BACE1 - The β-secretase enzyme in Alzheimer's disease. *Journal of Molecular Neuroscience*, **23**, 105–113.

von Heijne G (2006) Membrane-protein topology. *Nature Reviews Molecular Cell Biology*, **7**, 909–918.

Wallin E and von Heijne G (1998) Genome-wide analysis of integral membrane proteins from eubacterial, archaean, and eukaryotic organisms. *Protein Science*, **7**, 1029–1038.

Walsh DM, Klyubin I, Fadeeva JV, Cullen WK, Anwyl R, Wolfe MS, Rowan MJ, and Selkoe DJ (2002) Naturally secreted oligomers of amyloid β protein potently inhibit hippocampal long-term potentiation in vivo. *Nature*, **416**, 535–539.

Walter J, Capell A, Hung AY, Langen H, Schnölzer M, Thinakaran G, Sisodia SS, Selkoe DJ, and Haass C (1997) Ectodomain Phosphorylation of β-Amyloid Precursor Protein at Two Distinct Cellular Locations. *J Biol Chem*, **272**, 1896–1903.

Watanabe N, Takagi S, Tominaga A, Tomita T, and Iwatsubo T (2010) Functional Analysis of the Transmembrane Domains of Presenilin 1: Participation of transmembrane domains 2 and 6 in the formation of the initial substrate-binding site of γ-secretase. *J Biol Chem*, **285**, 19738–19746.

Watanabe N, Tomita T, Sato C, Kitamura T, Morohashi Y, and Iwatsubo T (2005) Pen-2 Is Incorporated into the Î³-Secretase Complex through Binding to Transmembrane Domain 4 of Presenilin 1. *J Biol Chem*, **280**, 41967–41975.

Weggen S, Eriksen JL, Das P, Sagi SA, Wang R, Pietrzik CU, Findlay KA, Smith TE, Murphy MP, Butler T, Kang DE, Marquez-Sterling N, Golde TE, and Koo EH (2001) A subset of NSAIDs lower amyloidogenic A β 42 independently of cyclooxygenase activity. *Nature*, **414**, 212–216.

Weggen S, Eriksen JL, Sagi SA, Pietrzik CU, Ozols V, Fauq A, Golde TE, and Koo EH (2003) Evidence that nonsteroidal anti-inflammatory drugs decrease amyloid β 42 production by direct modulation of γ-secretase activity. *J Biol Chem*, **278**, 31831–31837.

Weidemann A, Eggert S, Reinhard FBM, Vogel M, Paliga K, Baier G, Masters CL, Beyreuther K, and Evin G (2002) A Novel e-Cleavage within the Transmembrane Domain of the Alzheimer Amyloid Precursor Protein Demonstrates Homology with Notch Processing. *Biochemistry*, **41**, 2825–2835.

Weiss MS, Brandl M, Sühnel J, Pal D, and Hilgenfeld R (2001) More hydrogen bonds for the (structural) biologist. *Trends in Biochemical Sciences*, **26**, 521–523.

White SH, King GI, and Cain JE (1981) Location of Hexane in Lipid Bilayers Determined by Neutron-Diffraction. *Nature*, **290**, 161–163.

Whitmore L and Wallace BA (2008) Protein secondary structure analyses from circular dichroism spectroscopy: Methods and reference databases. *Biopolymers*, **89**, 392–400.

Widmaier S (2009) A Comparative Molecular Dynamics Study of Wildtype and Mutant Transmembrane Segments of the Amyloid Precursor Protein - Implications for Alzheimer's Disease. Master Thesis. München. Technische Universität München, Lehrstuhl fÃ¼r Chemie der Biopolymere.

Wolfe MS (2009) Intramembrane Proteolysis. *Chemical Reviews*, **109**, 1599–1612.

Wolfe MS (2010) Structure, mechanism and inhibition of γ-secretase and presenilin-like proteases. *Biol Chem*, **391**, 839–47.

Wolfe MS, De los Angeles J, Miller DD, Xia WM, and Selkoe DJ (1999) Are presenilins intramembrane-cleaving proteases?: Implications for the molecular mechanism of Alzheimer's disease. *Biochemistry*, **38**, 11223–11230.

Wolfe MS and Kopan R (2004) Intramembrane proteotysis: Theme and variations. *Science*, **305**, 1119–1123.

Woodward CK and Hilton BD (1980) Hydrogen isotope exchange kinetics of single protons in bovine pancreatic trypsin inhibitor. *Biophysical Journal*, **32**, 561–575.

Woody RW (1995) Biochemical Spectroscopy, vol. 246 of *Methods in Enzymology*, chap. Circular-Dichroism. 34–71.

Xu Y, Shen J, Luo X, Zhu W, Chen K, Ma J, and Jiang H (2005) Conformational transition of amyloid β-peptide. *PNAS*, **102**, 5403–5407.

Yang AS and Honig B (1995) Free energy determinats of secondary structure formation. 1. α-helices. *J Mol Biol*, **252**, 351–365.

Yildirim MA, Goh KI, Cusick ME, Barabasi AL, and Vidal M (2007) Drug-target network. *Nature Biotechnology*, **25**, 1119–1126.

Younkin SG (1998) The role of Aβ42 in Alzheimer's disease. *Journal of Physiology-Paris*, **92**, 289–292.

Yu N, Hayik SA, Wang B, Liao N, Reynolds CH, and Merz KM (2006) Assigning the protonation states of the key aspartates in β-secretase using QM/MM X-ray structure refinement. *Journal of Chemical Theory and Computation*, **2**, 1057–1069.

Zhang YZ (1995) Protein and peptide structure and interactions studied by hydrogen exchange and NMR. Ph.D. thesis, Philadelphia.

Zhang Z, Li W, Logan TM, Li M, and Marshall AG (1997) Human recombinant [C22A] FK506-binding protein amide hydrogen exchange rates from mass spectrometry match and extend those from NMR. *Protein Sci*, **6**, 2203–2217.

Zhao G, Cui MZ, Mao G, Dong Y, Tan J, Sun L, and Xu X (2005) γ-Cleavage is dependent on zeta-cleavage during the proteolytic processing of amyloid precursor protein within its transmembrane domain. *J Biol Chem*, **280**, 37689–97.

Zhao G, Mao G, Tan J, Dong Y, Cui MZ, Kim SH, and Xu X (2004) Identification of a new presenilin-dependent zeta-cleavage site within the transmembrane domain of amyloid precursor protein. *J Biol Chem*, **279**, 50647–50.

Zhong L and Johnson WCJ (1992) Environment affects amino acid preference for secondary structure. *PNAS*, **89**, 4462–5.

Zhou YZ, Moin SM, Urban S, and Zhang YK (2012) An Internal Water-Retention Site in the Rhomboid Intramembrane Protease GlpG Ensures Catalytic Efficiency. *Structure*, **20**, 1255–1263.

A Appendix

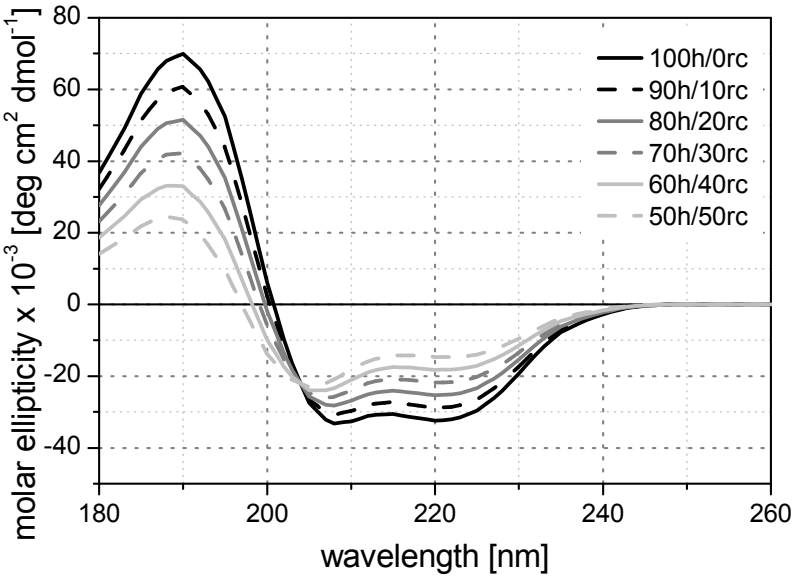

Figure A.1: Artificial spectra with different helix - random coil ratios

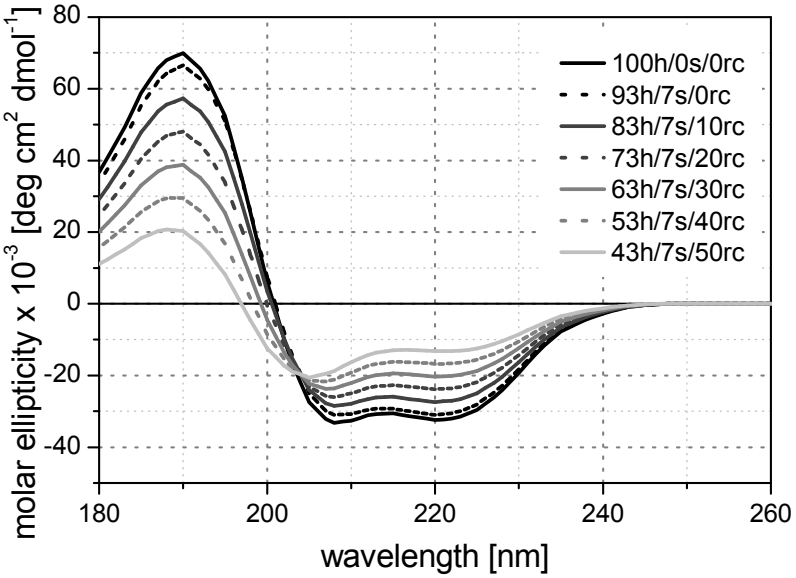

Figure A.2: Artificial CD spectra with different helix, sheet and random coil proportions

Table A.1: No. of protected deuterons with standard deviations at selected time points for Thr mutants, DHX at pH 5

time [min]	A 37–55	T43V	T43I	T48V	T43/48V
0	15.5 ± 0.3	15.6 ± 0.3	15.4 ± 0.2	15.5 ± 0.6	14.9 ± 0.3
1/6	13.9 ± 0.1	13.3 ± 0.2	12.9 ± 0.2	13.5 ± 0.1	12.7 ± 0.1
5	9.9 ± 0.5	10.1 ± 0.2	9.7 ± 0.6	9.3 ± 1.0	9.2 ± 0.2
20	7.9 ± 0.1	7.9 ± 0.05	7.5 ± 0.2	7.2 ± 0.2	6.8 ± 0.1
180	5.2 ± 0.1	4.9 ± 0.1	4.8 ± 0.3	4.5 ± 0.3	3.4 ± 0.1
240	4.7 ± 0.1	4.3 ± 0.02	4.1 ± 0.2	3.9 ± 0.4	3.0 ± 0.1

Table A.2: No. of protected deuterons in DHX kinetics of AL peptides

time [min]	L19	AL 35-42	AL 39-46	AL 42-49	AL 45-52	AL 45-52M
0[a]	16.4 ± 0.3	16.3 ± 0.4	15.2 ± 0.4	16.5 ± 0.5	16.1 ± 0.1	19.3 ± 0.4
0[b]	18.9 ± 0.4	18.4 ± 0.3	18.8 ± 0.3	18.5 ± 0.3	18.6 ± 0.5	21.6 ± 0.4
240[b]	11.5 ± 0.2	8.7 ± 0.0	9.6 ± 0.2	8.9 ± 0.3	10.7 ± 0.3	12.4 ± 0.4

[a] measured in isotropic solution, equation 3.4 on p. 46 used for calculation; the deuterated peptide stock solution was in 100 % HFIP from which the 100 µM deuterated working solution was prepared. A 1:20 (v/v) dilution of a 100 µM deuterated peptide solution (10% (v/v) dHFIP, 70% (v/v) dTFE and 10 mM ND_4Ac, pD 5) into 80% (v/v) TFE and 10 mM NH_4Ac, pH 2.5 at 0°C was performed.
[b] measured in liposomes, equation 3.5 on p. 46 used for calculation

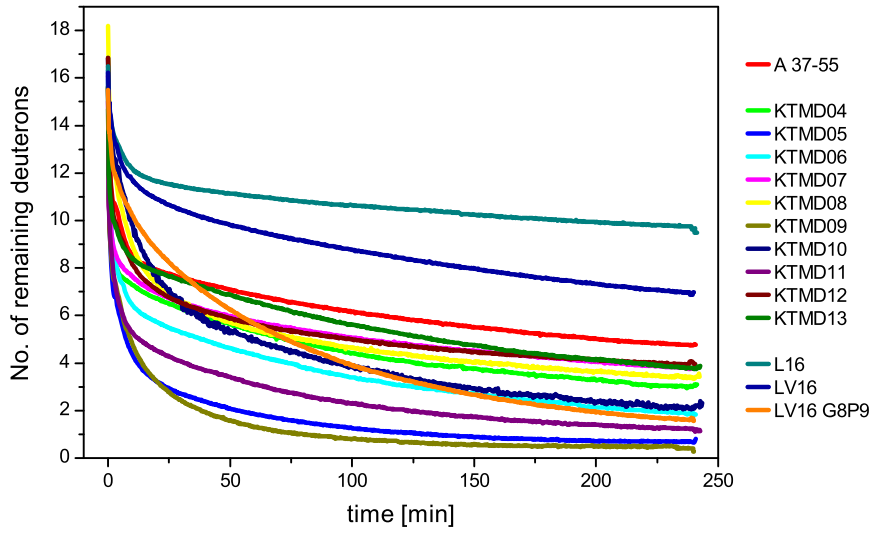

Figure A.3: Comparison in DHX kinetics between KTMD and LV peptides

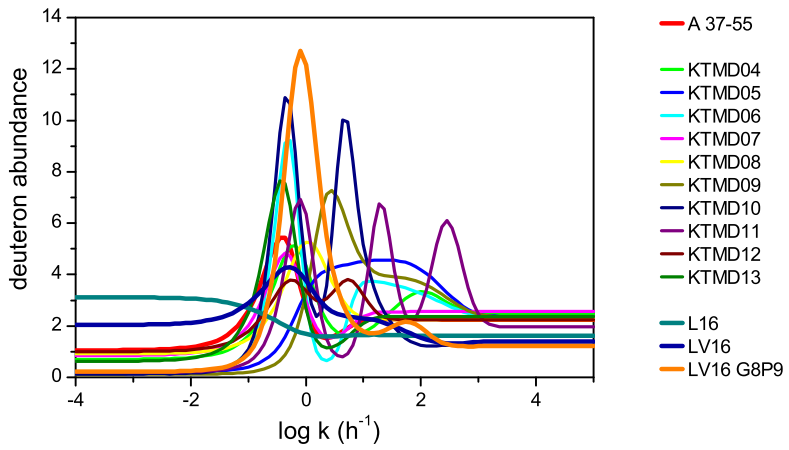

Figure A.4: Comparison in MEM Analysis between KTMD and LV peptides

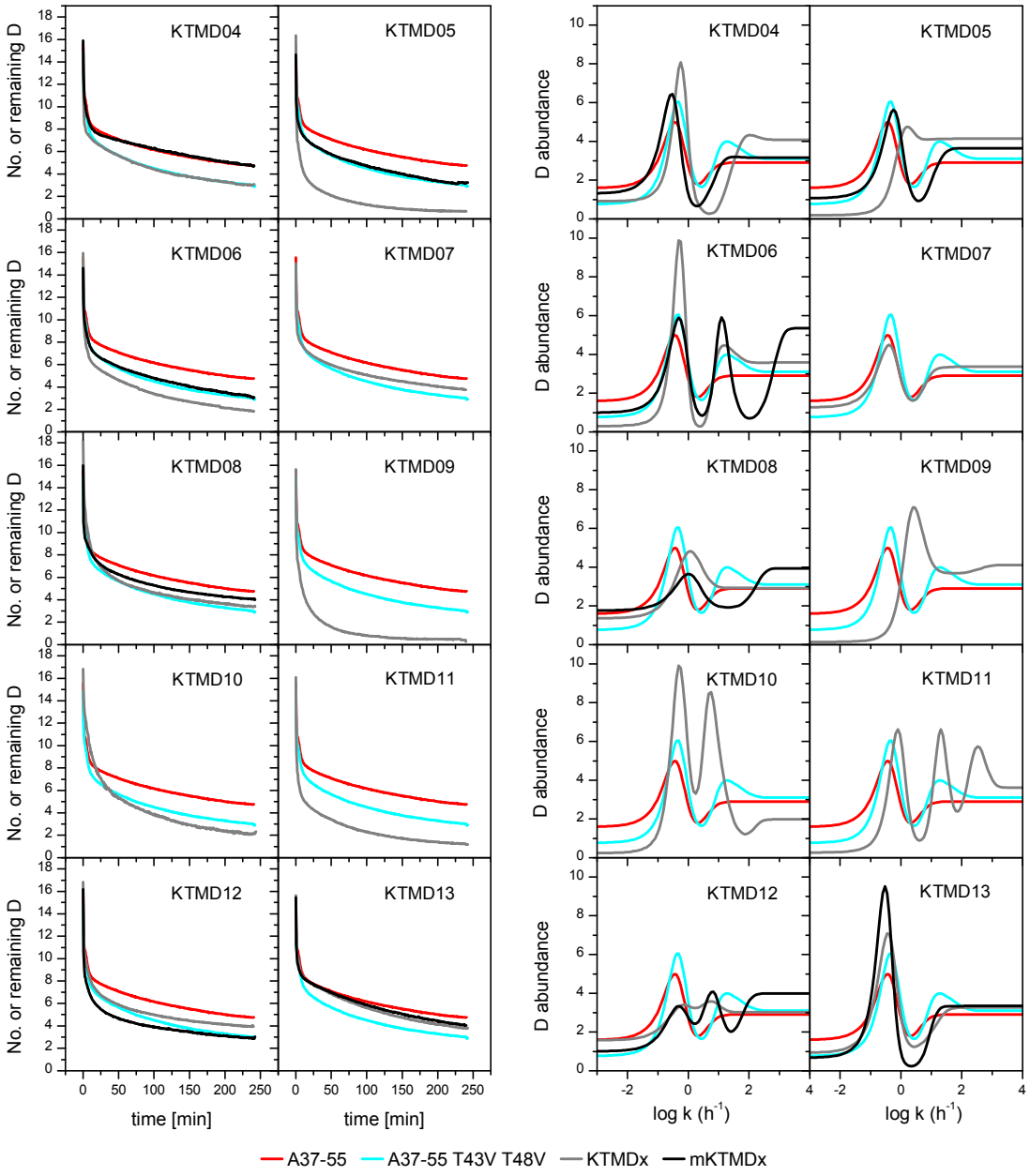

Figure A.5: DHX and MEM analysis of KTMDs compared with A37–55 and its Thr double mutant.

Publication List

Parts of the thesis are published in the following publications:

Pester O, Barrett PJ, Hornburg D, Hornburg P, Pröbstle R, Widmaier S, Kutzner C, Dürrbaum M, Kapurniotu A, Sanders CR, Scharnagl C, Langosch D (2013) The Backbone Dynamics of the Amyloid Precursor Protein Transmembrane Helix Provides a Rationale for the Sequential Cleavage Mechanism of γ-Secretase. *Journal of the American Chemistry Society*, **135,** 1317-29.

Pester O, Götz A, Multhaup G, Scharnagl C, Langosch D (2013) The Cleavage Domain of the Amyloid Precursor Protein Transmembrane Helix does not Exhibit Above-Average Backbone Dynamics. *manuscript to be submitted.*

Lebenslauf

Oxana Pester
am 29.Mai 1982 in Dresden geboren

Schulbildung

1989-1993	134. Grundschule, Dresden
1993-2001	Fritz-Löffler-Gymnasium, Dresden, Allgemeine Hochschulreife

Studium

2001-2007	Diplomstudiengang Chemie, Technische Universität Dresden
	Diplomarbeit: „Entwicklung einer ATR-FTIR-Datenbank zur Sekundärstrukturanalyse von Peptiden und Proteinen“
2004-2005	2-semestriger Erasmus-Austausch an der Northumbria University, Newcastle upon Tyne, Großbritannien
	Ganzjahresprojekt: „Charakterisierung von Makroamphiphilen in *Thermobifida fusca*“
2008-2013	Promotion am Lehrstuhl für Chemie der Polymere von Prof. Dr. D. Langosch, Technische Universität München, 85354 Freising
	Doktorarbeit: „Die Peptidrückgratdynamik der helikalen TMD des Alzheimerschen Amyloid-Vorläuferproteins - ein Substrat der γ-Sekretase“

Berufserfahrung

seit 2012	wissenschaftliche Mitarbeit im Proteinbioanalytik-Labor der Entwicklungsabteilung von Roche Diagnostics GmbH in Penzberg